Investigation of Wettability and Droplet Energetics on Micro-Scale Wavy and V-Grooved Surfaces

Thesis

M. Sc. Engg (Mechanical)

Submitted by

Md. Ikram Khan

Student No. 1018102051

Department of Mechanical Engineering
Bangladesh University of Engineering and Technology (BUET)

April 2022

Investigation of Wettability and Droplet Energetics on Micro-Scale Wavy and V-Grooved Surfaces

A Dissertation

by

Md. Ikram Khan(Student ID: 1018102051)

Under the Supervision of

Dr. Md. Ashiqur Rahman

MASTER OF SCIENCE IN MECHANICAL ENGINEERING

Department of Mechanical Engineering

BANGLADESH UNIVERSITY OF ENGINEERING AND TECHNOLOGY

April 2022

RECOMMENDATION OF THE BOARD OF EXAMINERS

The thesis titled "**Investigation of Wettability and Droplet Energetics on Micro-Scale Wavy and V-Grooved Surfaces**" submitted by Md. Ikram Khan, Student No.: 1018102051, Session: October 2018, has been accepted as satisfactory in partial fulfillment of the requirement for the degree of Master of Science in Mechanical Engineering on April 26, 2022.

BOARD OF EXAMINERS

_____
Dr. Md. Ashiqur Rahman
Professor
Department of Mechanical Engineering
BUET, Dhaka-1000

Chairman
(Supervisor)

_____
Dr. Muhammad Ashiqur Rahman
Professor and Head
Department of Mechanical Engineering
BUET, Dhaka-1000

Member
(Ex- officio)

_____
Dr. Mohammad Nasim Hasan
Professor
Department of Mechanical Engineering
BUET, Dhaka-1000

Member
(Internal)

_____
Dr. Chanchal Kumar Roy
Assistant Professor
Department of Chemistry
BUET, Dhaka-1000

Member
(External)

CANDIDATE'S DECLARATION

It is hereby declared that this thesis/project or any part of it has not been submitted elsewhere for the award of any degree or diploma.

Md. Ikram Khan

Dedicated to my family

ACKNOWLEDGEMENTS

TABLE OF CONTENTS

LIST OF TABLES

LIST OF FIGURES

droplet.

denotes the width and length of the droplet at the base measured in front and side views respectively.

NOMENCLATURE

Notation	Definition
G_E	Gibbs free energy
γ	Surface free energy
γ_{lv}	Liquid-vapor surface tension
γ_{sv}	Solid-vapor surface tension
γ_{sl}	Solid-liquid surface tension
γ_{LS}	Surface tension between liquid and solid phases
γ_{LG}	Surface tension between liquid and gas phases
γ_{SG}	Surface tension between solid and gas phases
A_{LS}	Interfacial or contact area between liquid and solid phases
A_{LG}	Interfacial or contact area between liquid and gas phases
A_{SG}	Interfacial or contact area between solid and gas phases
θ_Y	Young or equilibrium contact angle
θ_W	Wenzel contact angle
θ_{CB}	Cassie-Baxter contact angle
r	Surface roughness factor
f	Cassie roughness factor or solid fraction area
θ_{int}	Intrinsic contact angle
G^S	Droplet's free surface energy
G^G	Droplet's gravitational energy
G	Total droplet energy
G_{norm}	Droplet's normalized surface energy
T	Surface tension per unit length
θ_o	Orthogonal contact angle
θ_p	Parallel contact angle
W_p	Pillar width

Notation	Definition
W_g or λ_w	Groove width or pitch
D_g or H_w	Groove height or depth
$\Delta\theta$	Degree of Anisotropy
φ	Groove angle
V	Volume of droplet
h_{cr}	Critical amplitude height factor
r_{cr}	Critical surface roughness factor
R	Droplet expansion ratio
B	Length of the droplet
A	Width of the droplet
D_g/W_g or, H_w/λ_w	Aspect ratio

ABSTRACT

In order to develop micro-structured surfaces with tunable wetting properties, it is critical to understand the relationship between the surface roughness and wetting state. Basic research on developing hydrophobic surfaces with regulated wettability has piqued people's curiosity in the recent years. Surfaces having directional wetting properties and inducing anisotropic wetting behavior that encourage liquid drainage are beneficial in a broad variety of applications.

In this study, the wetting behavior on surfaces that can exhibit directional wetting, such as V-grooves and periodic wavy surfaces, are investigated using a numerical technique with a focus on the droplet stability and anisotropic wetting conditions. Surface Evolver, an open access software, is employed to develop 3D models of liquid droplets and to assess the shape and spread of liquid droplets for a broad range of parametric space. Along with a detailed examination of the stability and energetics of liquid droplets, the apparent contact angles on micro wavy and V-grooved surfaces are numerically quantified for a range of droplet volume. The effect of surface roughness parameters of micro V-grooved surfaces such as groove height, groove width, pillar width, groove angle and so on is examined and then compared to the same for the dimensional variation of pitch, amplitude and depth of the asperities of micro wavy surfaces. The findings are found to be consistent with the previously reported experimental studies and analytical models.

To distinguish the stabilities of liquid droplets on both micro V-grooved and micro wavy substrates, a dimensionless normalized version of interfacial energy is employed. For different anisotropic configurations, stable and metastable droplets with increasing droplet size on these surfaces is analyzed. It is found that multiple metastable wetting states can be obtained for constant droplet volume and larger number of pillars beneath the droplet is required for bigger droplet size to be stable. However, orthogonal contact angles are always larger than the parallel ones due to the free energy barrier caused by pinning, though this effect is less pronounced for micro wavy surfaces.

The essential characteristics that have a dominating influence on the anisotropy of droplets is explored using variation of the geometric properties of the surface roughness. Due to the larger dispersion of the liquid droplet along the groove direction, the Wenzel state of wetting showed a higher degree of anisotropy. The droplet height of Cassie droplets increased as the droplet volume increased, but the height of Wenzel droplets remained roughly constant regardless of the droplet size. The Wenzel state of wetting has a higher droplet expansion ratio than the Cassie state. Water droplets fall down the pillars and spread along the grooves on surfaces with a smaller groove depth and wider grooves, resulting in a lower apparent contact angle, whereas higher groove height and shorter groove width have the opposite effect due to the higher aspect ratio and larger energy barrier. The wetting properties of groove angles on V-grooved surfaces were likewise comparable.

Moreover, the chemical alteration of these rough micro-structured surfaces is also studied. With a higher intrinsic contact angle of the surface material, the apparent contact angle in both the parallel and orthogonal directions of the grooves increased, but with a faster increment rate of parallel contact angle than orthogonal contact angle, resulting in a lower degree of wetting anisotropy and a shift toward isotropic wetting.

In general, the developed numerical model provides reasonable predictions of anisotropic wetting behavior. This can be a useful tool in improving the design of micro-structured rough surfaces with directional wetting by means of optimizing the geometric parameters such as groove size, shape, spacing, as well as the chemical nature of the surface.

CHAPTER 01
INTRODUCTION

1.1 Preamble

From the water droplet on nature's spectacular masterpiece "lotus leaf" to the presence of liquid droplets in various forms on a range of manmade equipment, the interaction of liquids with solid surfaces has been discovered to be the widespread phenomenon in nature and our surrounds. However, the form of a liquid changes as it comes into touch with a solid surface owing to interactions at the solid-liquid interface, such as spreading or the development of distinct droplet forms. Two crucial characteristics – (a) the angle of contact between the liquid and the solid, and (b) the force of surface tension, which cause the liquid to alter form, can provide the better understanding about surface wettability. Necessity to comprehend the wetting phenomena on solid surfaces with configurable wettability has grown in recent years due to a wide range of applications, including refrigeration and air-conditioning systems [1], self-cleaning devices [2], microfluidic operations [3], and so on. So, this chapter's major purpose is to present the key elements of wetting physics that will be used throughout the thesis.

1.2 Surface Tension and Surface Energy

Despite the fact that steel is denser than water, if a little steel needle is put on top of a glass of water, it will float rather than sink. This is due to a phenomenon known as "surface tension". Basically, water molecules within this liquid are attracted to each other because of cohesion. In the bulk of liquid, each water molecule can form hydrogen bonds with other molecules around it from every direction,causing it to be drawn toward them, resulting in a zero net force. However, at the surface, attraction between water molecules is only lateral and downward and this unbalanced net force makes them less restricted.There are negligible intermolecular attractions above these molecules. So, on surface molecules, the net force is downward. Surface particles

are dragged down as a consequence of this downward force until the liquid's compression resistance counteracts it. Surface molecules are packed closer together near the surface, producing a type of skin on the surface, with less gap between them than molecules deeper in the liquid, allowing surface molecules to withstand pressure from above (Figure 1.1). That is why even after filling a glass with water up to the brim, still few more drops of water can be added till it overflows. So,surface tension is the tension in a liquid's surface film induced by the majority of the liquid's attraction to the particles in the surface layer, which strives to reduce surface area.
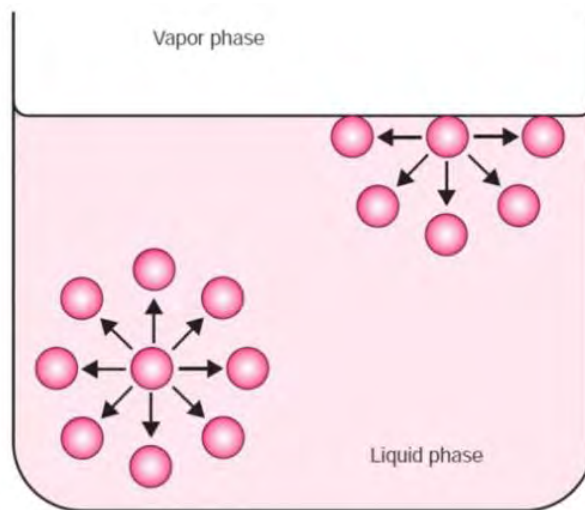
Figure 1.1: The imbalanced forces of liquid molecules at the surface generate surface tension.

Now, when compared to the molecules in the liquid's bulk, each molecule at the surface has a certain amount of potential energy. The more molecules with this surplus potential energy, the higher the liquid's surface. So, the energy of a liquid rises as the surface area of the liquid grows. This energy is known as "surface free energy" because it is proportional to the size of the free surface. Therefore, we know that in universe, everything tends to get less energy. So, liquid tends to attain a lesser surface area with minimal surface energy. As a result, since a sphere has the lowest surface area per unit volume, it has been observed by all that water flowing from a faucet takes on a spherical form. This phenomenon has also been detected in liquid drop without gravity.

By using thermodynamics, the concept of surface energy can be more elaborately described with the help of Gibbs model [4].It is known that between two immiscible phases, a surface or interfacial region forms over which properties are in transition. By convention, when one phase is a condensed phase (solid or liquid) and other one is gas or vacuum, the region between them is referred as a surface and when both are condensed phases, the region is called an interface. However, the term 'interface' is considered more general. The region between two immiscible phases is a region with unique properties. The interfacial region in liquids is so unstable that it will take any opportunity to eliminate itself as much as possible. At constant temperature (T) and pressure (P), this influence is reflected bythe surface free energy (γ), which employs Gibbs free energy (G_E). This surface energy (γ) can be expressed as:

$$\gamma = \left(dG_E / dA \right)_{T,P} \tag{1.1}$$

Dimension of this surface free energy is energy per unit area and commonly reported in mJ/m^2. This definition tells us that surface free energy must be greater than zero for an interface to exist. If it were negative, a spontaneous expansion of surface area (A) would occur, resulting in complete dissolution. The equation also tells us that surface area contracts spontaneously, in other words, interfaces exist, even though it is not energetically favourable. Hence, the time spent by a molecule at a liquid interface tends to be fleeting and molecules at solid surfaces tend to be markedly more reactive due to their desire to change. The integration of the equation (1.1) results in an expression for calculating the reversible work with an increase in surface area.

$$\Delta G_E = \gamma \Delta A \tag{1.2}$$

Equation (1.3) provides Gibbs free energy in terms of enthalpy (H) and entropy (S) which defines the surface enthalpy (H^s) and surface entropy (S^s) values.

$$G_E^s = \left(\frac{dH}{dA} \right)_{T,P} - T \left(\frac{dS}{dA} \right)_{T,P} = H^s - TS^s \tag{1.3}$$

Differentiating this expression with respect to temperature provides a useful equation (1.4) relating interfacial free energy with surface entropy, which indicates this quantity can be gauged experimentally.

$$\left(\frac{dG_E^s}{dT}\right)_{P,A} = \frac{d\gamma}{dT} = -S^s \tag{1.4}$$

The surface enthalpy equal to the total surface energy (U^s) plus pressure multiplied by volume. But for the Gibbs approach, surface is a plane and has no volume.

$$H^s = U^s + PV^s \approx U^s \tag{1.5}$$

This allows to write surface free energy in a form that can be used for molecular contribution analysis.

$$G_E^s = U^s - TS^s \tag{1.6}$$

$$\gamma = U^s + T\frac{d\gamma}{dT} \tag{1.7}$$

"Surface tension" and "Surface free energy" are theoretically similar, however their interpretations of the surface vary somewhat. The tension force per length operating in all directions along the surface is known as surface tension, and it is measured in mN/m or dyn/cm. The energy needed to develop additional surface area is known as surface free energy, and it is measured in mJ/m^2 (equal to mN/m). The surface free energy of a solid-vapor surface is an important feature that determines how a liquid will wet it. This energy is useful in a variety of applications, including coatings, water resistant textiles, improved oil recovery, and more.

1.3 Contact Angle and Wettability

Consider the impact of a little liquid droplet on a solid surface. The liquid will have a distinct clear boundary termed as"three-phase contact line" or "wetting line" or "contact line", if it does not fully wet the surface. The three-phase contact line is generated when three phases that make up the system of a liquid drop, a solid surface, and a surrounding fluid all come together and meet, as the name indicates. From the top view of a transparent liquid drop placed on a solid surface, circular shape of three-phase contact line can be observed at the base of the droplet (Figure 1.2, left).
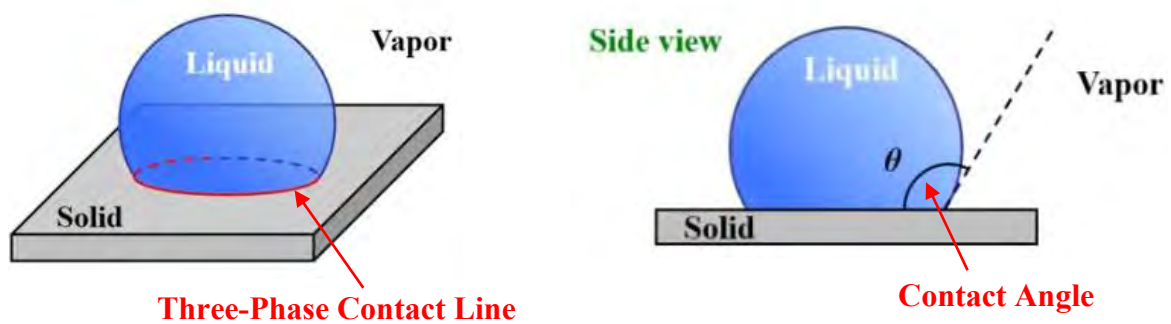
Figure 1.2: Sessile droplet on substrate: (left) drop's 3-D view shows the circular form of three-phase contact line at the wall where solid, liquid and vapor phases meet; (right) drop's side view reveals the contact angle (θ), angle liquid makes with solid surface at contact line.

Moreover, the contact angle (θ) can be best defined from the side view of a droplet on a substrate (Figure 1.2, right). It is the angle formed between the solid surface and the tangent to the liquid surface at or very close to three-phase contact line. Contact angle (CA) can theoretically range from 0° up to 180°. In the study of wettability, the contact angle is a key metric. It determines how effectively (or badly) liquid spreads over a surface. To determine the relationship between contact angle and surface wetness, we must first understand two major surface divisions based on wetting. The first is a "hydrophilic surface," whereas the second is a "hydrophobic surface"."Hydro" refers to water, while "philic or phil" denotes a strong attraction to or affection for something. "Phobia" or "phobic" on the other hand, refers to a dread of something. So, "hydrophobic" means "afraid of water", whereas "hydrophilic" implies "love of water". As water is polar and hydrophilic compounds break down to be surrounded by water, hydrophilic substances dissolve in water. Hydrophobic compounds, on the other hand, are

difficult to dissolve in water. Hydrophobic compounds include oils and other lipids, as well as non-polar chemicals. Now, while a liquid droplet is on a solid substrate, its interface is just the solid surface with which the liquid comes into touch and liquid molecules are attracted towards the interface by Van der Waals forces. Therefore, if the attractions of these molecules to the solid are strong, the solid substrate is said to be wetting or "hydrophilic" and the solid is non-wetting or "hydrophobic" if these attractions are weak [5]. The static contact angle, created between the droplet's edge and the surface underneath it, determines wettability, or whether a surface is hydrophobic or hydrophilic. The contact angle for hydrophilic surfaces is always less than 90°, while the contact angle for hydrophobic surfaces is always more than 90°.

The general categories of wetting based on contact angle defines spreading when contact angle is 0° and wetting simply when the angle is less than 180°. A more refined categorization system identifies 90° as the dividing angle between wetting and non-wetting conditions (Figure 1.3).
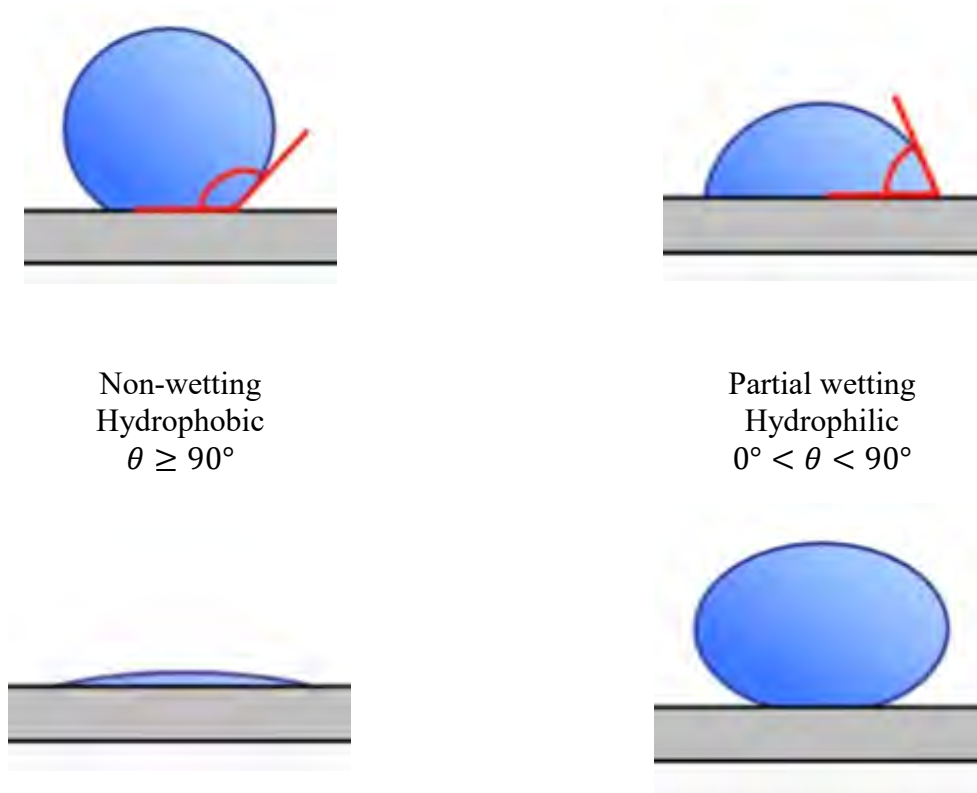
Non-wetting
Hydrophobic
$\theta \geq 90°$

Partial wetting
Hydrophilic
$0° < \theta < 90°$

Figure 1.3: Categorization of wetting depending on contact angle of liquid on a solid surface.

- When contact angles for liquid on a surface are greater or equal to 90°, these are said to be non-wetting conditions. Themore hydrophobic the surface is, the greater the contact angle from 90°. Completely un-wetted refers to a solid in the non-physical condition when contact angle is equal to 180°.

- Partial-wetting circumstances are defined as contact angles for liquid on a surface that are higher than 0°but less than 90°. The lower the contact angle from 90°, the more hydrophilic the surface will be.

- Complete wetting occurs when contact angle is very close to zero or the drop boundary is simply unable to form.

- A surface is considered to be super hydrophobic when liquid creates a contact angle on the surface larger than 150°[6]. Achieving such high contact angles for liquid has just as much to do with the physical structure or texture of the surface as with its chemical nature.

Sometimes identifying contact angles can be a bit more challenging. This is illustrated by the following examples. The contact angle of a liquid forming a bath produced on a submerged flat plate is the first example (Figure 1.4). This is indicative of how the Wilhelmy plate test is carried out. By performing this test, a direct measuring of the liquid surface tension can be done using a platinum plate for which an organic liquid will fully wet the surface that produces a contact angle of zero degrees. This method can also be used with other solid surfaces for which the aim is to measure the contact angle for a liquid of known surface tension. Surface tension forces draw down on the plate when the angle is less than 90°. When the angle is larger than 90°, however, the surface tension forces pull the plate up.
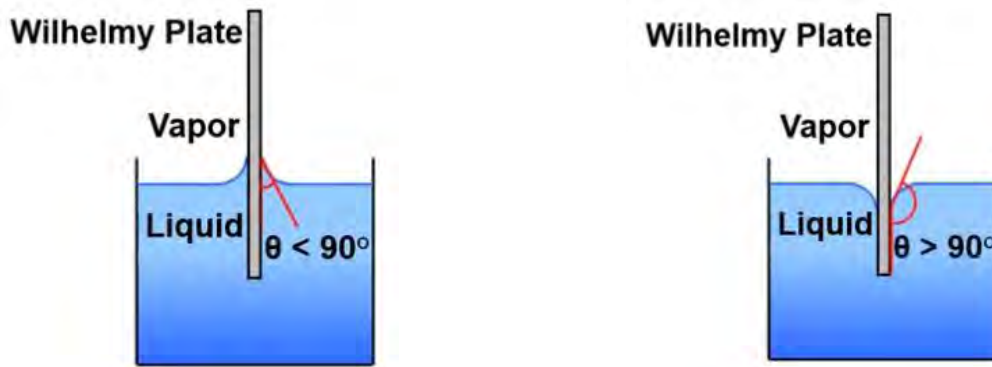
Figure 1.4: Wilhelmy plate test showing relation between surface tension and contact angle of the liquid on the flat plate.

The next example is that of a capillary tube which possesses a narrow diameter, is immerged in a liquid bath. The contact angle is the angle formed between capillary tube wall liquid and the liquid- vapor interface near the contact line. Figure 1.5 shows how the liquid will climb up into the tube when the angle is less than 90°, and when the angle is more than 90°, the liquid within the tube is really sunk below the liquid's surface. This is due to the orientation of the curvature of the meniscus which is fixed by the contact angle. This curvature will determine the direction and magnitude of the capillary forces.
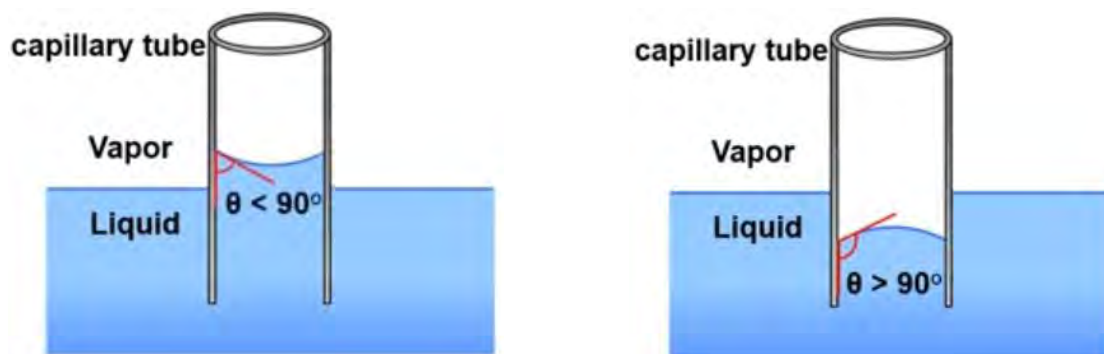
Figure 1.5: Relationship between contact angle and meniscus curvature direction for liquid within capillary tube.

Furthermore, demonstrating the contact angle between a liquid and a stiff rod put on the liquid surface, as well as a spherical particle at the interface between two immiscible liquids (lack of vapor phase) are also some complex cases.

1.3.1 Young's Equation

To understand how contact angle is related to the surface tensions at a solid surface, it must be understood what is occurring at the three-phase contact line. We know from previous section that surface tension acts parallel to an interface and perpendicular to its boundary. For a liquid drop at a solid surface, the boundary is the wetting or contact line where three interfaces – liquid-vapor, solid-vapor and solid-liquid interfaces, all converge and apply tension, which results in a balancing of forces and the resulting contact angle (Figure 1.6). In other words, the observed angle results from mechanical equilibrium in which the resulting forces on the contact line are balanced.
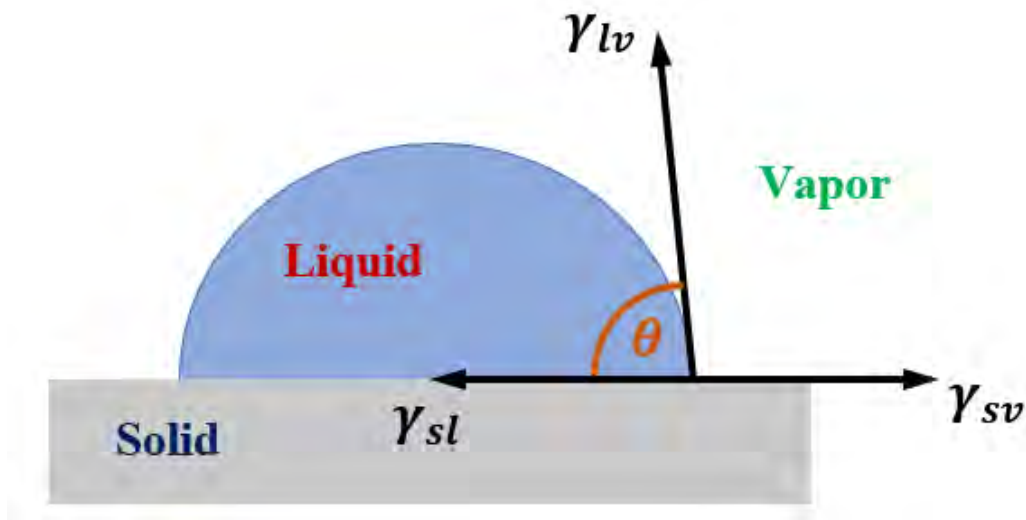
Figure 1.6: Interfacial tension forces acting on the contact line resulting Young's contact angle for a liquid droplet on a smooth solid substrate.

A horizontal force balance produces a relationship between the contact angle (θ), liquid-vapor surface tension (γ_{lv}), solid-vapor surface tension (γ_{sv}) and solid-liquid interfacial tension (γ_{sl}). Here, this angle 'θ' is known as Young or equilibrium contact angle and expressed as 'θ_Y'.

$$\cos \theta_Y = \frac{\gamma_{sv} - \gamma_{sl}}{\gamma_{lv}} \tag{1.8}$$

This equation developed in 1805 is attributed to Thomas Young.By solving Young's equation,we can isolate the cosine of the contact angle. If $\gamma_{sv} < \gamma_{sl}$, the $\cos \theta_Y$ will be negative, and 'θ_Y' is greater than 90°. But, if $\gamma_{sv} > \gamma_{sl}$, the $\cos \theta_Y$ will be positive, and 'θ_Y' is less than 90°.

This equation has been used without much thought over the past two centuries, but it has also been the subject of considerable debate in the area of wetting. Two issues have sparked these controversies. To begin, the equation relates surface tensions and is derived from mechanical equilibrium at the contact line, not from the system's thermodynamic equilibrium. As a result, its incorporation into thermodynamic connections is tenuous.The second point to consider is that, in addition to the horizontal force balance, the vertical force balance must be taken into account, i.e., the liquid-vapor surface exerts a vertical force on the solid surface, lifting it slightly. Because the extent of the deformation is determined by the solid's mechanical characteristics, the produced wetting ridge is often modest and might be overlooked. However, it might be rather considerable for some materials which complicates the force balance.

1.3.2 Factors Influencing Contact Angle

There are many factors that affect contact angle and wettability of solids which includes surface roughness, presence of functional groups on solid surface, impurities present on solid surface and the liquid, porosity, and the surface energy.

We all are aware of numerous applications of polymers. The poor wettability of these polymers makes product design difficult. To achieve the desired result, the surfaces of polymeric material are treated with various techniques such as corona, plasma, and ozone treatment, among others, which modify the surface energy of the polymeric surface by depositing different functional groups on the surface. Polyethylene (PE) has a very low surface energy and is particularly hydrophobic in nature owing to hydrophobic methylene groups. Corona treatment oxidizes it and deposits polar groups on its surface, increasing surface energy. The presence of carbonyl, alcoholic, acidic, and other oxygen-containing groups alters the wetting characteristics of PE by polar liquids such as water substantially. Similarly, corona or plasma treatment with fluorinated monomers may increase the water repellent qualities of cotton polyester fabric. Fluorination is a typical approach for increasing a substrate's hydrophobicity. Many polymers, such as polyethylene (PE) and polypropylene (PP), have insufficient absolute surface energy to interact with certain liquids, such as UV ink, coatings, and UV glue. The surface energy of the substrate must surpass the surface tension of the liquid by 2-10 mN/m in order for a suitable bond to form between the liquid and the substrate.

Moreover, the relationship between contact angle and surface energy or surface tension is very important because of a wide range of applications' reliance on it. To spread ink over the paper, for example, the surface energy of the paper must be powerful enough to overcome the surface tension of the ink. In this way, paint and coatings are also an excellent example. When dealing with any polymer, if the surface energy of the material is low, the coating will not flow effectively, resulting in pinholes, gaps, and air bubbles. Paint, ink, and coatings may blink and be difficult to manage if the surface energy of the substance is too high. As a result, the liquid's surface tension and the material's surface energy must be matched for the application. But, in general, if the surface energy of the surface is greater than the surface tension of the liquid molecule, the surface energy of the surface triumphs over the surface tension, causing liquid to spread across the solid surface, i.e., the higher the surface energy, the lower the contact angle, and the greater the wettability. If the substrate's surface energy is lower than the liquid's surface tension, the interaction between the two will be insufficient, and the liquid will not spread over the surface due to its high contact angle.

Surface contaminants or cleanliness are another aspect that influences contact angle and wettability. The contact angle is a common technique for determining surface contaminants or cleanliness. Any contaminant on the surface hinders wetting and increases the contact angle. The contact angle will be lower and wetting will be greater for a clean and free of impurities and contaminants surface. This approach is particularly valuable in semiconductor manufacture, where the contact angle is routinely employed to evaluate the wettability of silicon wafers in order to assess the success of the manufacturing process and surface changes.

Porosity is another important factor. Pores on solid surfaces behave as microscopic capillaries, allowing liquid to collect on the surface. However, the intermolecular force between the liquid and the substrate, as well as the cohesive force inside the liquid, determine whether the liquid will spread over the surface or sit as a droplet. The liquid may spread across the surface if the intermolecular interactions between the liquid and the solid surface are greater than the cohesive intermolecular forces inside the liquid. Because of the intricate structure and varying shapes and sizes of holes, measuring contact angles on porous substrates is very difficult, which have been observed in Figure 1.5.

However, chemical coatings are prone to wear owing to viscous forces, hence physical texturing is recommended over chemical approaches. Because they promote hydrophobicity, roughening the surface using micro-posts and microgrooves is one of several ways for texturing a surface, as shown in Figure 1.7, which will be broadly discussed on next section.
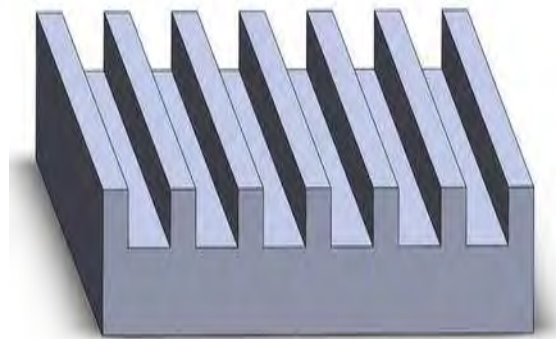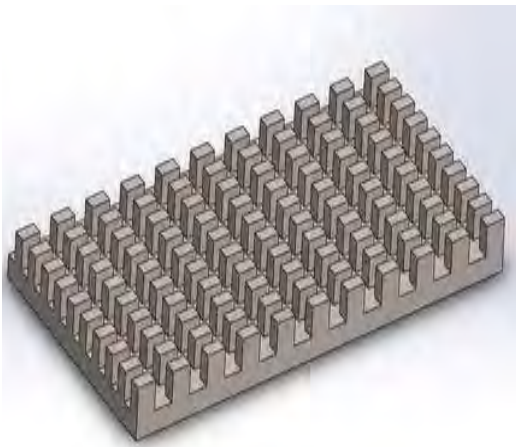
Figure 1.7: Different rough surfaces with surface modification: (a) square micro-pillar array on solid substrate and (b) parallel rectangular micro-grooved surface.

1.4 Wetting on Rough Surfaces

Previously, wetting on ideal surfaces, which are uniformly smooth solid, were only considered. However, in reality, actual surfaces are not completely smooth (Figure 1.8 (b)). Roughness or surface texture has a significant influence on the contact angle of a liquid droplet in equilibrium on a solid. The equilibrium configuration for rough or textured surfaces is established by a surface energy balance that takes into consideration the substrate's topography.

(a) (b)
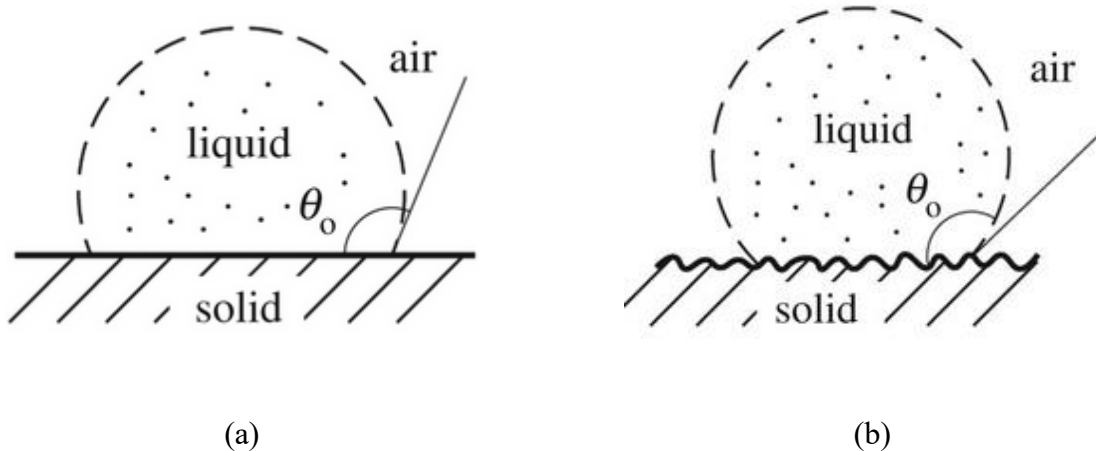
Figure 1.8:A liquid droplet placed on (a) smooth ideal surface and (b) realistic rough surface [7]

1.4.1 Wenzel State and Cassie-Baxter State of Wetting

Wetting conditions on a rough surface is usually defined in terms of two wetting states, namely "Wenzel state or non-composite state" and "Cassie-Baxter state or composite state".

The wetting situation in which the liquid dips into the cavity imprinted on the surface, making total contact with the solid (that means no vapor or air is trapped between liquid and solid) and forming a greater liquid-solid contact surface area than the apparent contact surface is known as the "Wenzel state" or "non-composite wetting state". Whereas, when a liquid displays a stable

condition on a composite surface made up of solid and air, the "Cassie-Baxter wetting state" or "composite state" is generated. The liquid droplet does not slide down into the surface cavity under this wetting situation, resulting in a smaller solid-liquid surface area than the apparent one. Both of these states are distinguished by certain wetting characteristics. Wenzel's model, which was introduced in 1936, is based on the subtle observation that surface tension acts on the projected area, while the solid-vapor and solid-liquid components act on the contour of the area [8]. This observation allows us to modify Young's equation as shown here:

$$\cos \theta_W = r \left(\frac{\gamma_{sv} - \gamma_{sl}}{\gamma_{lv}} \right) \tag{1.9}$$

<div align="center">(a)   (b)   (c)</div>
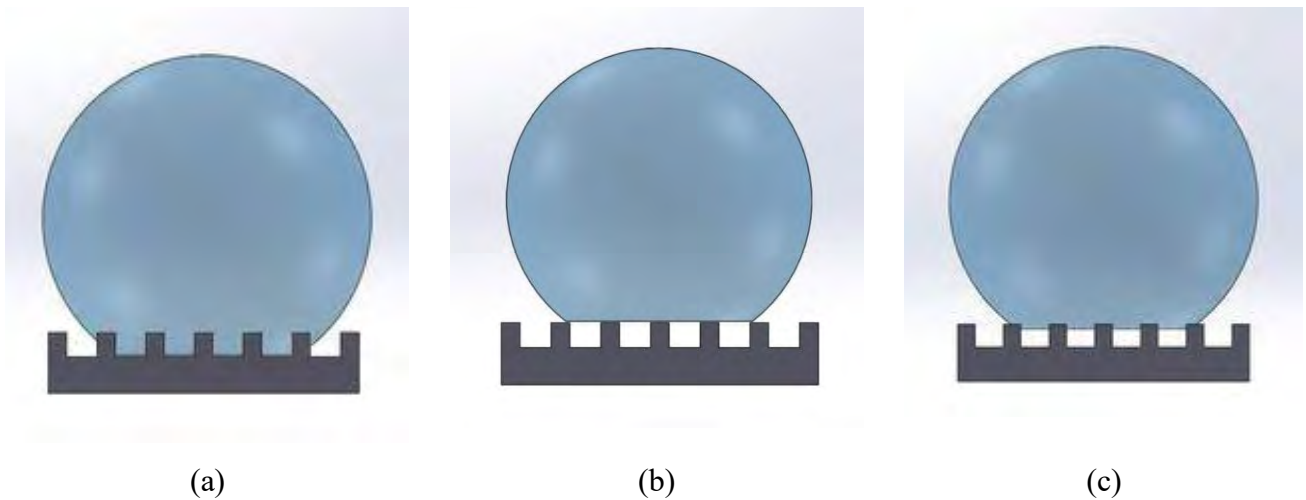
Figure 1.9: Different types of wetting states for a liquid droplet sitting on a rough surface - (a) Wenzel or non-composite state; (b) Cassie-Baxter or composite state and (c) Special type of composite or Cassie-Baxter state.

Where, 'r' is the roughness factor of the surface, which is defined as the ratio of the contour surface area to the projected surface area. Surface roughness factor, 'r' is always greater or equal than unity. It's equal to 1 for a perfectly smooth surface.

In 1944, Cassie and Baxter published their expression for wetting state, which was obtained by contemplating water spreading across a grid of cylindrical threads [9]. The following equation is

generated by combining the formula for the change in free energy associated with this process with Young's equation:

$$\cos \theta_{CB} = f\left[\left(\frac{\gamma_{sv} - \gamma_{sl}}{\gamma_{lv}}\right) + 1\right] - 1 \qquad (1.10)$$

Here, 'f' is the Cassie roughness factor which represents the fractional contact area between the water and the solid surface. For a perfectly smooth surface, 'f' will be equal to 1. And under these conditions Cassie-Baxter equation reduces to Young's equation.

Furthermore, a unique sort of composite wetting condition has been identified, in which liquid enters the cavities to some degree but does not reach the bottom of the asperity (Figure 1.9 (c)). As a result, there is still a space between the droplet's base and the cavity's bottom. This intermediate wetting state is also known as Cassie-Baxter or composite state [10, 11].

However, there have been several reported studies that point out the false premises behind the derivations of both Wenzel and Cassie-Baxter equations [12-15]. The derivation of the Cassie-Baxter equation is based on energy changes associated with liquid spreading across a rough surface, which is a source of contention. The energetics at the contact line, rather than the region under the drop, are said to determine the contact angle. The objections of the Wenzel model are more ambiguous, and they seem to center on the difficulties of attaining equilibrium contact angles. These models supplied a critical theoretical framework for wetting of rough surfaces and are accurate in forecasting general wetting patterns, despite the apparent problems that also exist for Young's equation. When Young's equation is included, these rough surface equations become more user-friendly, with the caveat that this Young's equation only applies to perfect surfaces. Substituting this relation into both Wenzel (Equation 1.9) and Cassie-Baxter (Equation 1.10) models, relationships between measured angles on rough surfaces and the angles for ideal surfaces is obtained:

$$\cos \theta_W = r \cos \theta_Y \qquad (1.11)$$

15

$$\cos\theta_{CB} = f\cos\theta_Y + f - 1 \tag{1.12}$$

Now, some general trends for the wetting of rough surfaces by water, for Wenzel and Cassie-Baxter states, is reviewed (Figure 1.10). In case of Wenzel wetting and for a droplet of water placed on a hydrophobic surface (i.e., intrinsic contact angle is greater than 90°), if surface roughness factor (r) increases, contact angle (θ) also increases. However, when a water droplet is sitting on a hydrophilic surface (i.e., intrinsic contact angle is less than 90°) and surface roughness factor (r) increases, contact angle (θ) decreases. It revealsan important parameter of droplet motion called contact angle hysteresis (CAH). If a droplet's volume is progressively raised, the three-phase contact line will initially stay static in its original position, but the contact angle will grow. Adding additional liquid to the droplet will eventually cause the three-phase contact line to alter its location. The advancing contact angle (θ_A) is the contact angle generated at this point (Figure 1.11 (a)). Similarly, when the droplet's volume decreases, the contact angle decreases as well, despite the three-phase contact line being static. The receding contact angle (θ_R) is the angle produced right before the contact line moves position owing to the volume drop (Figure 1.11 (b)). Contact angle hysteresis (CAH) is the difference between an advancing contact angle (θ_A) and a receding contact angle (θ_R) [16]. CAH can be observed by placing a drop on a surface and tilting it. A droplet must both advance (on the downhill side or front end of the droplet) and recede (on the uphill side or at back end of the droplet) in order to travel on a slanted surface.Hence, the front end of the droplet will make an advancing angle and the rear end of the droplet will form a receding angle. CAH evaluates the liquid's mobility on the solid surface, while CA measures the liquid's affinity for the solid surface.
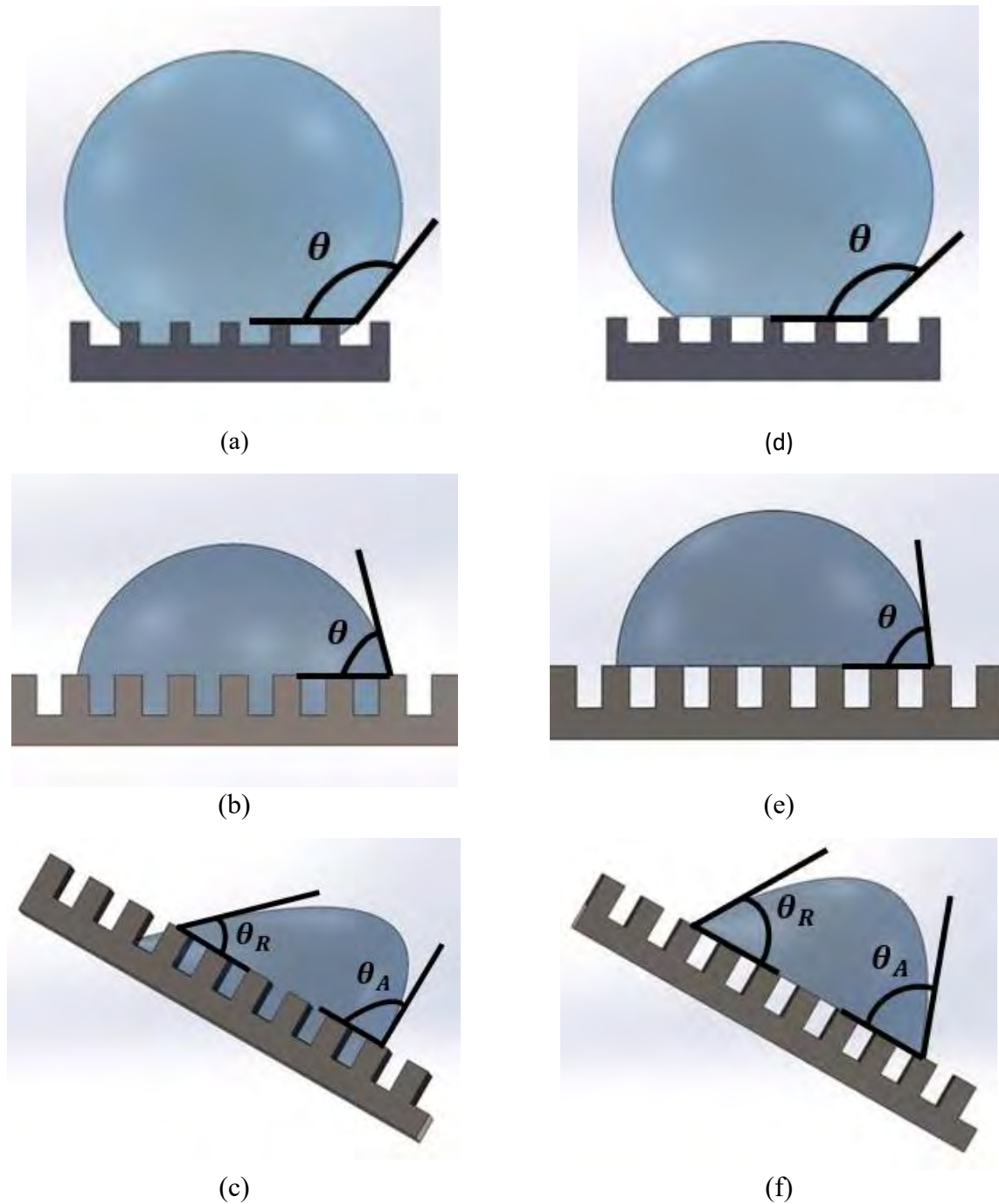
Figure 1.10: Two main wetting states for different types of surfaces with mobility of the droplet. Wenzel wetting for a liquid droplet - (a) on hydrophobic surface, (b) on hydrophilic surface, (c) showing contact angle hysteresis (CAH) for sliding motion; Cassie-Baxter wetting for a liquid droplet - (d) on hydrophobic surface, (e) on hydrophilic surface, (f) showing contact angle hysteresis (CAH) for sliding motion.
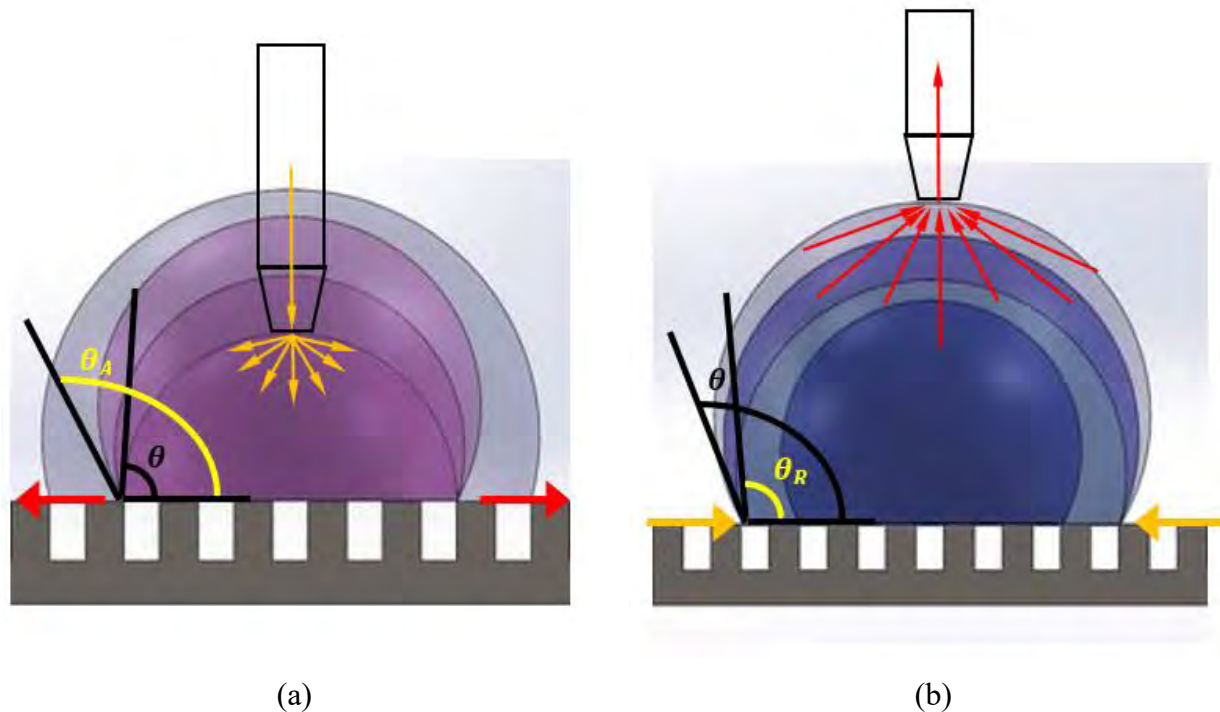
Figure 1.11: Cassie liquid droplet showing - (a) advancing contact angle (θ_A) while adding liquid to the droplet and (b) receding contact angle (θ_R) while taking away the liquid from the droplet.

Because of its slippery nature, a liquid droplet on a solid hydrophobic surface with Cassie-Baxter wetting qualities has the least resistance to being attached to the surface. As a result, the droplet will travel more easily. That is why, the term 'slippery' surfaces refer to hydrophobic surfaces with Cassie-Baxter wetting. On contrary, Wenzel wetting properties on hydrophobic surface makes it difficult to move on the surface. The liquid in this surface seeks to attach to the solid. In this situation, there was more wetting of the surface. So, this type of surface is called as 'sticky' surface.

From thermodynamic point of view, Gibbs free energy curve demonstrates multiple minimum energy minima points for a droplet on rough surfaces, providing the proof of contact angle hysteresis, which is different from ideal surface (Figure 1.12) [17]. In case of droplet residing on an ideal surface, this curve has only single minimum energy point. Despite the fact that a real surface might have various metastable apparent contact angles, the system eventually achieves the global energy minimum, which corresponds to the most stable state.
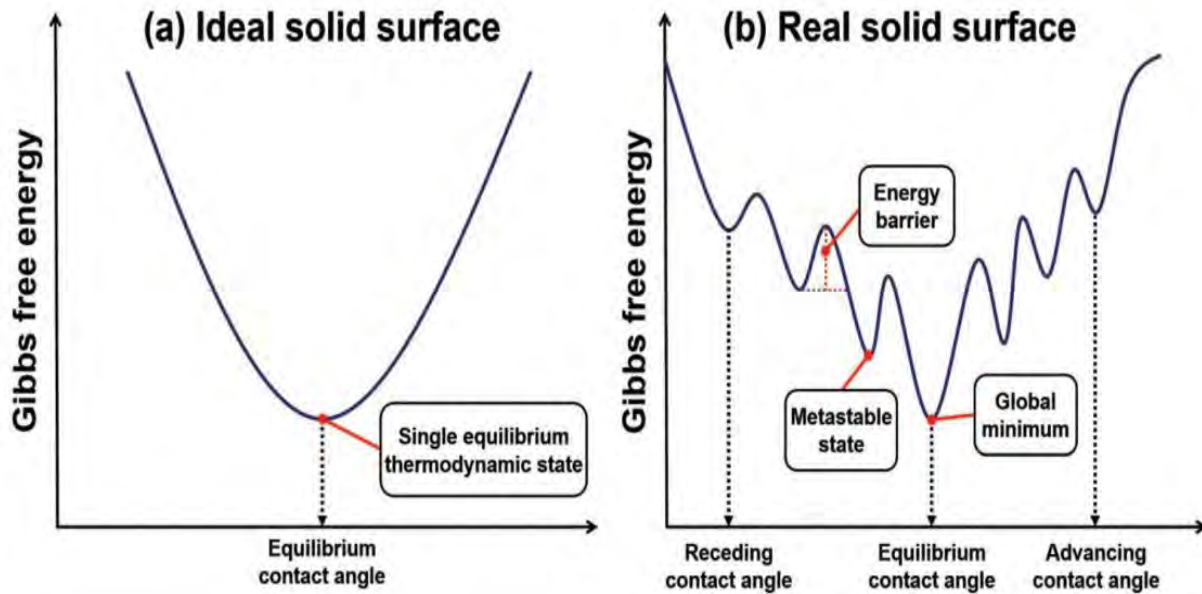
Figure 1.12: Gibbs free energy curve for a liquid droplet placed on (a) an ideal solid surface and (b) a real rough solid surface [18].

Thus, for Wenzel wetting state, when 'r' grows, the disparity between θ_A and θ_R is increased. As a result, contact angle rises in hydrophobic surfaces as roughness increases, whereas contact angle reduces in hydrophilic surfaces as surface roughness factor increases. And as the roughness of the surface rises, so does contact angle hysteresis. Now, in case of Cassie-Baxter wetting state, in which water droplet is balanced on surface roughness, if the contact between water and solid surface narrows, contact angle increases. So, when the water droplet is placed on a hydrophilic surface and contact between surface and liquid is reduced, i.e., solid fraction area with liquid in contact (f) is decreased, it is found that as with the hydrophobic surface, contact angle increases. Now, when it comes to contact angle hysteresis, after the reduction of contact between solid surface and liquid, there is much less adhesion between that surface and the contact angle hysteresis actually decreases.

1.5 Anisotropic Wetting

The form of a droplet may vary greatly as a result of various surface alterations. "Isotropic wetting", which implies the condition of equal apparent contact angle along the three-phase contact line, results in the typical spherical cap worn by droplets in equilibrium, which means that the direction of vision has no bearing on the contact angle. Unless the spreading of the contact line is confined to any direction, pillar-like roughness characteristics generally result in isotropic wetting. There is, however, another kind of droplet equilibrium condition in which the contact angle along the triple contact line is not uniform, i.e., apparent contact angle is dependent on the direction of the view. This type of wetting is referred as "anisotropic wetting". It describes the situation in which a droplet has distinct contact angles from different orientations. Anisotropic wetting states, in which liquid spreads unidirectionally on solid surfaces, are common on micro-grooved or chemically striped surfaces. Static qualities (different static CAs in various directions) and dynamic features (different sliding angles and directional movement) are both present in anisotropic wetting processes. A stationary droplet on a solid surface is usually exposed to external forces that are counterbalanced. Anisotropic wetting happens when the external forces are imbalanced, which implies the driving force is big enough to overcome the resistance. Liquid movement is hampered by a resistance force, F_R. Contact angle hysteresis causes the resistance force, which may be characterized as:

$$F_R \sim \pi R \gamma (\cos \theta_R - \cos \theta_A) \qquad (1.13)$$

Where, R is the droplet radius, γ denotes liquid's surface tension, θ_R and θ_A depicts advancing and receding contact angle respectively. As a result, reduced contact angle hysteresis (CAH) promotes droplet directional mobility.

Anisotropic wetting is caused by both sudden and ongoing changes in chemical or structural characteristics. The causes of these varied anisotropic wetting behaviors may be divided into two categories: non-uniform surface wettability and asymmetrical surface geometric forms. To demonstrate the anisotropic wetting behavior of a droplet on rough surfaces, two kinds of views are often employed. The first is an orthogonal view, which is in the grooves' perpendicular direction, and the second is a parallel view, which is in the grooves' parallel or along the grooves' direction. The angle is called "orthogonal or perpendicular contact angle (θ_o)" when it

is viewed from the orthogonal direction, whereas "parallel contact angle (θ_p)" is foundwhen formed angle between the liquid and the surface viewed from the parallel or side view. Both isotropic and anisotropic wetting conditions are illustrated in Figure 1.13.
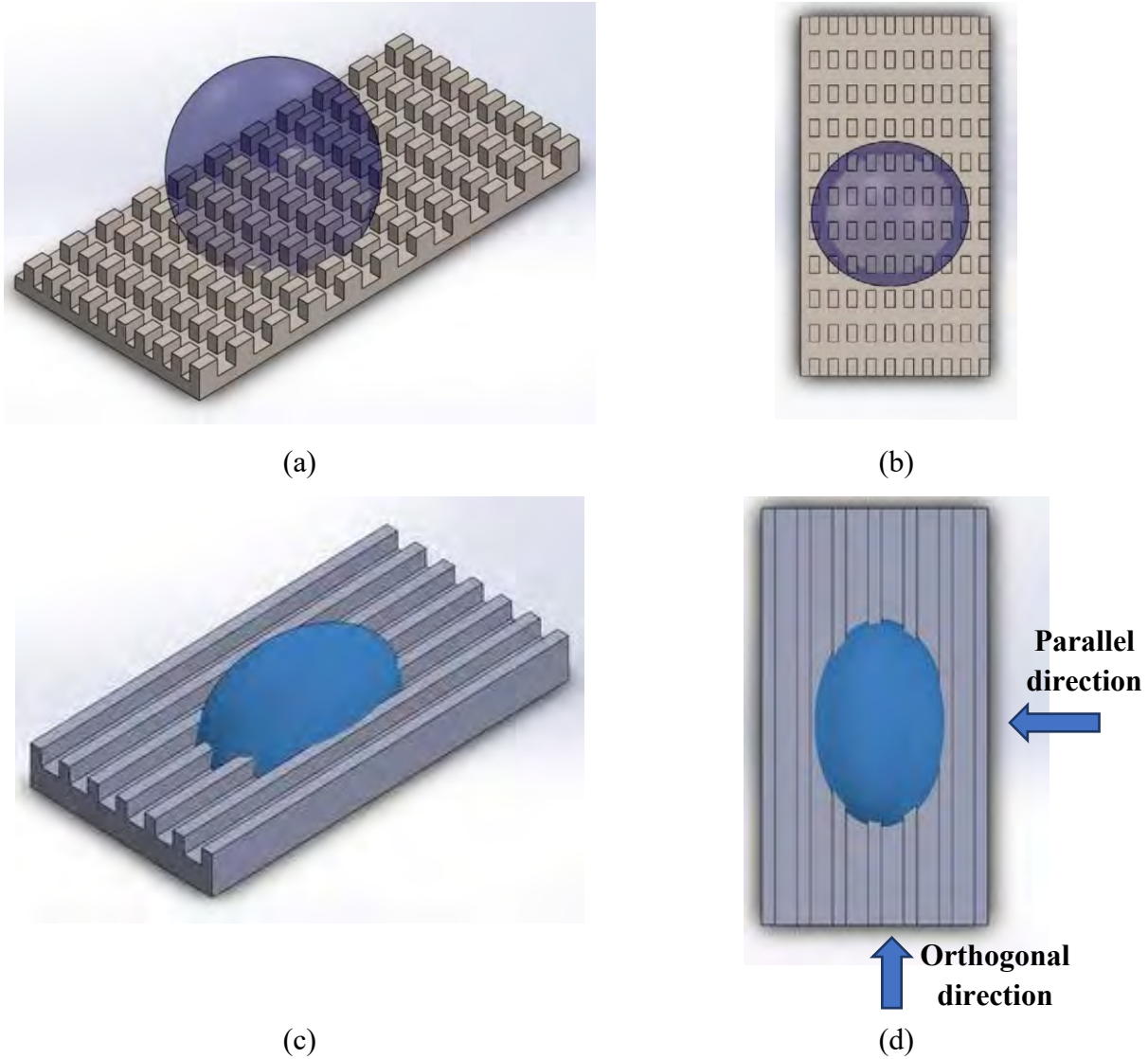
Figure 1.13: (a) 3-D view and (b) top view of a spherical base of liquid droplet on square micro-pillared surface showing isotropic wetting; (c) 3-D view and (d) top view of anisotropic wetting demonstration for a liquid droplet on parallel micro-grooved surface with orthogonal and parallel view directions.

Droplets on chemically heterogeneous surfaces have an extended morphology with varied water contact angles in different directions, resulting in anisotropic wetting. Due to the existence of a surface energy differential on the solid surface, droplets tend to flow from a lower to a higher

surface energy side on gradient chemical heterogeneous surfaces.Moreover,the contact line is pinned at the edge of the pillar edges when a droplet encounters a sudden change in physical morphology on a micro-grooved surface, and the contact line discontinuities generate anisotropic wetting behavior, which might be represented by the Gibbs inequality effect. The contact line encounters a periodic shift in perceived surface energy as it goes perpendicular to the pillars or grooves due to the micro-grooved structures. The contact line is stuck at the edge of the pillar due to the increase in surface energy until the pillars can be bridged. As a result, compared to spreading along the grooves direction or parallel direction, a substantially greater energy barrier must be overcome. That is why, a liquid droplet spreading preferred along the grooves, resulting in an extended shape with a substantial variance in terms of the contact angle, depending on the direction of the droplet observation, in case of tailoring a surface with parallel microgrooves. Also, chemically striped surfaces show anisotropic behavior due to the similar reasons as it is found in micro-grooved surfaces.

In other words, anisotropic wetting phenomena of liquids are caused by surfaces having asymmetric energy barriers in opposite directions. Furthermore, by integrating structural and chemical anisotropy, new anisotropic wetting phenomena might be achieved. The driving forces for anisotropic wetting of droplets on micro-/nanostructures are usually made up of many forces acting in distinct directions.

Anisotropic wettability has been reported on a number of biological surfaces in nature. Rice leaves, for instance, roll in an anisotropic manner. Water droplets are more likely to move in a path parallel to the leaf edge than in a perpendicular one. On superhydrophobic butterfly wings, directed water droplet attachment has been discovered. On butterfly wings, water droplets move readily in a radial outward direction, but they are trapped in the opposite direction.Furthermore, the distinctive fan-shaped micro-nanostructures of goose feathers were discovered to have directional adhesion phenomena. In addition, due to the presence of complex micro-nanostructures on natural cactus spines, water droplets flow reliably in a specified direction. Also, directional water transportation system has been observed on spider silks.

Due to its unique wetting capabilities, which include directing liquid to flow in one direction while pinning in all others, this directional anisotropic wetting behavior is of great scientific interest. Many thermal management applications rely on the drainage of frost melt water. Defrost cycles, for example, handle the inevitable deposit of frost on the air-side surface of the heat exchanger in domestic heat pumping and refrigeration systems. Defrosting is required because unchecked buildup of a frost layer causes severe machine performance deteriorationHowever, defrosting uses more energy, resulting in less efficientfunctioning.Defrosting should be done as rapidly as possible, using as little energy as feasible, and removing as much water as possible. As a result, in these and many other applications, it is critical to drain the frost melt water off the surface. In such instances, developing a surface with reduced frost melt water retention qualitiesis critical for which unidirectional surface wetting is required.Furthermore,controlled wettability in a specific route and surfacemodification are required for microfluidic devices. Anisotropic wetting surfaces, which enable precise control over the wetting or spreading direction of liquids, improve both open and enclosed microfluidics. Using anisotropic wetting surfaces in microfluidics to regulate the flow behavior of microfluids has emerged as a possible alternative to traditional microvalves that need external control elements, lowering preparation costs, increasing analysis efficiency, andconsiderably simplifying microfluidic system design. Many artificial materials with directional liquid movement or transportation capabilities were developed and used for fog/water collecting, inspired by natural spider silks, desert beetles, and cactus spines. Moreover, because of pressing environmental and economic concerns, oil-water separation technology has become an important study area in environmental protection and cost-cutting in which employing anisotropic micro or nano structured materials have been proved effective and desirable. Also, as the water droplet rolls off the surface,it cleans the surface along with that.

There has already been a slew of experimental andnumerical studies published in various journals, articles, books, etc., reflecting scholarlycommunity's ongoing as well as rising interest in this subject area, which has been discussed elaboratively in Section 1.6.7.

1.6 Review of the Literature

1.6.1 Studies on Natural Surfaces

For more than quarter of a century, wettability of chemically varied and abrasive surfaces has been studied in both nature and artificial settings. Long before the fabricated and altered surfaces, mother nature has shown its inherent properties to solid-liquid interactions. The typical form of wetting state has been observed in "Lotus leaf". This special leaf has a slick surface, which it takes use of by allowing water droplets to roll off the surface, cleaning it of any contaminants they come across. The roughness of the leaf surface is caused by papillose epidermal cells, which create asperities or papillae. Barthlott and Neinhuis, twoGerman botanists, coined the term "Lotus-effect" to describe the Lotus leaf's combination of self-cleaning and high water-repellency properties [19]. Following that, further investigation and study were carried out in order to get a better understanding of the surface chemistry and composition for future non-wettability applications. Because air bubbles fill the troughs of the hierarchical structure underneath the droplet, water droplets on these lotus leaves surfaces easily perch on the apex of nanostructures. As a result, these leaves have a high level of superhydrophobicity [20]. Among all other plant leaves, because of its contact angle of waterlarger than 160° and tilting angle smaller than 5°, lotus leaf always stays clean in filthy-muddy environment. When rain drops hit the surface of lotus leaves, they instantly congeal into sparkling spherical balls and roll away, accumulating dirt and scraps along the way because of its self-cleaning characteristics [21]. Spherical droplet of water cleans the lotus surface by rolling off the lotus leaf because of the higher adhesion between the water droplet and dirt materials than the surface and dust, exhibiting excellent self-cleaning process [22]. Apart from these non-wetting characteristics, lotus leaves can self-heal themselves over a lifetime because of their superhydrophobicity [23].Tulipa, asphodelus, euphorbia,drosera, eucalyptus, iris, and gingko biloba are among the plants having superhydrophobic leaves [19, 24].

It is not only lotus leaves that have superhydrophobicity in nature. This particular wetting property is shared by a number of different plants, animals, and insects. Water-striders are one of those unique products of nature. Cheng illustrated that their resistance to wetting and skating capabilityon the surface of water due to their outstanding adaptable bodily characteristic [25]. Later Anderson examined semi aquatic bugs body structures, especially body hair layers and morphology of spiracles. Fine structure of micro and macro layered hair pile was discovered in

ocean skaters, which prevented them to be wet due to pressure variations [26]. Later, Gao and Jiang created force–displacement curves for a water strider's legs while pushing on the water surface using a high-sensitivity balancing system. And ultimately came to the decision that water-striders legs' unique hierarchical structure with super hydrophobic coatings, which is covered by a high number of aligned microscopic hairs (microsetae) with fine nanogrooves, is more crucial in causing this water resistance [27]. Although the conventional hydrophobic coating offers adequate support for the water strider to float, superhydrophobic coating is required. By injecting a tiny layer of air around the surface, superhydrophobic coating may reduce fluidic drag, allowing the water strider to go quicker on fluid surface, because drag force developed by fluid causes the resistance of solid's relative motion [28].Superhydrophobicity is also seen in the wings of butterflies. The superhydrophobicity of these wings is thought to protect water droplets from clinging to the wing surface and preventing them from sticking together [29]. While these insects employ superhydrophobicity to remove water droplets from their bodies, Nambibian beetles use it for a different purpose: gathering rather than repelling water droplets [30]. To fulfill their water needs in desert settings, water rolled down to their mouth utilizing their superhydrophobic grooved channel, which is around hydrophilic elytrae where water droplets are accumulated from fog or dew.

1.6.2 Studies on HierarchicalFabricated Surfaces

Surface textures with micro and nano hierarchical structures enhance hydrophobicity to superhydrophobicity, which is a common motif in all natural instances. Both a high-water contact angle and a low tilting angle require this dual scale roughness. By integrating hydrophobic chemical composition and geometric variations, different synthetic ways for preparing superhydrophobic surfaces and coatings have been created based on these concepts (Figure 1.14) [31].
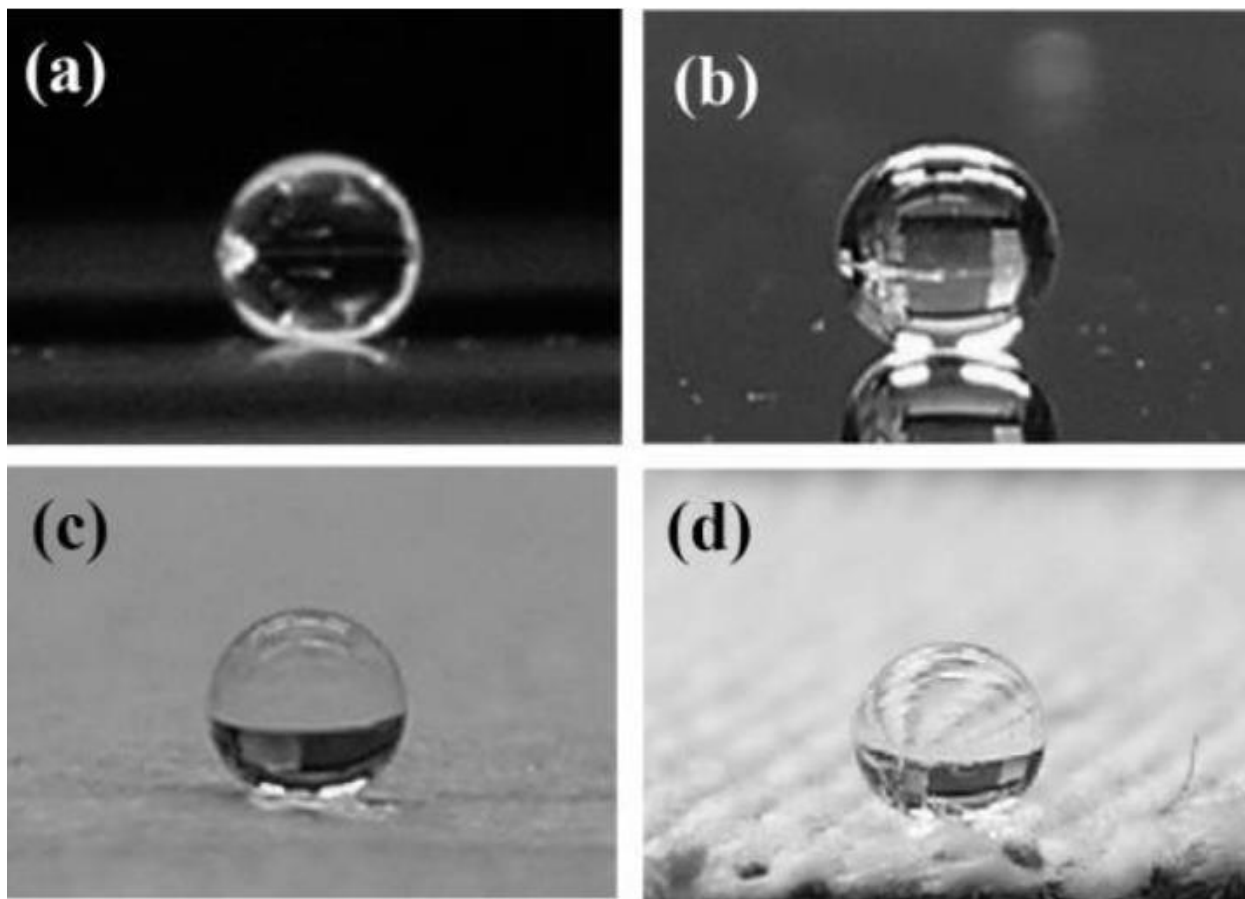
Figure 1.14: Incorporating superhydrophobic coatings on (a) Gold film, (b) Si wafer, (c) Kimwipe, and (d) cotton showingsuperhydrophobicity[31].

Johnson and Dettre constructed a glass substrate with waxes and controlled roughness by heat-treatments in the first systematic research of roughness influence on contact angle hysteresis of water. They discovered that when surface roughness increases, advancing contact angle increases as well, but receding contact angle falls at first but then leaps closer to advancing contact angle value after reaching a critical value of surface roughness. This is referred to as the "Wenzel to Cassie-Baxter wetting transition" [32]. They discovered that the Wenzel wetting was dominant up to a certain roughness factor (~1.7) on sinusoidal surface, which is the ratio of a rough surface's real area to its projected area. However, they found that when the roughness factor surpassed the specific value, the prevailing hydrophobic wetting behaviorexperienced Wenzel to Cassie transition owing to an increment in the fractional area of air at the cavities. After that, more advanced superhydrophobic surfaces were created by covering anodized metal

surfaces with fluorinated silanes and developing fractal architectures of alkyl ketene dimer wax. [33, 34].Since then, scientific articles on man-made techniques for producing superhydrophobic surfaces have flourished. Water contact angles of more than 160° and water slide angles of less than 5° have been observed on hydrophobic polymer Polydimethylsiloxane(PDMS) surfaces treated with laser abrasion [35]. Moreover, superhydrophobic characteristics can be obtained by roughening the surface of hydrophobic hydrocarbon compounds. According to an earlier study of Bartell and Shepard, it was proved that superhydrophobicity could be achieved by producing roughness of paraffin surfaces via cutting [36]. Also, by inducing coatings of polypropylene on the surface suited for superhydrophobicity had been carefully fabricated [37].

1.6.3 Studies on Intrinsically Hydrophobic Surfaces

Many researchers introduced various surface geometry modification like- square and circular micro-pillared surfaces, rectangular micro-grooved surfaces, etc., into intrinsically hydrophobic surfaces to obtain increase hydrophobicity or superhydrophobicity. Bico*et al.* [38] embossed spike and holed patterns on surfaces with a predetermined surface roughness and found excellent agreement between Cassie and Baxter's hypothesis for apparent contact angles. When a little drop of water is dropped on a hydrophobic rough surface with completely non-wetting condition, it seems to be a pearl. However, they only looked at a few structures and did not investigate the phenomena further by altering structural factors. Also, Patankar presented a method for creating a rough superhydrophobic substrate that takes into consideration the various equilibrium droplet forms in order to maximize a droplet's advancing contact angle [39]. He then created a model to optimize the receding contact angle so that hysteresis could be minimized. In the study of Li *et al.*, a 2-dimensional model was used to study the thermodynamics of a trapezoid microtextured superhydrophobic surface in which effects of geometric parameters like height, base angle, base width, base spacing had been observed on equilibrium contact angle and CAH. Some basic concepts for designing the optimum shape of perfect superhydrophobic surfaces are proposed in this study [40]. Micro level hierarchical surface structures stabilize superhydrophobic state by increasing energy difference between Cassie and Wenzel states and greatly reduces the contact area, effectively reducing adhesion between solid and fluid [41]. Dong *et al.* presented a computational technique for calculating

apparent contact angles on heterogeneous rough surfaces with a variety of wettable materials for the dual-scale structures and bases [42]. The Herminghaus technique had been improved using this numerical computation method. They proposed that this model has the potential to become a revolutionary technique to designing heterogeneous superhydrophobic surfaces. Ding *et al.* developed conical structured surfaces which can be used as a template for creating superhydrophobic surfaces with invariant wetting properties [43]. When designing surfaces, they found out that the apex angle of cones and the intrinsic contact angle were the crucial characteristics to consider. Lowering the pitch between the cones improved the surface's resilience, whereas decreasing the apex angle of the cones restrained the Wenzel condition in hydrophobic materials.In a recent study, both nylon taffeta and non-woven templated membranes, intrinsic contact angle of 133.8° and 118.3° respectively, consisting of repeating arrangement of macro-valleys and micro-grooves, resulting in a greater contact between air and the membrane [44].As a result, the contact area between solid membrane and the droplet of water is reduced and made contact angle higher than 150° and tilting angle smaller than 10°, which demonstrated their superhydrophobicity.

1.6.4 Studies on Intrinsically Hydrophilic Surfaces

Although beginning with a hydrophobic surface helps creating superhydrophobicity easier, it is not a must. According to Cassie-Baxter equation, it is also feasible to construct a metastable superhydrophobic condition using a material that has an intrinsic contact angle smaller than 90°, i.e., intrinsically hydrophilic material.One of the precise instances of surface engineering was achieving superhydrophobicity with Si-surfaces with the termination of hydrogen that had an intrinsic contact angle of water about 74° when particular micro-textures consisting of with well-defined overhang structures are produced [45]. Roughening the surface and then applying hydrophobic treatments to change the surface chemistry is a more prevalent approach. Inherently rough surface materials can exhibit superhydrophobic behavior by the application of hydrophobic coatings. Feng experimentally used nanofabrication to change the hydrophilic surface property of poly (vinyl Alcohol) (PVA) and created a superhydrophobic surface with contact angle of water around 172°[46]. According to their findings, owing to the rearrangement of the hydrophobic groups in the PVA molecules in the nano fiber, the surface energy was

decreased, resulting in a hydrophobic behavior. Also, CH_4 atmospheric rf plasma treatment technique was implemented on rough hydrophilic surfaces such as cotton, which resulted in superhydrophobicity [47].Patankardemonstrated that rough hydrophilic surface with asperities can increase the hydrophobicity of the surface by creating larger apparent contact angle of liquid on the surface and reduced hysteresis [48]. This occurred as a result of the dominating pressure force based on ambient value having a lower wetting of the cavities than the surface tension force.Abdelsalam haveproved for regularly structured gold surfaces that apparent contact angle's conversion from 70° (hydrophilic surface) to 130° (hydrophobic surface), if the substrates have holes with a diameter of 400–800 nm [49].By creating double re-entrant aperture in surface micro textures, Domingues*et al.* discovered exceptional hydrophobic behavior for inherently hydrophilic silica surfaces [50].Furthermore, Zhang *et al.* recently showed that without any chemical alterations, T-shape microstructures can elicit superhydrophobic behaviors on hydrophilic surfaces [51]. Electrospinning process has also been proved as one of the straightforward methods for the conversion of intrinsically hydrophilic surface to superhydrophobic surface [52].

1.6.5 Studies on Cassie-Wenzel Wetting Transition

Several researchers have outlined the conditions that must be met for the Cassie or Wenzel wetting transition to occur on rough surfaces.Netz and Andelman provided some general theoretical bases for roughness-induced wetting, where they derived a certain limiting value of surface roughness as well as required relationship among interfacial tension forces among solid, liquid, vapor for wetting transition phenomenon [53].Wetting transitions observed on molecularly rough surfaces due to their stronger liquid-solid interaction than on smooth surfaces [54]. Later, by using a homogenization technique, Alberti and DeSimone studied wetting phenomenon forrough surfaces composed of both hydrophilic and hydrophobic substrates theoretically [55].Dorrer and Rühestudied the metastable Wenzel wetting state to thermodynamically stable Cassie-Baxter state, both experimentally and theoretically [56]. According to their findings, the volume of a liquid droplet dwelling on a surface with four micro-posts steadily rises due to a continuous condensation process, culminating in the Cassie form of droplet. Also, when the accumulating liquid droplet began to travel by overcoming the

energy barriers that had previously held it back. The droplet was able to overcome the pinning strength in each of these wetting transition scenarios. Moreover, they observed that the measured contact angle changed as a consequence of the varied wetting conditions. Jung and Bhushan, in their study on evaporation, found that liquid droplet size was the major factor in the transition from Cassie-Baxter to Wenzel states on patterned Si surfaces with varied geometric changes [57]. They demonstrated that on a pillared surface, droplets bigger than the depth of the asperity facilitated this transition. Decreasing the Si surface's micro-pillar spacing also increased the probability of the droplet being on top of the pillar arrangement without sinking through the gaps between them, retaining the surface's superhydrophobicity for a given volume of droplet. Patankar theorized that the only way to get from Cassie to Wenzel is to overcome the energy barrier between the two states, which was attainable for square-shaped micro pillar surface arrangements owing to lower gravitational potential energy [58]. They also argued that in absence of energy barrier between Cassie and Wenzel states, transition from Cassie to lower energy Wenzel state would always occur which was matched with Marmur's findings [59].Bico*et al.* developed critical intrinsic contact angle to evaluate the favorable wetting states between Wenzel and Cassie using differential energy balance equation [60]. And then later, Milne and Amirfazli defined another equation to find critical intrinsic contact angle relating the area fraction of liquid in contact with both solid and air as well as surface roughness parameters [61].Yao *et al.* investigated the wetting conditions of a hybrid surface made up of micropillars of hydrophilic and hydrophobic materials [62]. They observed dropwise condensation and dropwise-filmwise condensation on the surface, which has never been reported in the literature before, despite previous research on droplet impingement on such a surface indicating better water repelling properties. They had to create a surface energy-based condition to forecast the wetting transition since two forms of condensation resulted in distinct wetting processes. They discovered that the pillar spacing was a key factor in the wetting fluctuation. Gong *et al.* used the Lattice Boltzmann approach to statistically investigate the wetting transition process, and the key causes for this transformation were gravitational forces and the intrinsic contact angle of the patterned surfaces [63].In their analytically built model, Alen *et al.* presented two wetting transition conditions for inherently hydrophilic surfaces [64]. The first requirement was determined by equating the cosine of both Wenzel and Cassie states' apparent contact angles, while the second condition was calculated using surface free energy of both wetting states.

Using both conditions, wetting transition prediction became more transparent than when simply surface roughness was used.In recent years, further experimental work on the wetting transition has been done, including surface topography dependence for this wetting transformation[65]. Recently, Wilke *et al.* developed surfaces roughening with micro re-entrant specifications for introducing the new doorway for thermofluidic systems applications. They demonstrated that even for intrinsically hydrophobic surface made of the material having intrinsic contact angle of 143°, non-wetting features transformed into wetting by making apparent contact angle of 35° for mercury on these rough silicon surfaces [66].

1.6.6 Studies on Wettability Using Thermodynamics

From a thermodynamic standpoint, wetting characteristics such as stability, contact angle, hysteresis, energy, wetting transitions, etc. on various kinds of surfaces have been explored in several literatures. In subsection 1.4.1, it has been already described that in contrast to an ideal surface with a single Gibbs energy minimum, a real surface's Gibbs energy curve has many minima points corresponding to numerous potential metastable equilibrium states, as seen in Figure 1.12 [17, 18]. So, metastable liquid droplets satisfy both the thermodynamic and geometric conditions, resulting in the apparent contact angle's multiplicity. These metastable liquid droplets have to overcome the energy barriers to ultimately reach the most stable state by attaining global energy minimum. Mechanical, thermal, and electrical energy have all been reported as ways to generate the external energy required to initiate the transition between thermodynamic states [67-69]. By undertaking a thorough thermodynamic investigation, Long *et al.* used an analytical model to describe equilibrium contact angle on rough surfaces and classified it into three different types based on a parameter called "surface feature factor" [70]. Li *et al.*took thermodynamic approach for free energy analysis of Cassie and Wenzel systems and discovered that the wetting transition is strongly influenced by the pillar depth to pillar gap ratio rather than ratio of the depth of pillar to width of the pillar [71].According to Chen *et al.*, depending on the liquid droplet volume and pillar number on which they are placed, the droplet will assume an equilibrium form matching to the local energy minimum [72].By fastening the smaller number of pillars on which the droplet resides, makes its contact angle along the grooves lower with the increment of droplet volume. That is why optimum number of pillars for

larger droplet size should be selected to find more spherical shape of the droplet, as wetting across the grooves would be difficult for high energy barrier. Chatain*et al.* examined the form of the liquid droplet as well as its stability based on the energy of the droplet on the rough surfaces by incorporating circular micro posts and holes over the surface [73].Dimensionless number termed as "normalized energy" was employed to determine the droplet size dependency on various types of surfaces. This energy was found constant for a sessile liquid droplet on smooth surface. However, on rough surfaces, this dimensionless number reveals a dependence on droplet volume. Relative stabilities of the drop were investigated by normalized energy as a function of droplet volume on these micropatterned surfaces. From this relation, the normalized energy curves usually offer a minimum matching to the steadywetting configuration, according to their findings. As a result, over a rough surface, the droplet size that gives the lowest normalized energy value corresponds to the most stable Cassie droplet. They also showed that total energy increased gradually with the larger droplet size. From liquid droplet on two micro-pillared surfaces, in which one pillar was made of hydrophilic material and another one consisted of hydrophobic material, Cui et al examined both substrates' free energy and free energy barrier, as well as their apparent contact angle [74]. Wenzel state had been the balanced form of wetting in case of hydrophilic substrate, while hydrophobic substrate exhibited stabile free energy characteristics for the Cassie state. Increment in the pillar heights for hydrophilic materials led to composite states, which demonstrated the unstable condition for the liquid on these surfaces.Pomraksa and Chen found out multiple metastable states of the droplet on cosine-wave like square array patterned rough hydrophobic surface consisting of two different roughness features [75]. The most stable contact angle was defined as that particular contact angle corresponding to the minimum energy among the multiple metastable states. Contact line's shape variation with droplet size had also been discussed. In their other study, they examined droplet's stability on sinusoidal surfaces with multiple roughness and demonstrated that small roughness induced model produced the firm contact angle near to the receding contact angle and it gradually shifted towards the advancing contact angle with surface roughness increment [76]. In order to achieve stable composite wetting, necessity of minimum droplet size on a surface with only circular pillared roughening, had been illustrated for evaporation of droplets by Dubov et al [77]. Guo *et al.* presented a general theory to calculate the threshold pressure for Cassie to Wenzel wetting transition on solid surfaces with porous or

projecting microstructures using an energy method [78]. Later, Anjan *et al.* demonstrated similar type of work for square array micro-pillared rough surfaces to find out the stability along with the energetics and shape of the liquid droplet for different droplet configurations [79]. They also extended their work to determine the stability nature of the droplet as well as apparent contact angle for pillar geometry like width, spacing and structure variation on those rough surfaces.Largest apparent contact angle had been obtained for least solid fraction area at the base of the droplet for equilibrium condition which was consistent with Cassie-Baxter formula. Also, stable form of droplet changed for different pillar width and spacing for similar pillar configurations. Normalized energy value along with stable droplet size had been elevated for higher pillar spacing and lower pillar width from these square pillared surfaces due to the reduced fractional area between solid and liquid. Effect of droplet on stability and energy had shown similar trend like Chatain*et al.* [73]. However, for larger droplet volume superhydrophobic nature had been induced for these rough surfaces. They concluded the fact that in order to achieve the most stable balance, a larger droplet needed a greater number of pillars underneath it. Anjan *et al.* also exhibited this energetics and wetting stability of liquid droplet on parallel micro-grooved surfaces [80]. For higher number of pillared surfaces, normalized energy values were lower than those for designs with smaller number pillars for a larger volume of liquid droplet, resulted in requiring a higher pillar number for larger droplet size. Furthermore,He *et al.* numerically studied this energetics and stability of liquid droplet on chemically striped heterogeneous surface utilizing dimensionless energy method and also discovered that minimum dimensionless energy value for the stable droplet shape on these surfaces [81]. The stability and formation of droplets developing across a vast number of V-grooves were studied quantitatively by Semprebon*et al.* [82]. In a recent study on energetics of liquid droplets placed on micro-grooved surface, Ding *et al.* proved that a droplet's normalized free energy on micro-grooved surfaces was not constant, and it dropped as the ridge width increased [83]. The droplet wetting form characteristics were associated with the normalized free energy.

1.6.7 Studies on Anisotropic Wetting

For highly dynamic application domains including anti-fogging, anti-fouling, and biomedical devices, directional wetting is acrucial and essential feature of the surface [84]. Anisotropic surface texturing may be used to produce directional wettability, or the changing of wetting qualities based on the surface orientation. Many studies have been conducted on directional wettability in order to incorporate anisotropic liquid behavior on various types of surfaces. Earlier in 1950, Bikerman observed anisotropic behavior of liquid on parallel grooved surface, where droplet was stretched along the direction of the grooves [85]. Good *et al.* also showed anisotropic wetting of liquid onTeflon FEP polymeric film [86]. According to their results, the anisotropic force field of the orientated polymer molecules is most likely to blame for the anisotropy of the measured contact angle.In 1981, Hitchcock *et al.* developed a relation between surface texture parameter with anisotropy [87]. This parameter was the ratio of average amplitude to the average wavelength of the surface features. With the increment of this ratio, the isotropic equilibrium condition gradually switched to the anisotropic wetting mode on that rough surface by spreading the liquid more along the grain than across the grain of the surface. Later in 1986,similar type of anisotropic behavior also exhibited by introducing more roughness on the SiO_2 substrate [88].Schonhorn did notfully support the reason 'anisotropic force field' given behind the anisotropic behavior by Good *et al.* [86], rather they proposed to use the surface roughness as the criteria to interpret the stretched liquid droplets [89]. Effect of various liquid on anisotropic behavior had also been demonstrated in their work. By utilizing the roughness, contact angles parallel and perpendicular to the grooves, and the drop form, the equilibrium contact angles on a flat surface had been computed, which provided better agreement with experimental findings. In 1989, Sung *et al.* proved that surface roughness and topology are the prime responsible parameters for anisotropic wetting behavior rather than molecular orientation by experimental observation of wetting characteristics on three types of polymers [90]. By molding tetramethylorthosilicate in shallow holed, striped, and spiked patterns on a silicon wafer to form a superhydrophobic surface, Bico*et al.* observed isotropic wetting arrangement on spiky and holed surfaces with larger apparent contact angle, while their striped surface was anisotropic, since apparent contact angles observed from orthogonal and parallel to the directions of the stripes were different [38]. Chen *et al.* investigated and described anisotropic wetting of an inherently hydrophobic PDMS surface adjusted by parallel microgrooves, as well as experimentally demonstrating the substrate's superhydrophobicity

34

[72]. They developed a numerical model for the ultimate elongated liquid droplet form, assuming both elliptical and cubic contact lines. The cubic contact line assumption performed better than the elliptical contact line assumption in terms of matching experimentally observed outcomes. Because the droplet was trapped on the pillar edge and so stretched along the groove and compressed perpendicular to the groove, the number of pillars it rested on, dictated the equilibrium form it acquired. They also saw the estimated contact line created by the spherical droplet on the same substrate, which was an average of parallel and perpendicular lines, and measured the length of the contact line both parallel and perpendicular to the groove direction. The apparent contact angle estimated using the Cassie formula for a spherical drop shape was also between the parallel and perpendicular contact angles of the elongated droplet as observed experimentally. Both parallel and perpendicular contact angles were greater than the intrinsic contact angle of the base surface, suggesting higher hydrophobicity. Anisotropic behavior had been found by Feng *et al.* in a natural product called 'rice leaf', on which droplet can move in a particular direction by maintaining anisotropic de-wetting properties because of the presence of micropapillae positioning on that particular surface [91]. Afterthat, they mimicked this process by incorporating carbon nanotubes alignment on a surface. Similar kind of unidirectional movement of the droplet had been found for this surface, opening the doorway for future designing of controllable wettability.Sommers *et al.* fabricated the parallel grooves on the aluminum plate with proper UV exposure and etching to observe the effect of the tunable anisotropic wetting and effect of these roughness of the surface for wetting qualities [92]. At horizontal condition, 54° of degree of anisotropy had been found, as along the grooves the contact angle was 75° and across the grooves it become 129°. Due to the lower energy barrier and continuity of the three-phase contact line along the grooves, droplet can spread parallel to the grooves direction easily and made the contact angle smaller in this direction. However, with the presence of grooves, contact line was pinned at the edge of the grooves and needed sufficiently larger amount of energy to surpass the increased surface energy to cross the grooves and move to the next pillar edge, which increased observed contact angle from the orthogonal direction of the grooves. In the sinusoidal rough surfaces fabricated by Chung *et al.*, three-phase contact line structure was the dominant factor rather than increasing surface roughness for droplet wetting anisotropy [93]. Pinning of the contact line, whose motion displayed periodic stick-slip behavior, accounted for the larger orthogonal contact angle. And,because there were

no obstructions in the way of the contact line causing pinning, it expanded parallel to the grooves owing to preferred stretching along the grooves, resulting in a reduced contact angle in parallel directions. They also observed higher perpendicular contact angle, for increasing height of sinusoidal grooves due to higher energy barriers. Moreover, Zhao *et al.* showed groove height dependency on the anisotropic wetting on sin wave like grooved surfaces [94]. Degree of anisotropy ($\Delta\theta = \theta_o - \theta_p$) which is nothing but the difference between contact angles measured from parallel and perpendicular to the groove's directions, had been raised with the increasing groove height for two different wavelengths of the sinusoidal surfaces due to the increased energy barrier. In order to fully comprehend the mechanics of anisotropic wetting behavior, they also devised a thermodynamic model based on surface energy change. From free energy curve, due to absence of energy barrier along the groves for three-phase contact line movement, lower contact angle along this direction had been developed. contact angle hysteresis for the contact angle measured perpendicular to the grooves increased with the increment of groove depth and with the decrement of the groove wavelength due to the higher energy barriers for the liquid to fill the grooves. But no hysteresis was found for the contact angle along the grooves, as advancing and receding contact angles were found equal to the equilibrium contact angle because of the smooth free energy curve for contact line movement along the grooves. Another work on tunable anisotropic wettability had been performed by Zhang *et al.* [95]. They, at first, introduced micrometer and sub-micrometer scaled hierarchical structures on polystyrene (PS) and poly (methyl methacrylate) (PMMA), which altered their isotropic wetting characteristics when used without any roughening and converted into anisotropic wetting behavior by getting higher degree of anisotropy for rough hierarchical structures on PS and PMMA.For PS film, $8° - 38°$ of anisotropic wettability had been accomplished for different hierarchical structures whereas, this range had gone higher for PMMA film with $6° - 54°$.They also described that the anisotropy induced by the rough structures on both hydrophilic surfaces was due to higher energy barriers across the gratings. As a result, stretched and elongated droplet structure had been observed along the gratings for preferential spreading movement in that particular direction. Xia *et al.* showed strong anisotropic behavior for photoresist (PR) patterns on silica surfaces during the conversion of hydrophibicity to hydrphilicity mode [96]. Though during this process, degree of anisotropy reduced from $79°$ to $30°$, higher value of 'droplet distortion' (8-10) had been found which is nothing but the ratio of length of droplet which is directedalong the

grooves to the width ofthe droplet which is in the orthogonal direction of the grooves, because of the hydrophilic wetting condition. Again, in other study, Xia *et al.* compared the degree of anisotropy for surfaces with different chemical composition by incorporating positive PR, negative PR and Si on the parallel grooved surfaces modified with plasma treatments [97].

A series of researches on the anisotropic wetting and frosting/melting of parallel rectangular micro-grooved brass surfaces had been conducted by Rahman and Jacobi by altering the surface geometry and roughness [98-100]. Parallel micro-grooves were machined by them on the four series of brass alloy surfaces,three of which had constant pillar and groove width and another one had same groove height [98]. Observed contact angle hysteresis was much lower along the grooves than across the groove directions for all the cases. As a result, 7° to 48° ranged wetting anisotropy of contact angle hysteresis had found for the droplet's Cassie wetting behavior which was induced by huge deviation of advancing contact angles measured between orthogonal and parallel groove directions. Obstructed movement across the grooves due to higher energy barrier and no pinning along the groove directions made it possible to increase the higher anisotropic wetting for continuous volume addition of liquid droplet on the grooved surfaces. Effect of surface roughness had also been demonstrated here on anisotropic wetting variation by contact angle hysteresis. In their other study, these effects had been described for static contact angle difference between orthogonal and parallel direction of the groove [99]. They fabricated the brass surface with parallel rectangular micro-grooves with same surface processing and roughening procedures in the absence of chemical modifications but with varied geometry of groove width, pillar width and pillar height. Like the other cases, larger static contact angle in orthogonal direction of the grooves had been pronounced for all the cases than the parallel contact angles. This anisotropic wetting variation had also been observed for different sizes of droplets. "Droplet elongation ratio", which is similar to the parameter called "droplet distortion" [96], and "droplet height" were defined to describe the effect of volume. Droplet exhibiting Wenzel wetting state had higher droplet elongation ratio (3.5 to 6) than the Cassie droplet (1.05 to 1.5). Droplets having lower parallel contact angle for stretched along the grooves and sunk down the grooves were the main reason for Wenzel droplets having higher rate of elongation ratio, while Cassie droplets had shown almost circular shape, resulting in less anisotropy. Also, height of the droplet did not vary for Wenzel state for the increasing droplet volume because

droplet addition was only responsible for increasing the droplet elongation in parallel direction of grooves. However, Cassie droplets increased with the increment of droplet size. For droplet size increasing from 3 µL to 10 µL, static orthogonal contact angle increased about 5° for 10^{-5} J/m of line tension, but no definite dependence of droplet volume had been observed for parallel contact angles. Ratio of groove depth to groove spacing named as "aspect ratio" was also been taken into account for determination of static contact angles in both directions. For low aspect ratio (less than 0.23), Wenzel wetting state was favorable for small groove height, whereas for higher aspect ratio cases (0.28 ≤ aspect ratio ≤ 0.75), because of the prevention of droplets intrusion inside the grooves for taller height of grooves, they provided Cassie wetting. However, due to shape and slope of the edge, Cassie to Wenzel transition happened again for more depth of grooves. Higher contact angles had been observed for higher pillar width but for too small width of pillar, droplet again couldnot help butenter into the cavities for the same reason of lower aspect ratio results. Same type of results had been produced for the observation of defrosting characteristics on parallel grooved brass surfaces by Rahman and Jacobi [100]. They had proved that degree of anisotropy increases with the increment of aspect ratio, but decreased with pillar width value increment. However, in the above literatures of Rahman and Jacobi, only rectangular micro-grooved surfaces had been employed and stability of droplets on those rough surfaces had not been discussed.

Later, Naziaet al. numerically obtained the apparent contact angles showing anisotropic wetting for eight parallelly rectangular micro-grooved brass surfaces with groove parameters variation and compared with the experimental values, which had been found in a good agreement [101]. At first, 3-D model of the droplet shape was developed using a numerically founded open-source software, "Surface Evolver" [102]. This software had been used for many research works described above [72, 73, 75, 76, 79-81, 101, 106]. Then they extended their work by analyzing droplet and wetting characteristics on V-grooved surfaces to compare with their rectangular grooved surface findings. But, effect of volume and groove width had not been observed in their studies. Because of their aim of finding proper surface roughness for hydrophobic nature and Cassie droplet, they didnot extend their work much for V-grooved surfaces because of their Wenzel characteristics for the compared results. However, wettability gradient had been applied on the surface which had increased parallel contact angle. Asakura and Yan found that higher

contact angle had obtained for steeper grooved orientation that means for lesser groove angle which is the angle between two inclined faces of the pillar [103] of V-grooved brass surfaces. They demonstrated that after a certain groove height, increasing trend of contact angle would suddenly go down. Li *et al.* in 2004, experimentally obtained contact angles defined anisotropic wetting by the liquid droplet on micro V-grooved Si surfaces fabricated using micro-grinding technique [104]. They observed that increased groove height and groove pitch were responsiblefor better anisotropic behavior, since orthogonal contact angle were found higher than the parallel ones in these cases. For groove pitch of 52 µm and groove height of 36 µm, orthogonal and parallel contact angles were 135.7° and 127.8°, respectively, while contact angle in perpendicular direction was 144.5° and in parallel direction was 119°, for the groove height and pitch of 80 µm and 98 µm, respectively. Stick-slip behavior due to pinning of the droplet at the edges of the groove was the dominantfactor for this anisotropic behavior. Fan and Bandaru showed the effect of solid fraction area as well as surface energies on anisotropy of liquid droplets for Si patterned surfaces with Parylene-C coatings [105]. For higher solid fraction area, contact angles in both parallel and perpendicular to grooves decreased. Because when solid fraction area was lower, fraction area of air increased which reduced the wetting of top of the pillars and ultimately resulted in a larger apparent contact angle. They also developed relation between the anisotropy and liquid droplet penetration length. Song *et al.* in a partially grooved surfaces, demonstrated the effect of fraction of groove area and groove width on anisotropic wetting phenomenon both experimentally and numerically as well as developed relation between intrinsic contact angle and apparent contact angles in both directions along with degree of anisotropy [106]. They found that degree of anisotropy gradually reduced with the enhancement of intrinsic contact angle. Qi *et al.* illustrated the effect of grove width or pitch and height on wetting anisotropy for fabricated micro sine grooved aluminum surfaces [107]. With constant groove pitch (30 µm), apparent contact angle in orthogonal and parallel directions of the grooves increased with the increment of height of the groove (12 µm to 24 µm). However, when the groove height was fixed at 24 µm and groove pitch was increased (30 µm to 60 µm), orthogonal contact angles decreased. Moreover, orthogonal contact angle had been observed larger than the parallel contact angles due to energy barriers deviation in different directions to surpass by the droplets. Recently, combined experimental and simulation analysis had been conducted on parallel micro-groove surfaces to study the anisotropic wetting behavior

for Cassie-Baxter droplets by Ding *et al.* [83]. In this study, they also found out that perpendicular contact angles values are much higher than parallel contact angles and also build some relations between droplet base ratio with wetting parameters. They further added that Cassie droplets did not break down, even if dominant gravitational effect was there for anisotropic variations. More significantly, biomedical applications are a prominent application direction in this regard [108]. Chemical and bio-analysis may benefit from directional liquid transportation on anisotropic wetting surfaces. Microfluidic devices with a variable fluid flow rate may be used to replicate blood flow in pathological examinations. Finally, it can be said that anisotropic wetting surfaces govern directional liquid transportation, which is a potential technology used in digital microfluidics, liquid accumulation, oil-water separation, and many other applications [109, 110].

1.7 Motivation of the Present Study

Many studies have sought to manipulate surface wettability by altering surface roughness and this is one technique to enhance water drainage from different surfaces for which water retention can be a critical issue [1-3, 38, 72, 94, 98, 100]. Directional wetting with tailored surface textures in a variety of key physical applications, as discussed in Section 1.5, has necessitated further research into the wettability phenomena, particularly anisotropic wetting. To obtain wetting anisotropy, it is crucial to be able to forecast how a particular surface shape will affect its wetting behavior.

Although a considerable number of studies have been reported on wetting and anisotropic wetting in general, there have been limited studies on tunable wettability on V-grooved and wavy surfaces and their comparative wetting behavior. Only a handful of studies, most of which are in experimental, have been reported on the wetting behavior of micro-structured wavy and V-grooved surfaces. However, comprehensive numerical simulations to aid the prediction of wettability and design of these surfaces are rare. This is in spite of the obvious importance of the V-grooved and wavy surfaces in achieving directional wetting behavior and the ease of fabrication of these surfaces from a micro-manufacturing point of view. Effects of surface

roughness parameters on anisotropic wetting behavior for both these surfaces are yet to be explained properly. Moreover, relative stabilities of metastable states along with the most stable state of liquid droplet on these surfaces have not been studied yet. Moreover, a comparison between the wetting characteristics on wavy and V-groove surface with roughness features of similar size has not been examined in detail. Therefore, in the thesis, detailed numerical analysis has been carried out to examine the wetting states, shape, and stability of droplets on micro-scale wavy and V-grooved surfaces with variations in surface geometry, surface chemistry, and liquid droplet sizes.

1.8 Objectives of the Present Study

The main objectives of the present study can be summarized as follows:

(i) To numerically investigate the wetting behavior of liquid droplets on micro wavy and V-grooved surfaces in terms of their total and normalized energies and apparent static contactangles.

(ii) To study the effect of geometric variation of the wavy surfaces such as wavelength or groove pitch, amplitude etc. on the wetting state and wettability of liquid droplets and to compare these results with the dimensional variations of V-grooved surfaces.

(iii) To analyze the effect of droplet size on the apparent contact angle and energy of the droplets by simulating drop shape for a range of dropvolume.

(iv) To study the effect of surface chemistry on the wetting behavior using surfaces of different types ofmaterials.

This present study is expected to be beneficial in the design of micro-scale sinusoidal and V-grooved surfaces with regulated wettability, and it might provide a reliable guideline for future surface design. Additionally, free energy analysis of wetting states would provide an additional value for the determination of stability of various droplet sizes and fluid types on these surfaces.

1.9 Outline of the Thesis

The goal of this dissertation is to establish a numerical approach in order to predict wettability and energetics of the liquid droplets placed on microV-grooved and microwavy surfaces for anisotropic wetting.

In **Chapter 01**, the fundamental concepts related to wettability and energetics of liquid droplets on surfaces have been discussed at the beginning. Following that, sequentially the previous relevant experimental discoveries as well as numerical studies of liquid wetting behavior were discussed. Finally, a synopsis of the thesis works has been offered.

In **Chapter 02**, detailed description of the numerical technique that has been devised to model 3-D liquid droplet form on rough surfaces for the wetting anisotropy is provided. "Surface Evolver" (SE), an open-source finite-element software, that has been used to calculate low-energy liquid surfaces over the last two decades, has been employed as a numerical tool in our research. In this chapter, the computational approach's whole technique is outlined in depth.

In **Chapter 03**, the influence of surface topology as well as liquid droplet volume on the stability of the liquid droplets in terms of the normalized energy parameter has been discussed. Also, the apparent contact angles have been determined to analyze the anisotropic wettability for geometric variations of surfaces and grooves and for the liquid droplet sizes.

Finally, in **Chapter 04**, major observations of this study are properly summarized, and future ideas or scopes of work are proposed.

CHAPTER 02

SIMULATION METHODOLOGY

The main objective of this chapter is to provide a detailed description of the numerical methods which was used to develop the numerical models to predict the wetting behaviour of 3-D liquid droplets on surfaces with micro-scaled wavy and V-grooves. The development of these kind of models allows researchers to explore characteristics of the liquid droplet that are complex or improbable to investigate through experimental procedures. "Surface Evolver", an interactive and the most widely used numerical tool in wettability modelling, has been utilized in this work to analyse the liquid droplet morphology and wetting state for structured surfaces, which will be thoroughly discussed in next sections.

2.1 Surface Evolver

Kenneth A. Brakke, professor of Mathematics department, Susquehanna University, created the free software tool, "Surface Evolver" (SE), for US National Science Foundation-sponsored research on geometry based fast and high-performance computation [102]. It is an interactive finite element-based open access software for exploring surfaces formed by surface tension and other energies while being constrained in different ways. Surface Evolver's numerical technique is based on reducing the system's free energy to produce the equilibrium liquid droplet form while accounting for Young's law and total free surface energy equations. In the beginning, a data file is used to specify an initial surface geometry (.txt file). The software then uses a gradient descent approach to develop the surface toward minimum energy. The surface evolver

handbook contains a full explanation of the concerning theoretical background and simulation technique [111].

The following sections include a short but concise description of the formulation of the model as well as the simulation processes.

2.2 Formulation of the Numerical Model

At the commencement of this numerical approach, a three-dimensional geometry of the surface and a user-defined droplet deposited on the substrate will be modeled. In our model, liquid droplet and the rough solid surface on which it is put are both exposed to the ambient fluid, which is air, and the liquid and the fluid (air/gas) are considered to be mutually incompatible. Surface tension and gravity - these two forms of energy are involved in a droplet of liquid placed on a rough surface. So, the total energy of a droplet is nothing but summation of free surface energy (G^S) and gravitational energy (G^G). Due to energy reduction, the droplet will attain a specific size and shape equilibrium.

The liquid drop's free surface energy, G^S may thus be confined to the addition of the energies at the interfaces, which can be expressed as [79]:

$$G^S = \iint_{A_{LG}} \gamma_{LG} dA + \iint_{A_{LS}} \gamma_{LS} dA + \iint_{A_{SG}} \gamma_{SG} dA \qquad (2.1)$$

Where, surface tension between the liquid-solid, liquid-gas, and solid-gas phases are indicated by γ_{LS}, γ_{LG}, and γ_{SG}, while A_{LS}, A_{LG}, and A_{SG} designate the interfacial or contact area between liquid-solid, liquid-gas, and solid-gas phases, respectively.

As specified by Young's equation in equation 1.8, from the horizontal force balancing of tensions at the interface at three-phase contact line, surface material's intrinsic contact angle (θ_{int}) can be calculated as:

$$\gamma_{SG} - \gamma_{LS} = \gamma_{LG} \cos \theta_{int} \tag{2.2}$$

Now, after combining equation 2.1 and 2.2, we can get:

$$G^S = \gamma_{LG} \left[A_{LG} - \iint_{A_{LS}} \cos \theta_{int} \ dA \right] \tag{2.3}$$

Moreover, the gravitational energy (G^G) can be written as [80]:

$$G^G = - \iiint_V \Delta \rho \vec{g} \cdot r \ dV \tag{2.4}$$

Where, $\Delta \rho$ denotes deviation between liquid phase density and air or gas phase density, $\vec{g}$ represents vector of acceleration due to gravity, r is the radius of the droplet and V indicates droplet volume.

So, ultimately, a liquid droplet's energy functional when exposed to a constant droplet volume, can be expressed by combining both equation 2.3 and 2.4, as follows:

$$G = G^S + G^G = \gamma_{LG} \left[A_{LG} - \iint_{A_{LS}} \cos \theta_{int} \ dA \right] - \iiint_V \Delta \rho \vec{g} \cdot r \ dV \tag{2.5}$$

The gravitational effect is ignored in our simulations because the droplets used in our work have a small enough volume (<10 µL) to ignore the effect of gravity. This type of sufficiently tiny liquid droplet is called "sessile droplet". That is why we simply address the liquid's surface tension and its interaction with the substrate surface in this situation.

As a result, after omitting the gravitation energy portion from the equation 2.5, we can write the total energy of sessile droplet (G) only as the free surface energy (G^S), given in equation 2.3. Then, G can be expressed as follows:

$$G / \gamma_{LG} = A_{LG} - \iint_{A_{LS}} \cos \theta_{int} \ dA \qquad (2.6)$$

This is the modified total effective free energy equation for the sessile droplet which have to be minimized in order to attain the equilibrium liquid droplet form for a constant value of droplet volume. Equation 2.6 reveals that the intrinsic contact angle (θ_{int}) is the only parameter that determines the equilibrium drop form on a surface since the free energy is reduced with reference to the liquid-air interface shape. G / γ_{LG} is minimized throughout the solution process. As a consequence, for the current case, the intrinsic contact angle (θ_{int}) is the only material feature we need to describe.

With the help of variational principles, the aforementioned restricted minimization approach can be demonstrated to be analogous to calculate Laplace equation for pressure fall at each liquid-gas interface's site by setting up the boundary condition as Young's equation (equation 2.2) at three-phase contact line, as follows:

$$2\gamma_{LG} / R_m = \Delta p \qquad (2.7)$$

Where, R_m denotes curvature's mean radius and Δp represents drop of the pressure, at a node on the surface of liquid droplet.

In a fixed atmospheric pressure, a static liquid droplet on surface will experience pressure drop at each location on the interface of liquid and gas phases, in the absence of gravity. As a direct outcome of the equation 2.7, a uniform average curvature surface should be observed of a sessile liquid droplet. While the circular surface is one of the several conceivable constant mean curvature surfaces in three dimensions, the circle arc is the only persistent average curvature surface.

After that, each point is shifted towards the lowest ever energy location using the gradient descent approach. The energy gradient may be written as follows [102]:

$$\vec{F} = -\nabla E = (\partial E / \partial x \, \hat{\imath} + \partial E / \partial y \, \hat{\jmath} + \partial E / \partial z \, \hat{k}) \qquad (2.8)$$

Where, the force exerted to each point is denoted by $\vec{F}$. The liquid droplet's equilibrium location is the final convergent solution since the gradient descent technique is applied to each point independently.

2.3 Development of the Numerical Model

Surface Evolver (SE) is a simulation tool that progresses towards the minimized energy state condition for a liquid droplet; however, it lacks capabilities to assist in the design or creation of the model. An initial surface is described as a model in a data file that acts as the input for this public domain program. To make the SE solver easier to use, creation of an optimized data file for each of the investigated instances using SE syntax is necessary. To effectively construct the complicated geometries and apply the boundary constraints, C-language subroutines are included into the data file. The data file also contains surface geometry, intrinsic contact angle of surface material, which illustrates the feasibility of solid-liquid phase combination and takes into consideration the nanoscopic roughness of the surface, liquid characteristics (γ and ρ), and droplet size. In order to explicate the model, the user must utilize a text file that is in the proper formatting (.fe). Given that it is a surface vertex-edge-facet element model, the surface will be produced by specifying its vertices, edges, and faces in the "Surface Evolver" application. A vertex is a spatial point in three-dimensional space. The coordinates of the vertices serve as the parameters that govern where the surface is positioned on the plane. Surface evolution occurs as a result of changes in the coordinates of the surface. In geometry, an edge is a one-dimensional geometric element formed by joining the head and tail vertices by a line. A facet is a flat triangle with three sides that are parallel to each other. A face is defined as an ordered collection of three or more edges that is arranged in a certain manner. Then, geometric, energy and volumetric constraints has been applied to the necessary vertices and edges of the surface. When a liquid droplet is in the Wenzel wetting state, the liquid-air boundary is thought to vanish, and the droplet receives the rough surface's energy locally, as determined by the intrinsic contact

angle of that surface.Cassie wetting state is presumed when the liquid-air interface at the air-gap which is in between the two edges of the pillar, receives the interfacial energy of liquid-air, with a contact angle of 180°.

The geometry of the liquid droplet is initially set up in a cubical form with the smallest mesh size possible (Figure 2.1 (a)). A series of iterations are carried out until the energy of the system does not vary appreciably; convergence condition is fulfilled. During this process, liquid-vapor interface vertexes are adjusted at each iteration in order to minimize the system's energy while staying within the given parameters like uniform volume, constant intrinsic contact angle, etc. Then, after successive refinement of meshes and energy minimizing iterative steps with some user-definedcommands, the initial model evolves to the desired final equilibrium droplet shape (Figure 2.1 (b)).Furthermore, in order to explore the impacts of changing scale, the model must be readily altered by tweaking the parameters of interest, which necessitates the inclusion of options for automated model modification from input data.

A liquid droplet is placed on a set of pillars or grooves in the desired models, with the droplet size, pillar width, groove width, groove height and surface energy all being customizable. In all our models in order to observe the effect of these surface roughness parameters along with droplets', water has been used generally as the liquid, therefore, interfacial tension of liquid-air interface (γ_{LG}) at 25℃ is 0.072 N/m. It should be kept in mind that the final equilibrium form of the droplet may not (and typically will not) be the absolute minimum energy arrangement, but rather the lowest local minimum in energy, i.e., the stable droplet shape attained throughout the simulation where total energy is continually dropping.

| (a) | (b) |
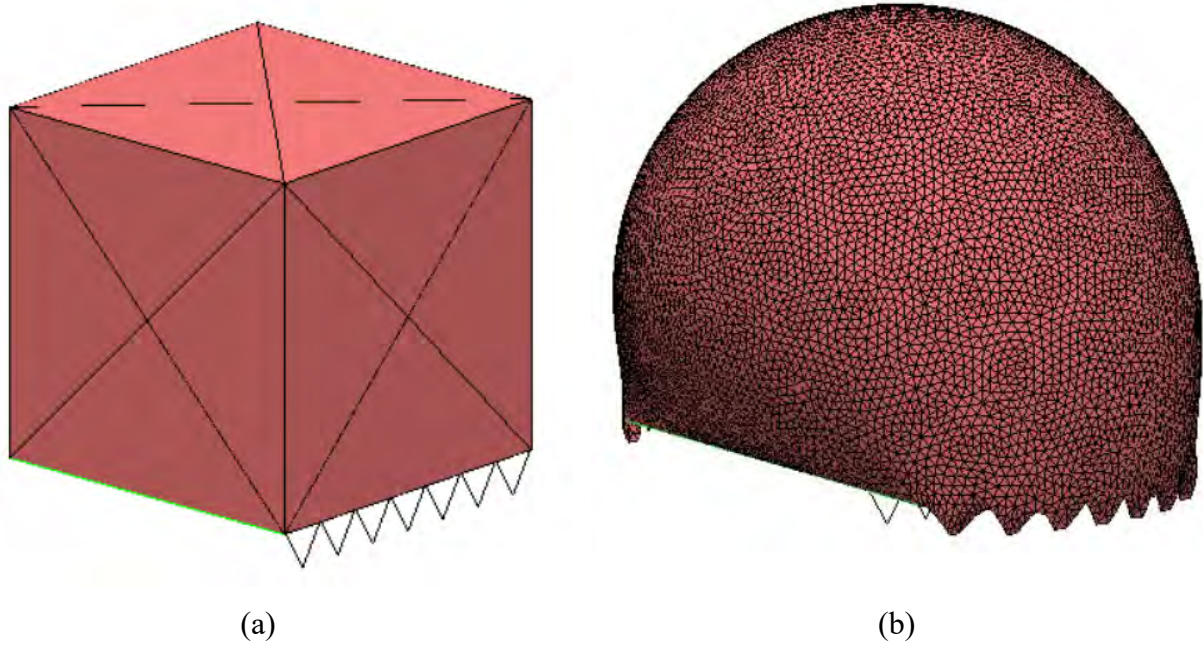
Figure 2.1: On microV-grooved surface of eight pillars - (a) Initial cube shape configuration of a droplet; (b) Evolved equilibrium droplet shape acquiring minimized energy state.

However, the geometric dimensions used in our simulation model for the micro V-grooved and wavy surfaces is presented in Table 2.1. The topographical data from all of the microV-grooved and micro wavy surface samples are summarized here. The micro V-grooved and micro wavy surface samples are referred as "$D_g{}^a W_g{}^b W_p{}^c$", and "$H_w{}^a \lambda_w{}^b$" respectively, where, groove height (micro V-grooved surface), groove width (micro V-grooved surface), pillar width, groove depth (micro wavy surface), and groove pitch (micro wavy surface) are depicted by D_g, W_g, W_p, H_w, and λ_w, respectively, as well as a, b, and c superscripts denote the quantitative values of these characteristics in microns. It has to be noted that the bold dark red colored surface sample specified in Table 2.1 for our simulation model has exactly the mimic roughness parameters of Li *et al.*'s experimental study on micro V-grooved surfaces [104] without the number of grooves, with which our simulation model has been validated at first (Section 2.6). But this experimental work has been limited on three different surface roughness's of micro V-grooved surfaces, which are all discrete values. So, to predict the effect of surface roughness on wettability, $\boldsymbol{D_g{}^{80} W_g{}^{98} W_p{}^4}$ rough sample surface has been first taken from that experimental study of Li *et al.*for our simulationon micro V-grooved surfacesfor a specific number of grooves and after that, dimensions of each surface roughness parameters

49

have been increased or decreased or both from the above mentioned sample surface to clearly demonstrate the effect of those surface roughness parameters on wettability. Also, the dimensions of those parameters have been chosen to perfectly picturize the droplet shape, anisotropic effect and wetting transitions under those parametric ranges of surface roughness. After that, to compare these results with micro wavy surfaces, which have almost similar geometric surface like micro V-grooved samples but smooth curvy peak and valley instead of sharp-edged corner, similar range of dimensions have been selected for micro wavy surface simulations. And as all the parameters dimension units are limited in microns, that is why these surfaces are called micro V-grooved and micro wavy surfaces. Moreover, droplet size range has been restricted within 5 µL for our whole simulation work. This has been done due to two reasons: (i) to neglect the gravitational effect by maintaining sessile droplet, and (ii) further increment of droplet volume does not change any trends of findings (for both energetics and anisotropic wetting) significantly.

Table 2.1 Summarization of micro V-grooved and micro wavy surfaces topographical data

Series	Samples	Groove Height or Depth, D_g or H_w (µm)	Groove Width or Pitch, W_g or λ_w (µm)	Pillar Width, W_p (µm) (V-groove)
	$D_g{}^{60}W_g{}^{98}W_p{}^{4}$Or, $H_w{}^{60}\lambda_w{}^{98}$	60		
	$\boldsymbol{D_g{}^{80}W_g{}^{98}W_p{}^{4}}$**Or,** $\boldsymbol{H_w{}^{80}\lambda_w{}^{98}}$	80		
	$D_g{}^{100}W_g{}^{98}W_p{}^{4}$Or, $H_w{}^{100}\lambda_w{}^{98}$	100		
01	$D_g{}^{120}W_g{}^{98}W_p{}^{4}$Or, $H_w{}^{120}\lambda_w{}^{98}$	120	98	4
	$D_g{}^{135}W_g{}^{98}W_p{}^{4}$Or, $H_w{}^{135}\lambda_w{}^{98}$	135		
	$D_g{}^{150}W_g{}^{98}W_p{}^{4}$Or, $H_w{}^{150}\lambda_w{}^{98}$	150		

	Configuration			
	$D_g{}^{80}W_g{}^{98}W_p{}^4$Or, $H_w{}^{80}\lambda_w{}^{98}$		98	
	$D_g{}^{80}W_g{}^{110}W_p{}^4$Or, $H_w{}^{80}\lambda_w{}^{110}$		110	
02	$D_g{}^{80}W_g{}^{130}W_p{}^4$Or, $H_w{}^{80}\lambda_w{}^{130}$	80	130	4
	$D_g{}^{80}W_g{}^{150}W_p{}^4$Or, $H_w{}^{80}\lambda_w{}^{150}$		150	
	$D_g{}^{80}W_g{}^{170}W_p{}^4$Or, $H_w{}^{80}\lambda_w{}^{170}$		170	
	$D_g{}^{80}W_g{}^{98}W_p{}^4$			4
	$D_g{}^{80}W_g{}^{98}W_p{}^{15}$			15
03	$D_g{}^{80}W_g{}^{98}W_p{}^{25}$	80	98	25
	$D_g{}^{80}W_g{}^{98}W_p{}^{50}$			50
	$D_g{}^{80}W_g{}^{98}W_p{}^{75}$			75
	$D_g{}^{80}W_g{}^{98}W_p{}^{100}$			100

2.3.1 Model Development for Droplets on Micro V-grooved Surface

The enclosure of triangular facets aligned by the surface normal is how SE represents bodies. The surface energy is defined to all along the pillar width, i.e., top face of the pillars as well as the inclined pillar walls corresponding to the intrinsic contact angle of the material ($\theta_{int} = 111°$) as $-\gamma_{LA}\cos\theta_{int}$, which has been suggested by Brakke [102, 111]. Each of these inclined walls of these pillars has been developed by the use of trigonometric formula consisting of the magnitude of groove width and height. The vertex coordinates of the groove portions of the surface, where the liquid-air interface has been observed during the initial cubical droplet shape, are not constrained. Only, the surface roughness geometry, especially the critical roughness factor (which will be discussedfrom analytic model in Section 2.7) will decide whether the droplet will enter the grooved cavities entirely and represent the Wenzel wetting state or there will be air-gap under the liquid-air interface to depict the Cassie wetting behavior.

As has already been discussed that in case of the Cassie state, droplet will not fully fill the groove cavities whereas, in case of Wenzel wetting, no air-gap will be found inside the asperities. And, in micro V-grooved surfaces, the contact line integral technique was employed for only the faces of solid wallswetting. Green's Theorem is applied to the assessment of surface energy at the interface faces of solid-liquid of V-grooved surface, which results in the transformation of a surface integral to a line integral, which is along edges of the three-phase contact line, because of this transformation. The oriented droplet surface in contact with the pillar top face and walls is denoted by $\vec{S}$. The unit basis vectors are represented by $\vec{i}, \vec{j}$ and $\vec{k}$.

Now, vector field $\vec{w}$ can be determined such that,

$$\iint_{face} T\vec{k} . d\vec{S} = \int_{edge} \vec{w} . d\vec{l} \tag{2.9}$$

Where, T is the surface tension per unit length which can be rewritten from Young's equation as:

$$T = -\gamma_{LA} \cos \theta_Y \tag{2.10}$$

Now, from Stoke's theorem [111], we can say that:

$$Curl \, \vec{w} = T\vec{k}$$

$$\text{Or, } \nabla \times \vec{w} = T\vec{k} \tag{2.11}$$

$$\begin{bmatrix} \vec{i} & \vec{j} & \vec{k} \\ \partial/\partial x & \partial/\partial y & \partial/\partial z \\ w_x & w_y & w_z \end{bmatrix} = T\vec{k} \tag{2.12}$$

So, there are numerous alternative answers (each varied by the gradient of a scalar function), but one simple approach is to takefor the surface energy at a horizontal face in contact with a pillar, $\vec{w} = -T_y\vec{\imath}$ or $\vec{w} = -T_x\vec{\jmath}$, which can be utilized like:

$$\text{For, } \vec{w} = -T_y\vec{\imath}, \qquad \begin{vmatrix} \vec{\imath} & \vec{\jmath} & \vec{k} \\ \partial/\partial x & \partial/\partial y & \partial/\partial z \\ -T_y & 0 & 0 \end{vmatrix} = T\vec{k} \qquad (2.13)$$

$$\text{For, } \vec{w} = -T_x\vec{\jmath}, \qquad \begin{vmatrix} \vec{\imath} & \vec{\jmath} & \vec{k} \\ \partial/\partial x & \partial/\partial y & \partial/\partial z \\ 0 & -T_x & 0 \end{vmatrix} = T\vec{k} \qquad (2.14)$$

In this way, contact surface energy in line integral form around three-phase contact line, which is constrained by the surface of each pillar along with its inclined walls, can be attained in this linear model.

Figure 2.2 illustrates the 3-D microV-grooved surface of our model with the roughness geometry of the surface.

(a)
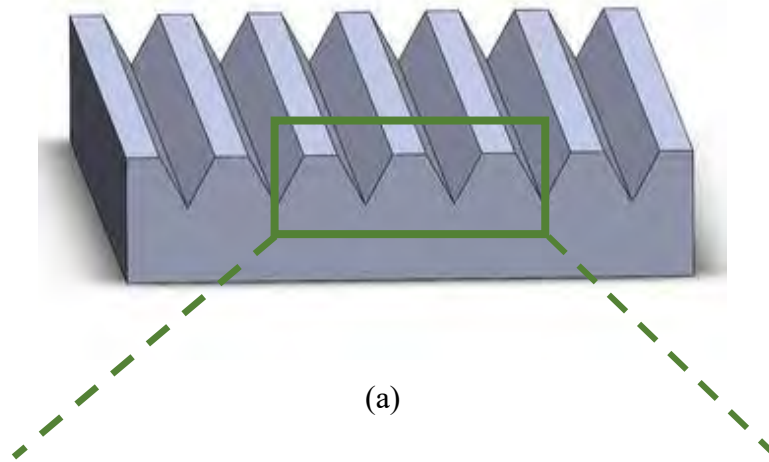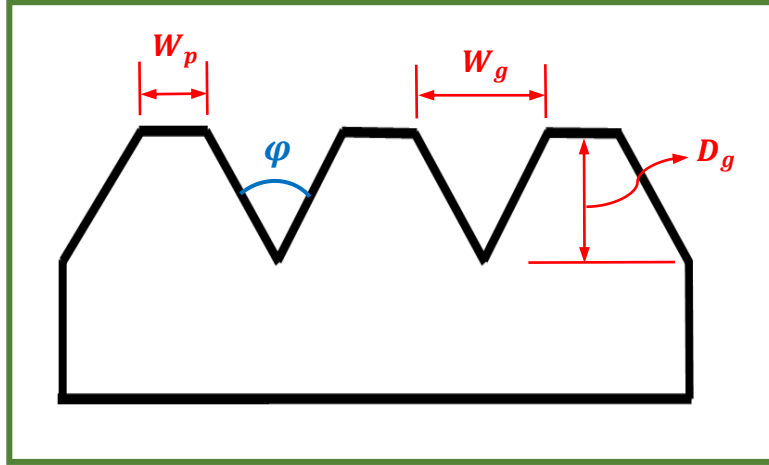
(b)

Figure 2.2: (a) 3-D view of microV-grooved surface of our simulation model; (b) Schematic 2-D view to address the surface geometry of the surface; Here, W_p denotes pillar width, W_g represents groove width, D_g depicts groove depth and φ is groove angle of the microV-grooved surface.

The simulation using Surface Evolver began with a cubic shaped droplet as the starting point, on which restrictions and associated energy functions are set. Among the four borders or edges which construct the bottom face of the initial droplet, the left and right borders are restricted to moving on the two outermost pillars (Figure 2.3(a)). The number of pillars on which the droplet dwells is physically defined by the drop production process, hence this boundary condition is required. Only the bottom face is regarded to be relevant for establishing the shape of the droplets when imposing constraints to the facets and edges in the simulation. The boundary conditions, which are applied to the edges of the bottom face of the droplet, contribute to the generation of the three-phase contact line for convenience (Figure 2.3(b)). More detailed information about boundary conditions as well as constraints implementation are given by Brakke [102, 111].

<div align="center">(a)   (b)</div>
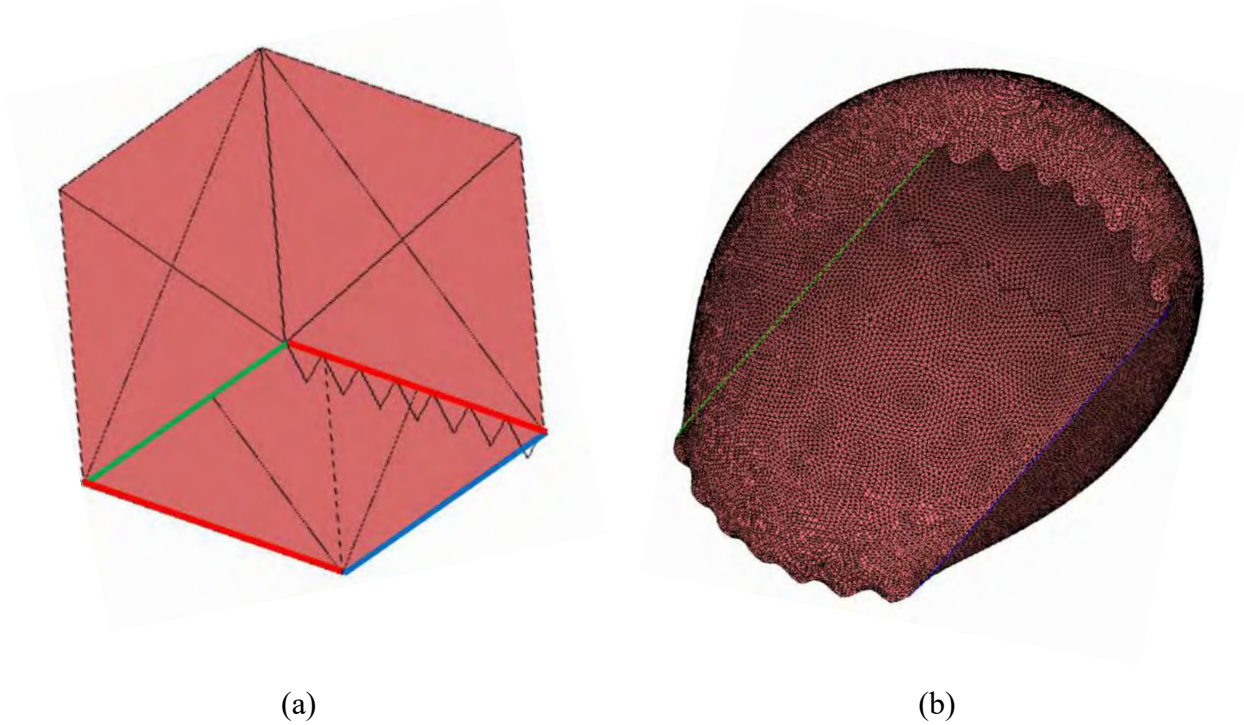
Figure 2.3: (a) Initial cubical droplet, in which bottom face has been shown by 4 different colored edges – left and right edges are denoted by green and blue color, respectively; (b) Equilibrium droplet's bottom face illustrating the constraints imposed on those left and right two edges along which the droplet moved to attain the final shape.

Finally, the anisotropic equilibrium droplet shape is determined by iterative refining and energy minimization phases in the numerical simulation of Surface Evolver (Figure 2.4).
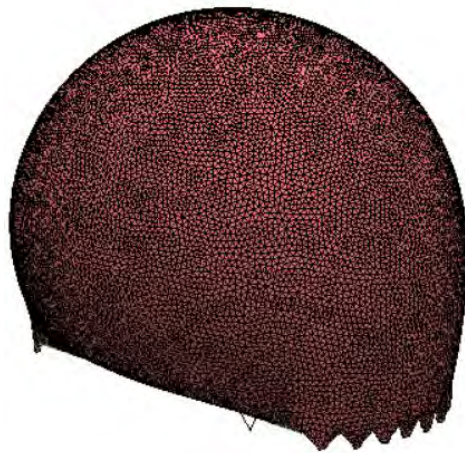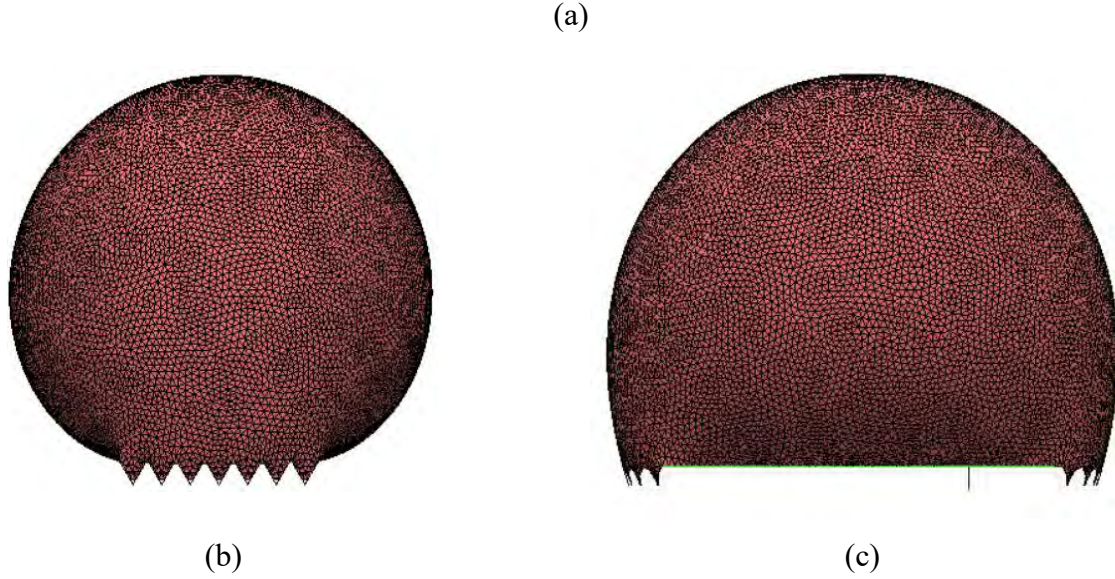
Figure 2.4: (a) Isometric view of equilibrium droplet shape on microV-grooved surface showing anisotropic wetting, (b) Orthogonal direction to the groove or front view of the equilibrium droplet, (b) Parallel direction to the groove or side view of the equilibrium droplet.

2.3.2 Model Development for Droplets on Micro Wavy Surface

The surface energy provided for the droplet surface and wavy surface for our simulation model is similar to that used in droplet on micro V-grooved surfaces. The overall surface has been defined by the equation of sinusoidal function, as follows:

$$z = \frac{H_w}{2} \times \sin\left(\frac{2\pi x}{\lambda_w}\right) \tag{2.15}$$

where, H_w denotes the groove depth and λ_w represents the wavelength of the groove or groove pitch. Here, $\frac{H_w}{2} (= A)$ depicts the amplitude of this sine curve.

(a)

(b)
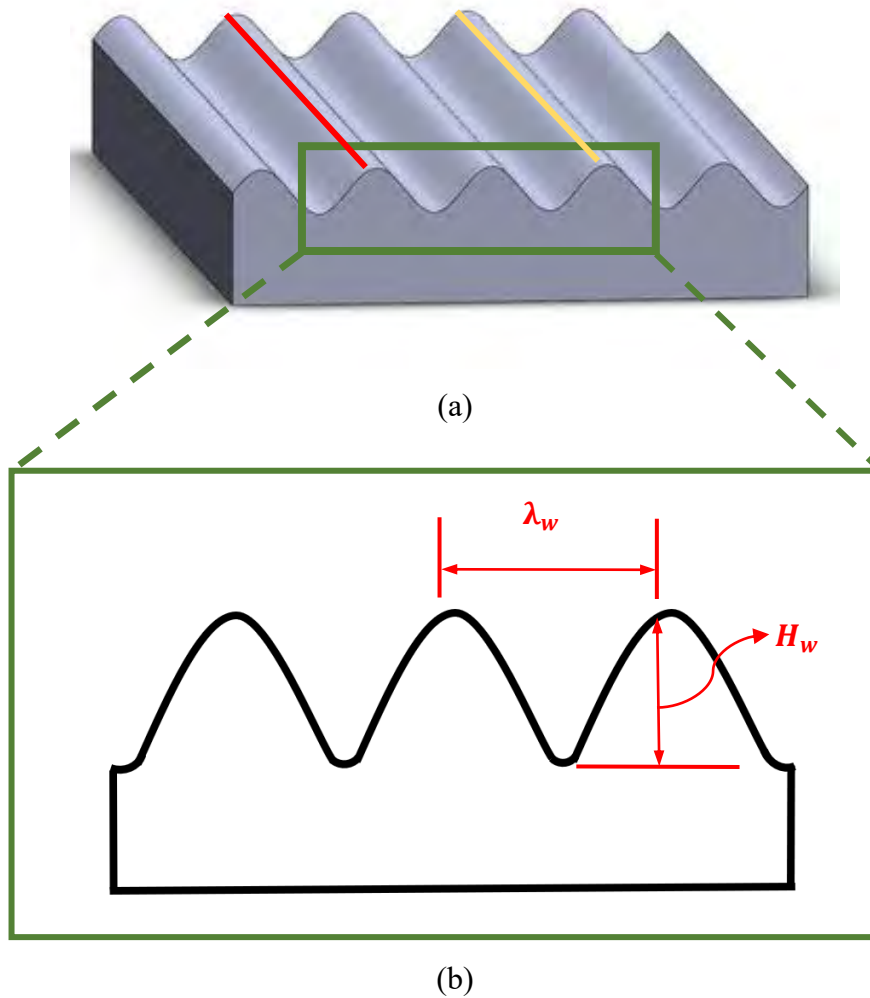
Figure 2.5: (a) Isometric view of micro wavy surface of our simulation model with the two bottom edges of the initial droplet – red line is for left edge and yellow line is for right edge of the bottom face; (b) Schematic 2-D diagram to address the surface geometry of the surface.

The z coordinates of the vertices of the wavy surfaces are found by the abovementioned equation 2.15 for different x coordinates of the vertices. During the initial cubical droplet modelling on the micro wavy surface, the bottom face of that droplet has been placed on top of the wave or peak points of the pillar of the surface, where the left and right edges of that bottom face has resided along the pillar or wave top nodes on two outermost waves, which has been shown in Figure 2.5 (a). The droplet again can move along these two edges like the micro V-

groove model because of the given boundary conditions. The surface energy for whole wavy surface has been set by introducing the intrinsic contact angle of the surface material.

(a)

(b)

(c)

(d)
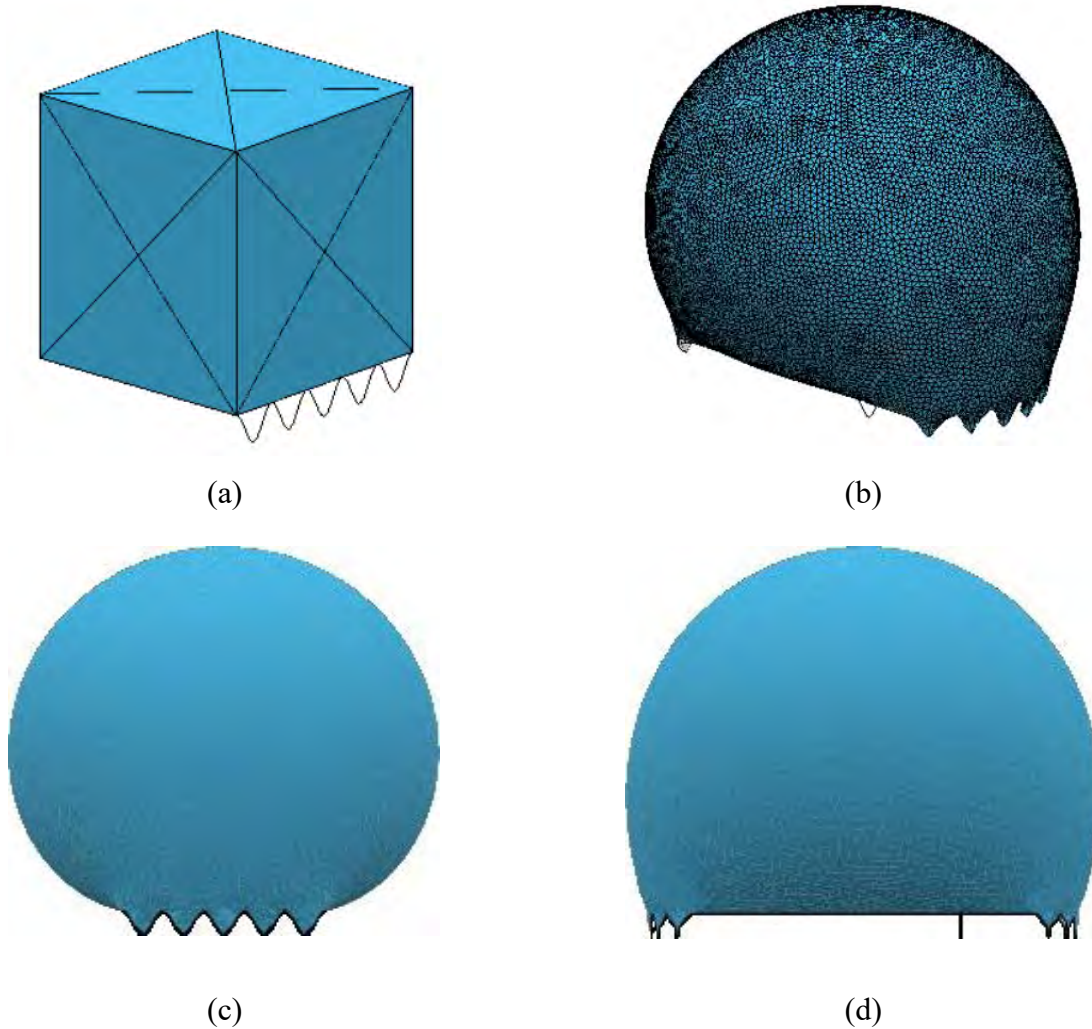
Figure 2.6: (a) Initial droplet shape as a cube above micro wavy surface; (b) Isometric view of final equilibrium droplet shape; (c) Orthogonal or front view, and (d) Side or parallel to the groove view - of the equilibrium droplet on micro wavy surface.

2.4 Meshing and Convergence

The mesh is modified at each iteration, which sets Surface Evolver apart from many other finite element software. Convergence and correctness of the final outcome can be difficult to determine. Surface Evolver is a tool that portrays surfaces with a triangular tessellation that may

be modified to achieve the desired level of precision. The Surface Evolver parameterizes surfaces in terms of their vertex coordinates for a specified triangulation, then changes a given initial interface form according to the conditions of the Gauss–Laplace equation. The Newton–Raphson technique is used to iteratively change vertices to discover the shape of the droplet within a given set of constraints, fast bringing the energy of the surface to a local minimum. The graph of the energy function resembles a mountainous landscape with hills, valleys, and passes. As a result, G, the energy function's gradient, can be considered the steepest upward direction. With each iteration step, the Evolver reduces energy by going downhill, or in a negative gradient direction, until a local minimum is reached.

The user must manually enter the sequence of simulation stages, which includes iteration, refinement, vertex averaging, and cutting of abnormally long edges created during refinement, because Surface Evolver does not automate the simulation process. The simulation starts with a coarse mesh and gradually improves and averages the vertex counts until it reaches the ultimate equilibrium shape. From the starting model, the equilibrium drop form is determined repeatedly. Iterations are done until the system's energy does not change significantly. Vertex averaging is done on a regular basis after refinement and iterations to make the vertices more evenly spaced. The simulation phases are established as user-defined identifiers in order to produce the best results during the model generation process. The degree of refinement, mesh modification, vertex averaging, and number of iteration steps appropriate for the level of refinement are all included in each identifier. These user-defined identifiers can be used to run the simulation's operations, making it easier and faster to finish. To make the refining process unbiased for comparative parametric evaluation, the same simulation technique with similar phases and identifiers is used for all analogous wetting scenarios on microV-groove and micro wavy surfaces. An example simulation technique for a liquid droplet on a micro wavy surface is shown in Figure 2.7.

*InitialCubical
Shaped Droplet*

*Single step
refinement
and after few
iterations*

*Minimizing
energy in few
more iterations*

*After
significant no.
of iterations*

*Further
refinements
and*

*Significant no.
of iterations*

*Final
equilibrium
droplet
shape*

Figure 2.7: Simulation procedure in a chronological order in which droplet approaching towards its ultimate equilibrium shape by attaining minimized energy state by necessary refining and meshing. Here, figure depicts only equilibrium drop shape evolution on a micro wavy surface. For equilibrium drop shape with energy minimization on microV-groove surface, similar approach is utilized.
[The figures are not all drawn to the same size]

60

2.5 Post-Processing Operation

After the conclusion of the simulation process in Surface Evolver, post-processing has to be done to find enough data, especially contact angles from the equilibrium droplet shape deposited on micro scale rough surfaces. First of all, the image of the final droplet is exported as .eps file and stored in a folder. Then, after extraction from that specific file, the image of the droplet has been saved as jpg form (.jpg file).
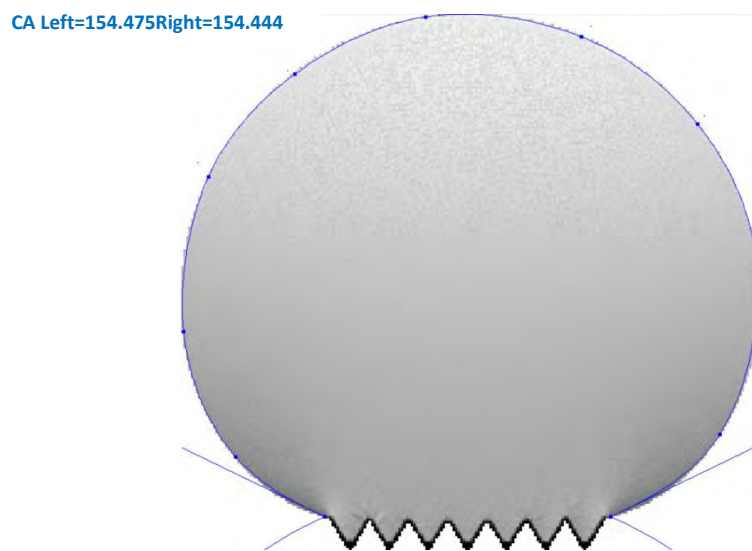
Figure 2.8: Contact angle measurement of the droplet using ImageJ software integrated 'dropsnake' plugin.

A Java-based public domain image processing software, "ImageJ" has been used to measure the apparent contact angles of the liquid droplets. Many researchers adopted this program to determine droplet's contact angles [113-116]. Specifically, "dropsnake" plugin under the software has been employed to meet the need of contact angle measurement. After detecting interface and minor slide of image with the help of drop reflection, by utilizing piecewise polynomial fit, contact angle of the droplet can be attained. In this process, to begin with, we have to load the image of the droplet into "ImageJ" and then 'dropsnake' plugin has to be launched to initialize the snake. After that, a few knots are placed on the drop contour while in

the "Add/move knot" mode. The drop contour starts at the left interface point and continues until it reaches the right interface point. After closing the spline by inserting the last knot, Drag and drop can be used to change the knot placements. Finally, contact angles are shown in the illustration and the table (Figure 2.8).

2.6 Validation of the Computational Approach

The created model was tested against the respective experimental work of Li *et al.* [104] on microV-grooved surfaces and Qi *et al.* [107] on micro wavy surfaces. First of all, these experimental studies have been selected based on the micro-structured rough surfaces (micro V-grooved and micro wavy surfaces) we have chosen for our model. Also, as the surface roughness parameters dimensions are in micro-scale unit in our work, it is better to validate our work with the studies that employed similar types of dimensions in surface roughness parameters. Both experimental studies that have been selected to verify our simulation model's validity, have the surface roughness parameters (groove width or pitch, groove height, pillar width) dimensions are also in the micron's unit, which is another reason to select these works for the validation. Moreover, both of the experimental works [104, 107] demonstrated effect of surface roughness on wettability to some extent, which has also been an important factor to select these studies.The results were found to be extremely consistent. The SE model findings showed a maximum variation of 1.4% (1.9°**)** and 1.08% (1.1°**)** in the apparent contact angle when compared to Li*et al.* [104] and Qi*et al.*'s [107] experimental data, respectively. Table 2.2 shows a summary of the findings. Figure 2.9 illustrates the similarity and accuracy of our numerical model with one of the findings of Qi *et al.*'s experimental results [107] on the water droplet placed on micro wavy surface.

Table 2.2 Summary of the validation results

Groove Shape	Geometry of surface roughness	Experimental Value		Numerical Value	
		Orthogonal CA	Parallel CA	Orthogonal CA	Parallel CA
MicroV-groove	Pitch, p = 73 µm Top width, c = 3 µm Depth, d = 60 µm Drop Volume = 2 µL **(Li *et al.*)**	**140.5°**	**121.3°**	**138.6°** (Deviation / Error = **1.4%**)	**122.7°** (Deviation / Error = **1.2%**)
Micro V-groove	Pitch, p = 52 µm Top width, c = 3 µm Depth, d = 36 µm Drop Volume = 2 µL **(Li *et al.*)**	**135.7°**	**127.8°**	**136.8°** (Deviation / Error = **0.8%**)	**126.5°** (Deviation / Error = **1%**)
MicroV-groove	Pitch, p = 98 µm Top width, c = 4 µm Depth, d =80 µm Drop Volume = 2 µL **(Li *et al.*)**	**144.5°**	**119°**	**145.8°** (Deviation / Error = **0.9%**)	**117.5°** (Deviation / Error = **1.3%**)
Micro-sine-groove	Pitch = 30 µm Height = 24 µm Drop Volume = 12 µL **(Qi *et al.*)**	**133.4°**	**102.3°**	**132.2°** (Deviation / Error = **0.9%**)	**101.2°** (Deviation / Error = **1.08%**)

Micro-sine-groove	Pitch = 40 μm Height = 24 μm Drop Volume = 12 μL **(Qi *et al.*)**	**130.6°**	**101.2°**	**129.2°** (Deviation / Error = **1.1%**)	**100°** (Deviation / Error = **1.2%**)

(a)

(c)

(b)

(d)

Figure 2.9: Comparison of the numerical results from SE: (a) orthogonal (130.6°) and (b) parallel contact angle (101.2°) of water droplet on micro wavy surface to those obtained by the experimental work of Qi *et al.* [107]; (c) orthogonal (129.2°) and (d) parallel contact angle (100°) of water droplet on micro wavy surface observed after simulationby SE.

2.7 Analytically Modelled Condition for Cassie-Wenzel Transition for Intrinsically Hydrophobic Surface

Among the two wetting states that have been developed, the wetting condition is Wenzel when a very modest roughness is initially added to a flat surface. In practice, we can see that a meniscus curve forms at the bottom of a spherical liquid drop due to the curvature of the drop. The wetting condition of the liquid (water) is Wenzel until the depth of the groove is expanded over a changeover or transition point.

Alen *et al.* have already provided analytical models forpredicting the wetting state of intrinsically hydrophilic surface (whose intrinsic contact angleθ<90°), where two conditions for Cassie-Wenzel transitions have been proposed [64]. However, in our thesis work, mainly the wetting states and characteristics of a roughintrinsically hydrophobic surface has been demonstrated.For an innately hydrophobic surface, the requirement for transitioning between the Wenzel and Cassie states is simple. Alen and Farhat also provided the Cassie-Wenzel wetting transition condition for intrinsically hydrophobic surfaces in their thesis work [117], which have been demonstrated here briefly. When the total surface energy at Cassie wetting state is smaller than the total surface energy at Wenzel state, a droplet is said to be in Cassie state. From previously indicated two conditions of Cassie-Wenzel wetting transition for intrinsically hydrophilic surfaces from Alen *et al.* [64], it has been known that the state of the droplet is Wenzel as the critical roughness has been approached shortly before the transition, thus they have used the apparent contact angle anticipated by the Wenzel equation, i.e., θ_w. However, in this case, transition event is not the concerning point; rather, energy inequality is the main focus here, i.e., surface energy values have been compared and attempted to determine a roughness minimum limit. As a result, Cassie's and Wenzel's energy states have to be forecast using a reference point. The initial state of roughing, when the apparent contact angle equals the intrinsic contact angle, is the best reference.

So, by formulating the above condition of $G_{Cassie} < G_{Wenzel}$, a limit for the roughnessvalue (r) in terms of the Cassie roughness factor (f) and intrinsic contact angle (θ_{int}) can be derived.The Cassie state is energetically advantageous once the roughness reaches the limiting value. And following these procedures, they have derived the condition for the wetting transition, especially that critical roughness factor (r_{cr}):

$$r_{cr} = f + \frac{f - 1}{\cos \theta_{int}} \tag{2.16}$$

This is the required condition, in case of an intrinsically hydrophobic surface, to determine the transition between Wenzel and Cassie wetting state. This specific condition has been used to compare our simulation result in order to observe the effect of roughness geometries of the microV-grooved surface on Cassie-Wenzel wetting transition. In this specific surface, Cassie roughness factor (f) has been defined same as other rough surfaces, which is the proportion of solid-liquid contact surface area to the apparent surface area.

$$f = \frac{W_p}{W_p + W_g} \tag{2.17}$$

However, to compare the roughness factor with the critical value, roughness factor (r) for microV-grooved surfaces has been defined by Alen *et al.* [117] as follows:

$$r = \frac{(W_p + (2 \times D_g)) / \cos(\emptyset/2)}{W_p + W_g} \tag{2.18}$$

Where, $\emptyset$ denotes the angle formed between the inclined wall surfaces which intersect at the bottom of the rough surface termed as 'groove angle', which has been formulated as:

$$\varphi = 2 \times \left(\tan^{-1} \left(\frac{W_g}{2 \times D_g} \right) \right) \tag{2.19}$$

Moreover, for droplets deposited on hydrophobic rough wavy substrates, Carbone and Mangialardi presented the critical amplitude height (h_{cr}) of the groove of the wavy surface for no load condition through thermodynamic model, which is as follows [118]:

$$h_{cr} = -(\lambda_w \tan \theta_{int}) / 2\pi \tag{2.20}$$

where, λ_w denotes wavelength of the wavy rough surface.

Critical roughness factor (r_{cr}) for micro V-grooved surfaces from equation 2.16 and critical amplitude height factor (h_{cr}) for micro wavy surfaces from equation 2.20 have been used in this study to compare our simulation results, mainly the Cassie-Wenzel wetting transitions of the droplets on these surfaces. According to the analytical model described above for micro V-grooved surfaces,if the roughness factor r is greater thanr_{cr}, then Cassie droplets should be found and if $r < r_{cr}$, then droplets should exhibit Wenzel wetting states on micro V-grooved surfaces. Similarly, from thermodynamic model of wavy surfaces, amplitude factor, h of our simulation has been compared with critical amplitude height factor (h_{cr}). Wenzel state should be transferred to Cassie state when$h > h_{cr}$ and vice versa. In the next chapter, comparison between these models with our numerical findings will further verify our computational approach.

CHAPTER 03
RESULTS AND DISCUSSION

3.1 Introduction

When the apparent contact angle along the three-phase contact line of the droplet is independent of the viewing orientation i.e., spherical droplet base shape has been developed on the surface, the wetting situation is referred as "isotropic wetting". However, in case of "anisotropic wetting", liquid droplet will spread in a specified direction and will have a distinct apparent contact angle along the contact line of the droplet depending on the viewing conditions. Two sorts of views are utilized to demonstrate this anisotropic wetting situation of the droplet: Orthogonal or front view (across the grooves direction) and Parallel or side view (along the groove direction). Because of the surface roughness properties, orthogonal contact angles are observed higher than the parallel ones in rough substrates such as- pillar patterned, parallel micro-grooved, V-grooved, wavy, chemically striped, and so on [71, 92-107]. Difference between these two apparent contact angles of the droplet is termed as "degree of anisotropy ($\Delta\theta$)" [92, 94, 106]. This degree of anisotropy has a significant impact on the unidirectional spreading of the droplet.

Few studies have experimentally investigated the wettability of liquid drops on micro-machined V-grooved and wavy surfaces with varying surface roughness [104, 107, 119]. Numerical simulations, on the other hand, which allow for the prediction of wettability, relative liquid droplet stability, and degree of anisotropy based on various design factors for these both kinds of surfaces, are currently underutilized, as well as the comparative discussions for the liquid droplets placed on both micro V-grooved and wavy surfaces are still unknown. Generally, from literature it has been observed that the fabrication of micro-grooves with straight edges is quite difficult by different microfabrication processes [98-100]. Most of the cases, inclined walls have been formed rather than proper vertical pillars for various reasons like- tool wear due to continuous passing of cutting tools through the surfaces, edge angle and rise angle formation during the machining processes, etc. That is why microV-grooved type surfaces having inclined pillar walls have been adopted for our thesis work for their ease of micro-fabrication and potential for practical applications with directional wettability. Wettingcharacteristics on this microV-grooved surfaces are then compared with quite similar shaped micro wavy surfaces, in which only the top and bottom portion of the pillars are smooth with no edges and corners. Since edges or corners formation of the rough surfaces will impose similar kind of difficulties like parallel micro-grooved surfaces, smooth continuous rough surfaces like wavy have been employed for further investigation of wettability, more importantly for the comparison with the findings of microV-grooved surfaces wettability. However,wavy surfaces may be exploited for phase change and transport phenomena in a wide variety of applications, including condensation heat exchangers, microfluidics, and desalination for their directional wetting capabilities. Continuous micro-grooved surfaces like wavy surfaces, favored droplet coalescence and sweeping and may considerably increase condensation heat transfer efficiency [107]. Synthetic rice leaf-like wavy surfaces with variable anisotropic wettability are produced, inspired by the hierarchical architectures of rice leaf surfaces [120].

In this study, Surface Evolver, an open-source software, has been used to investigate the anisotropic (i.e., unidirectional spreading of a droplet on the wetted plane) wetting properties as well as the stability of the liquid droplet on micro-scale V-grooved and wavy surfaces, and then compared the wettability characteristics for both rough surface configurations. To begin, the wettability of micro structured surfaces is quantitatively assessed by analyzing the apparent

static contact angle of droplets. The effect of geometric parameters on wetting anisotropy, such as pillar width, groove width, groove height, and so on, is the main focus of this research. Using micro-patterned surfaces with both micro V-grooved and wavy surfaces, the influence of droplet volume on perceived static contact angle is explored. Following that, a numerical technique for quantifying the relative stability of a droplet's metastable states is demonstrated. The relative stabilities of metastable droplets with different volumes under various wetting configurations are compared using a normalized form of the interfacial surface energy [73, 79, 80]. The numerical studies for the examination of apparent static contact angle and relative stabilities are then extrapolated to compare the quality of wetting on micro V-grooved and micro-wavy surfaces in order to determine the optimum surface topography for directional or anisotropic wetting design.

3.2 Analysis of Droplet Energetics

The energetics of droplets are investigated by examining how a liquid droplet's shape and energy alter as a function of droplet size or volume and surface roughness. Our research focuses on micro wavy and microV-grooved surfaces. Also, because we restricted our research to microdroplets, the gravitational effect is neglected in all scenarios involving droplet simulation. The interfacial surface energy that must be decreased to obtain an equilibrium droplet shape can be written from equation 2.6 of the previous chapter:

$$G = \gamma_{LA} \left[A_{LA} - \iint_{A_{LS}} \cos\theta_{int} \ dA \right]$$

If V denotes volume of the liquid droplet, then the aforementioned interfacial surface energy can be expressed in the following way as a normalized form [73]:

$$G_{norm} = G \Big/ \gamma_{LA} \left(V^{2/3} \right) \tag{3.1}$$

At first, let us discuss the energy and stability of liquid droplet on smooth flat surfaces. Promraksa*et al.* investigated the possibility of numerous metastable states of water droplets

displaying wetting on micropatterned surfaces [75]. It is convenient to compare this dimensionless energy called "normalized energy" (G_{norm}) of all the metastable drops of different volumes when studying their respective stabilities. The dimensionless number describes a drop shape's equilibrium state. Consistent value of G_{norm} has been observed for various quantities of liquid under identical wetting conditions. When considering a sessile liquid droplet on a smooth surface, for example, normalized energy (G_{norm}) is found to be a function of intrinsic contact angle only. Figure 3.1 and 3.2 shows that regardless of the droplet sizes on the smooth surface, it always spreads out throughout the entire surface, supporting the equilibrium contact angle with invariant normalized energy (G_{norm}). For a specific intrinsic contact angle of 80° (hydrophilic) and 111° (hydrophobic), normalized energy has a fixed value of 3.48 and 4.41, respectively, for all droplet volumes on smooth flat surfaces, as illustrated in Figure 3.1. From this graphical illustration, it is clear that normalized energy value will be higher for larger intrinsic contact angles, i.e., lower surface energy will represent higher normalized energy value. Figure 3.2 depicts the scenario of droplet spreading on both of these hydrophilic and hydrophobic flat surfaces for two different droplet sizes (1 μL, and 4 μL). The equilibrium droplet's bottom view is shown below the front views of the corresponding droplet, revealing that the apparent contact angle and stipulated intrinsic contact angle are of the same values in all situations. For all numerical calculations from Surface Evolver simulation, the surface tension for the water-air interface, i.e., γ_{LA}, is assumed to be 0.072 N/m at 25℃. These findings have also mimicked the results of Anjan *et al.*, where they observed similar independent behavior of droplet's normalized energy with intrinsic contact angle of 120° of smooth surface for different sizes of droplet [79].
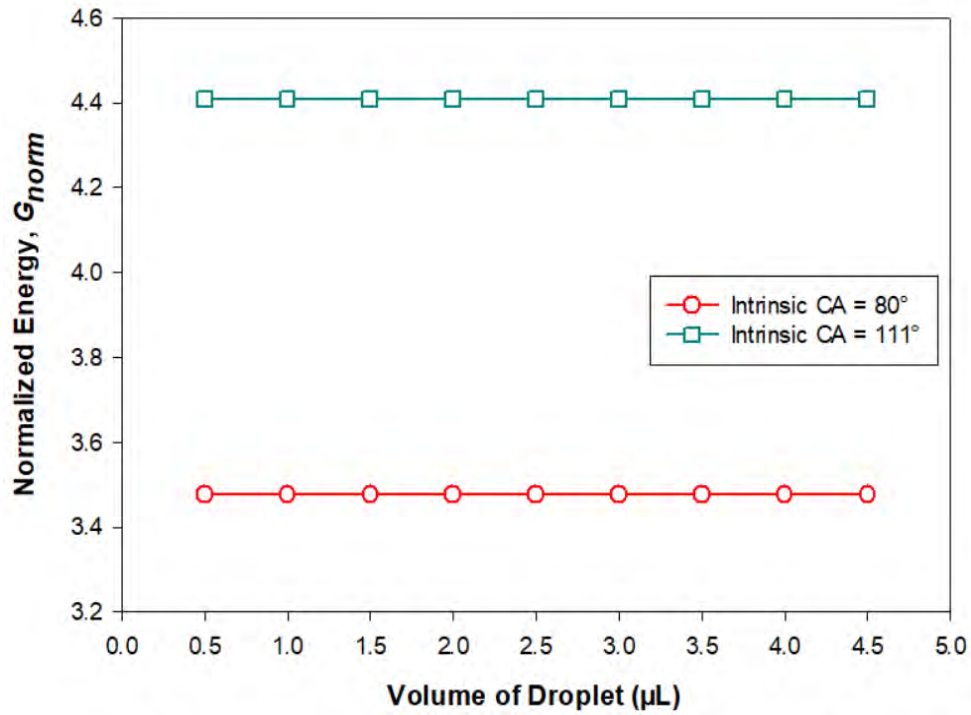
Figure 3.1: Normalized energy value of a sessile liquid droplet with the variation of droplet volumes on hydrophobic (intrinsic contact angle = 111°) and hydrophilic (intrinsic contact angle = 80°) smooth flat surfaces.

Front View	Bottom View	Droplet Size (Intrinsic CA)
		1 μL (80°)
		4 μL (80°)
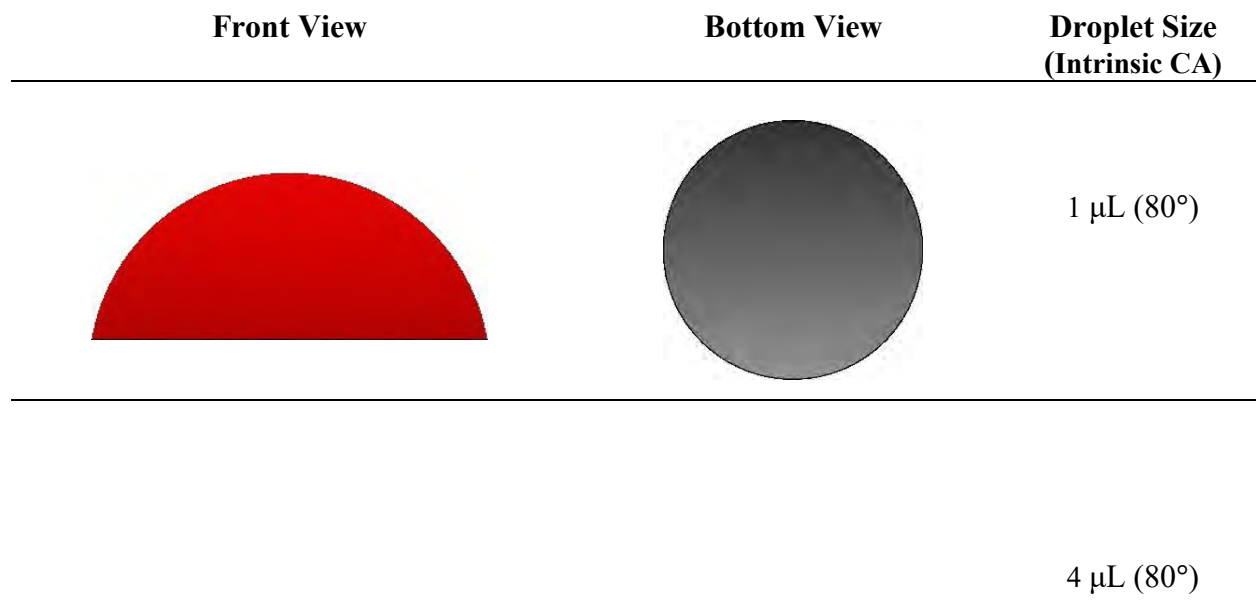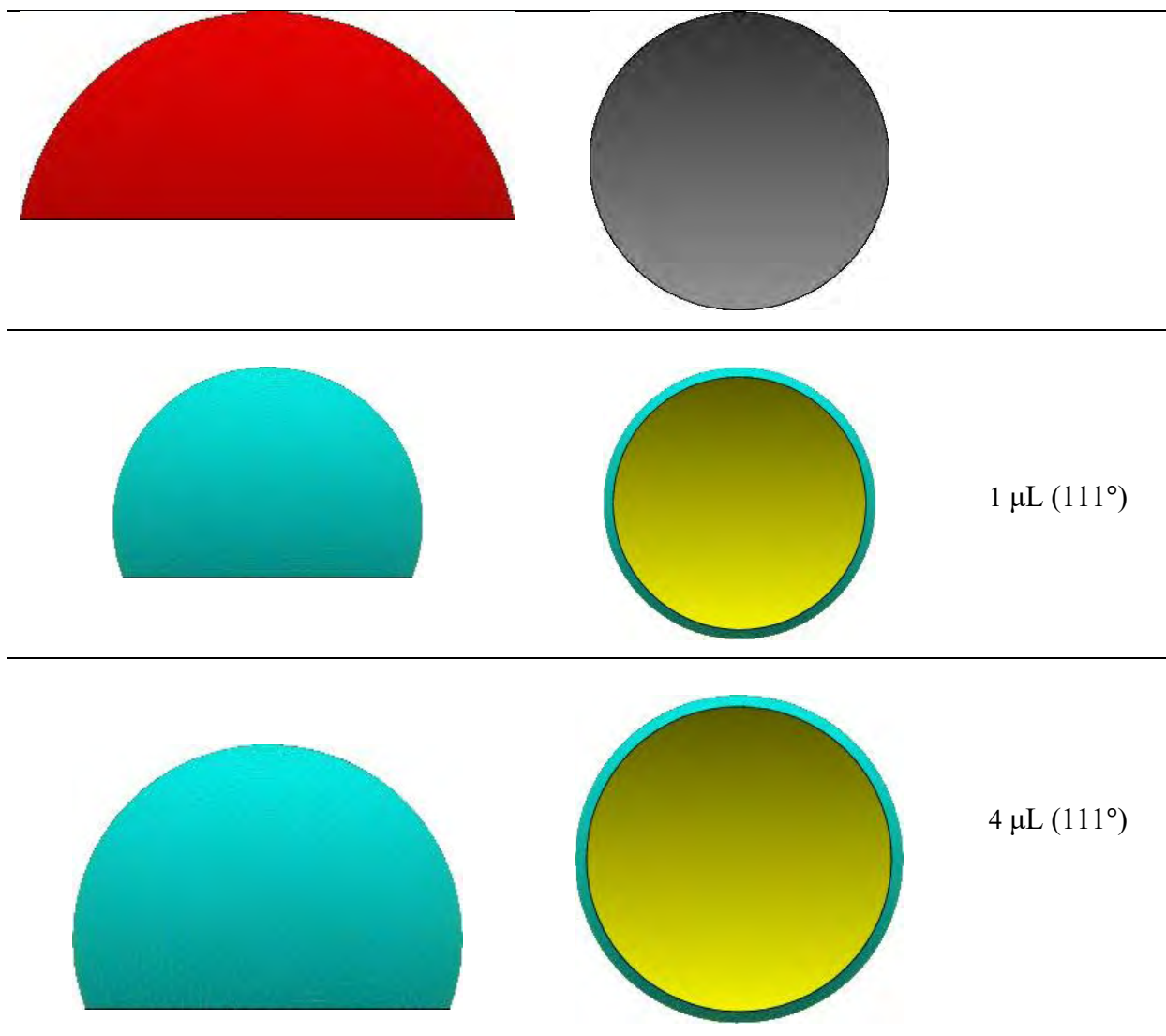
Figure 3.2: Front and bottom views of equilibrium water droplets of 1 μL and 4 μL for both hydrophobic and hydrophilic smooth flat surfaces.

However, for micro structured surfaces made of any kinds of materials, which have various types of roughness, normalized energy of the droplets does not exhibit the volume independency. Relative stability along with the most stable form of the droplet can be then easily determined from those values, which will be discussed in the next sections for our two different types of rough surfaces.

3.2.1 Effect of Droplet Volume on Droplet Energetics for MicroV-Grooved and Micro Wavy Surfaces

Figure 3.3 illustrates a liquid droplet demonstrating anisotropic wetting over a rough surface with microV-grooves and micro wavy grooves, where the intrinsic contact angle of the solid surface is 111°. This specific surface property along with the quantifications of pillar width, groove width, and groove height are set based on those found in an experimental investigation described in the literature for an identical wetting condition for microV-grooved surfaces, for justification of the surface design that confirms anisotropic wetting state [104], as specified in all three series of Table 2.1 ($D_g{}^{80}W_g{}^{98}W_p{}^4$). Then for comparison with microV-grooved surface wetting, these roughness geometries have been maintained the same in the case of micro wavy surfaces ($H_w{}^{80}\lambda_w{}^{98}$). For both rough surfaces, droplet volumes are restricted within 5 µL in our study to retain sessile droplets. By constraining the left and right edges of the droplet on the pillar of the surfaces, directional wetting has been maintained underneath the droplet, as a confined three-phase contact line cannot cross the boundary edges of the two outermost pillars, which have been defined in the simulation coding. In our overall simulations, mainly surface configurations consisting of six and eight pillars have been employed. Droplets of varied sizes or volumes have developed distinct metastable structures while simulations have been carried out.

(a)   (b)

| (c) | (d) |
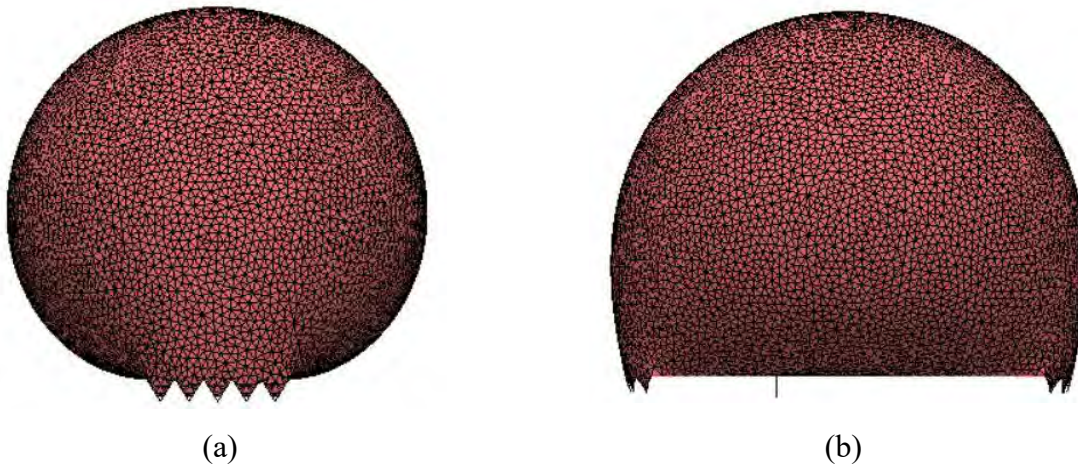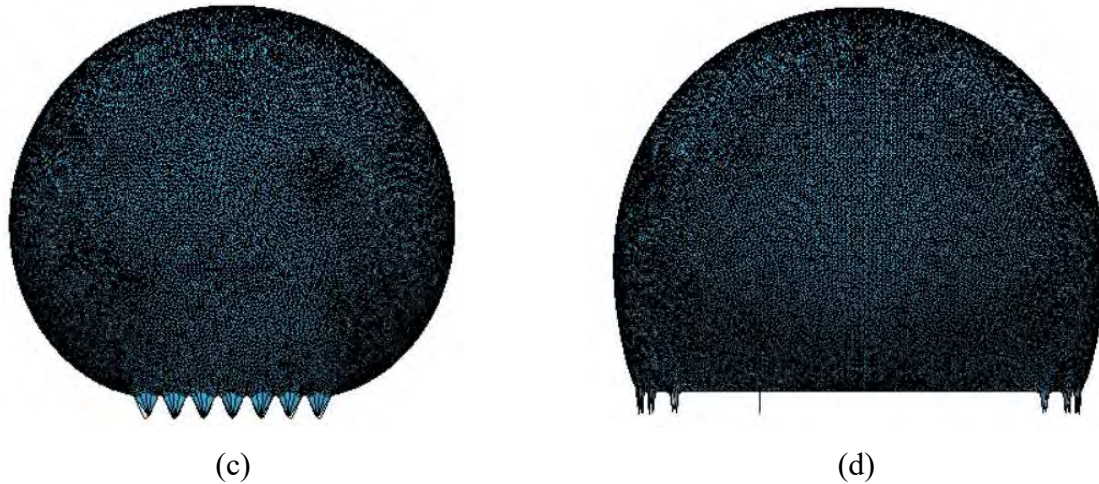
Figure 3.3: Front (across the groove direction) and side (along the groove direction) views of simulated droplets placed on rough surfaces, where different apparent contact angles from different viewing directions confirms the anisotropic wetting: (a) Front view and (b) side view of the droplet sitting on micro V-grooved surface of six pillars; (c) Front view and (d) side view of a droplet residing on micro wavy surface of eight pillars.

The total and normalized energy of the droplets are displayed as a function of volume in Figure 3.4 and Figure 3.5 for both of the micro-structured surfaces. For all situations, total energy grows continually with droplet sizes; however, the normalized energy hits a minimum around a particular volume for each of the wetting configurations. The steady droplet shape corresponds to this normalized energy minimum. As previously stated, the droplet form is metastable in any other volume.
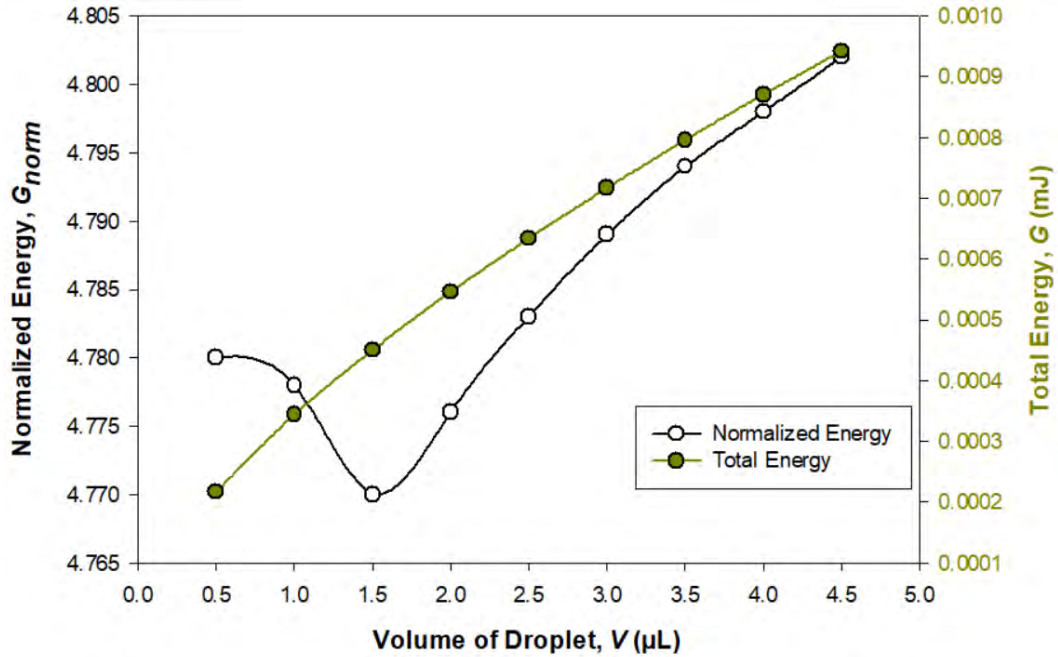
(a)
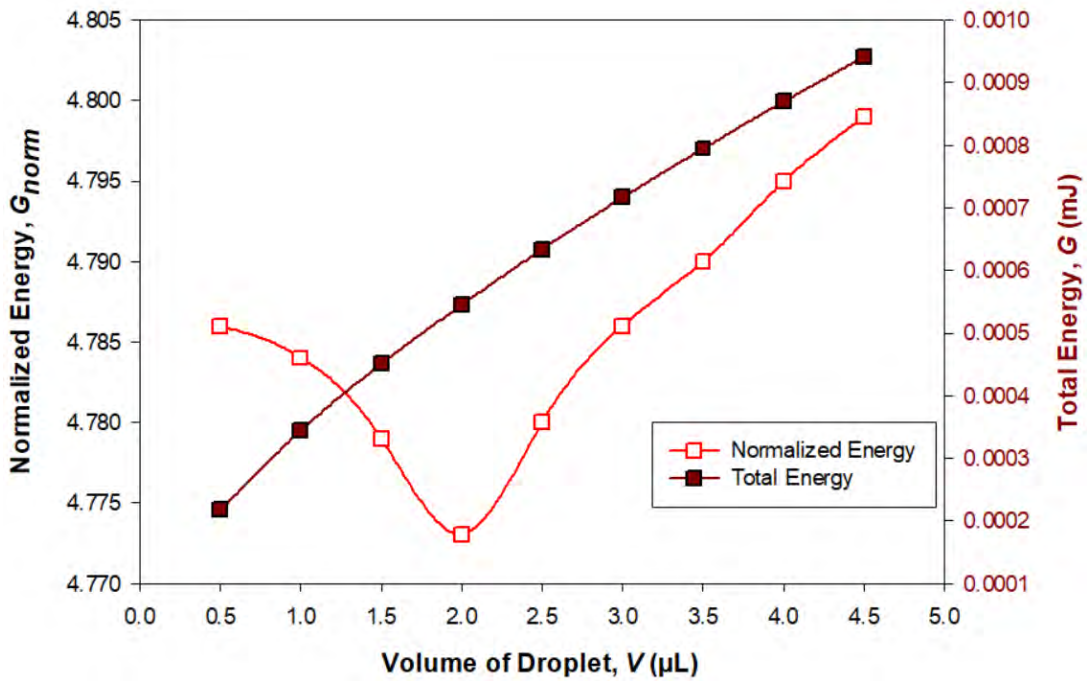
(b)

Figure 3.4: Variation of total and normalized energy of droplets deposited on (a) six pillars and, (b) eight pillars as a function of droplet volumeon micro V-grooved surfaces.
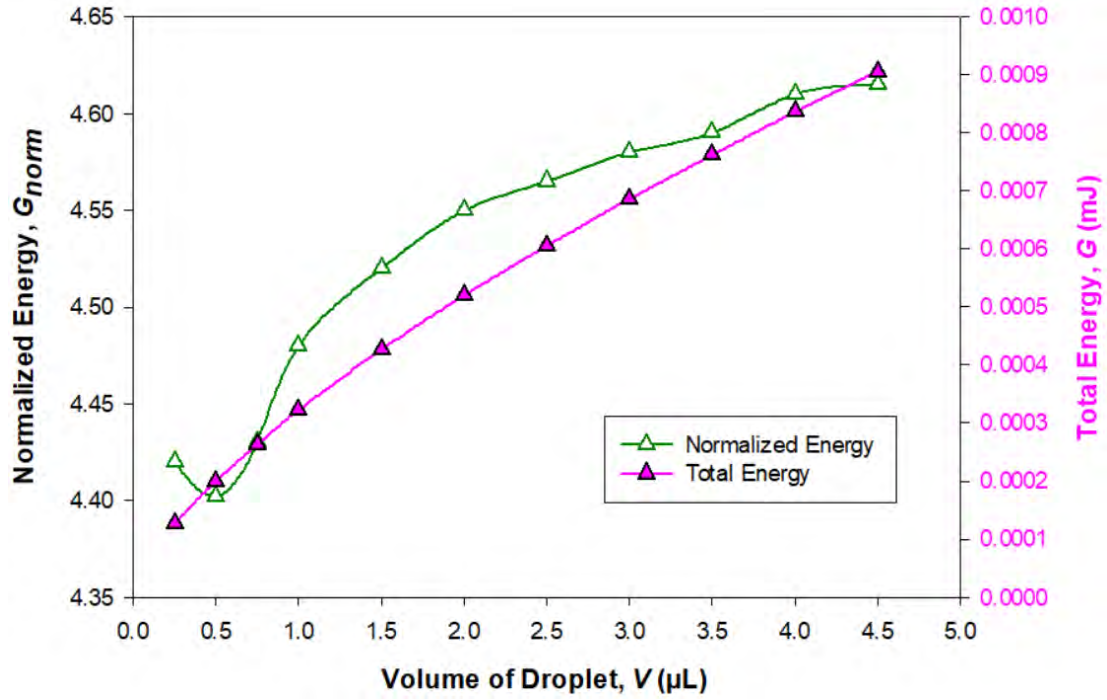
(a)
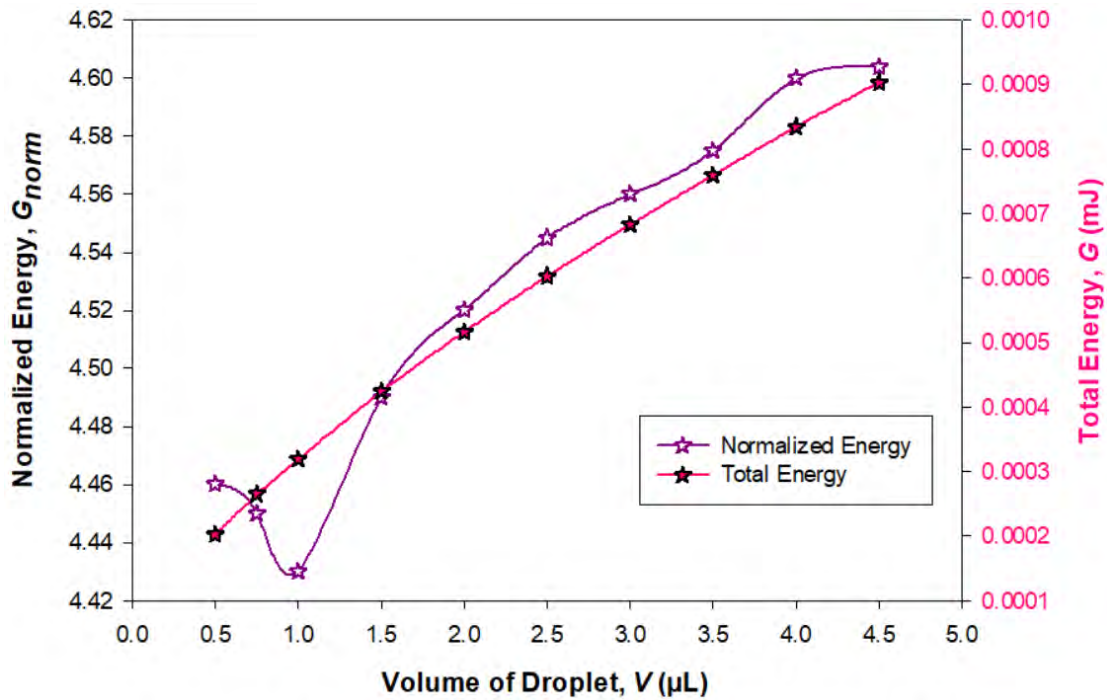
(b)

Figure 3.5: Variation of total and normalized energy of droplets deposited on (a) six pillars and, (b) eight pillars as a function of droplet volume on micro wavy surfaces.

There is a straight proportional relationship between total interfacial energy and droplet sizes or volume for droplets on six pillars, eight pillars, and ten pillars on micro V-grooved surfaces, although normalized energy (G_{norm}) reaches its lowest around the droplet volume of 1.5 µL, 2 µL, and 3 µL, respectively (Figure 3.6 (a)). This minimum normalized energy (G_{norm})corresponds to the stable droplet on these micro V-grooved surfaces.

For arrangements with more pillars, the normalized energies are lower than those for designs with fewer pillars for a larger size of the liquid droplet. In addition, a larger droplet necessitates more supports beneath it to be stable. The volume of the stable droplet grows from 1.5 µL to 3.0 µL as the no. of pillars carrying the liquid droplet rises from six to ten pillars for the given micro-Si surface (θ_{int} = 111°). By comparing the normalized energy of liquid droplets of various sizes on micro V-grooved surfaces, the relative stabilities of the droplets can be calculated. Anjan *et al.* for surfaces with parallel microgrooves and micro-pillared structures also observed that for larger droplets, higher pillar configurations were required to be in the stable state [79, 80].

Furthermore, similar tendencies have been identified for micro wavy surfaces for different anisotropic configurations (Figure 3.6 (b)). However, 0.5 µL for a droplet on six pillars, 1 µL for a droplet on eight pillars and 2 µL for a droplet on ten pillars have been observed as stable equilibrium droplets. Because the peak of the surface is curved and there is no edge like on a micro V-grooved surface, droplets on micro wavy surfaces have a more unstable or metastable tendency for larger droplet volumes. As a result, for the identical pillar configurations, the smallest normalized energy was observed in very small droplets for micro wavy surfaces. Also, the minimum normalized energy for droplets on micro wavy surfaces is substantially lower than for droplets on micro V-grooved surfaces (Normalized energies (G_{norm}) are 4.40, 4.43, 4.45 for droplets on six, eight and ten pillars, respectively for micro wavy surfaces, and 4.77, 4.773 and 4.78 for droplet on six, eight and ten pillars, respectively for micro V-grooved surfaces). Lower stable droplet size and non-pinning effect for smooth curved peak surface on the micro wavy surface may have played a major role in these results.

The stable liquid droplets of these various anisotropic configurations for micro V-grooved and micro wavy surfaces have been illustrated in Figure 3.7 from two prescribed views or directions.
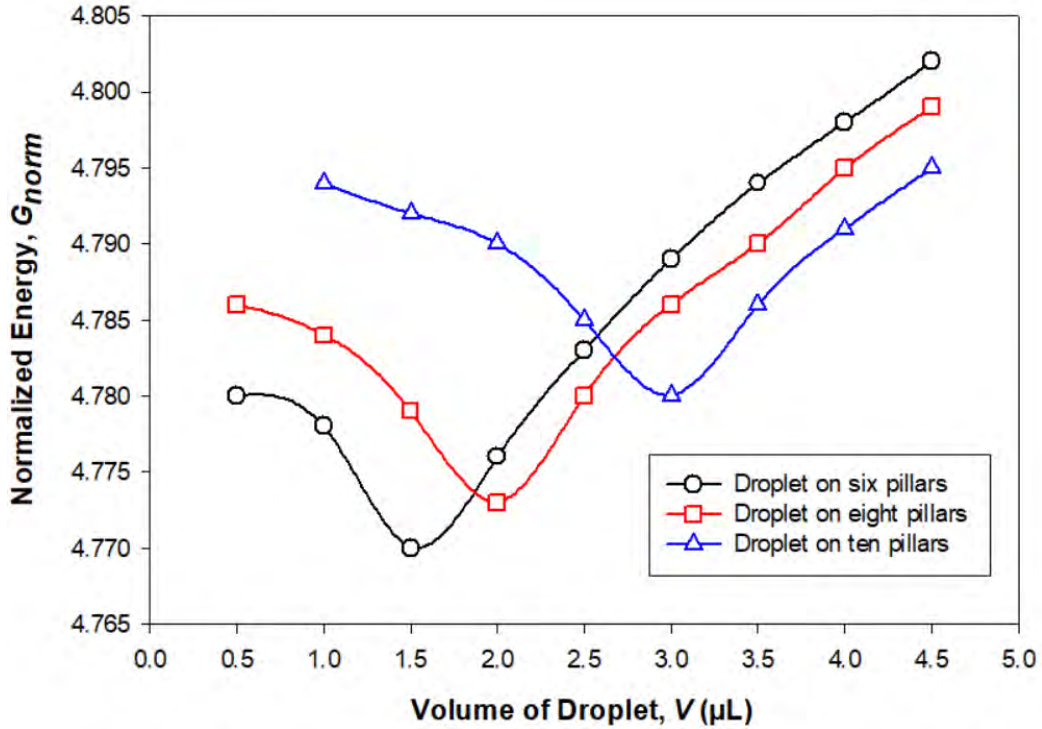
(a)
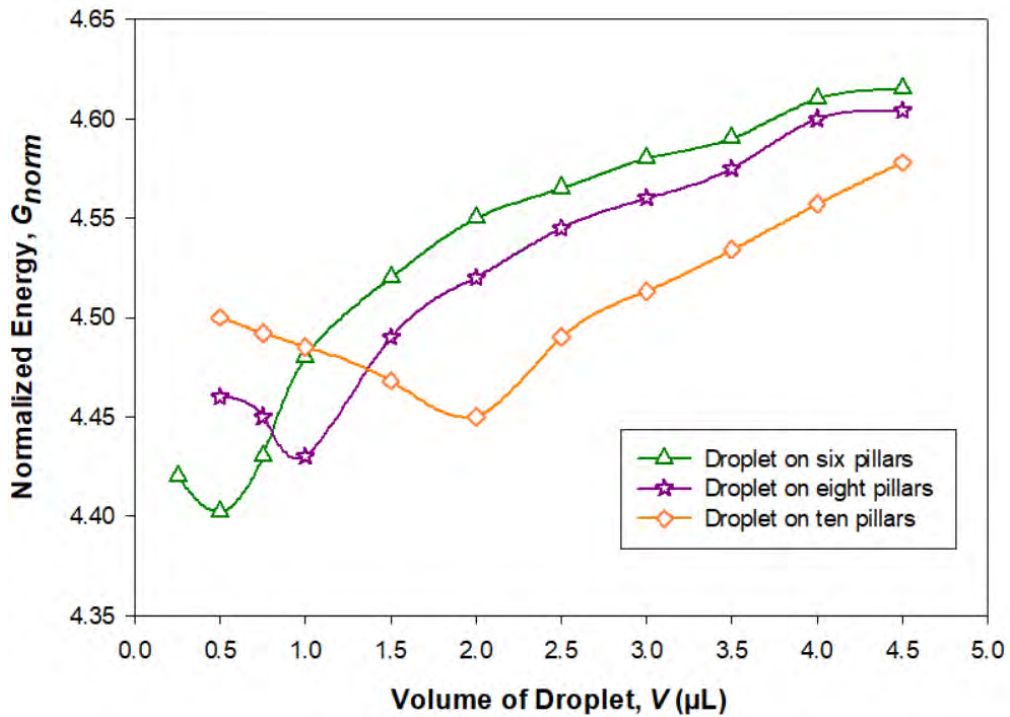
(b)

Figure 3.6: Variation of normalized energy of droplets of different anisotropic wetting configurations on (a) micro V-grooved surface and, (b) micro wavy surface.
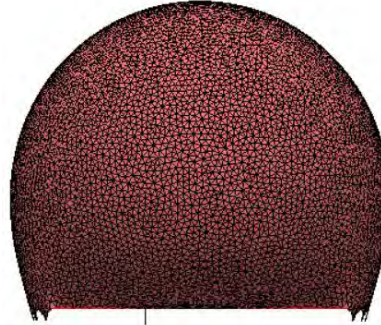
Front or Orthogonal View	**Side or Parallel view**	
		1.5 μL droplet on six pillars of micro V-grooved surface
		2 μL droplet on eight pillars of micro V-grooved surface
		0.5 μL droplet on six pillars of micro wavy surface
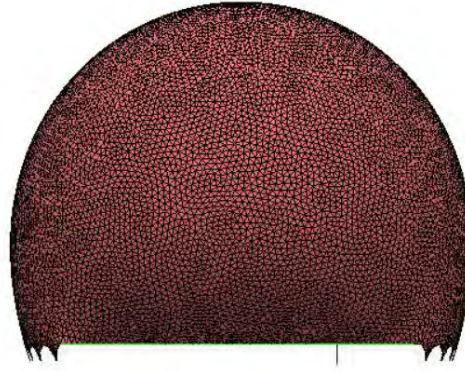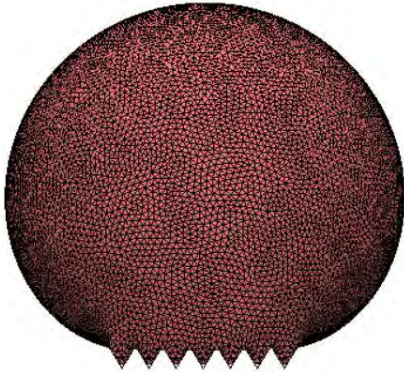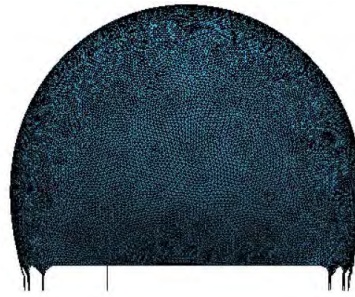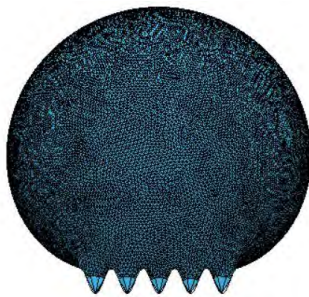
Figure 3.7: Stable simulated droplet shapes for different anisotropic configurations on micro V-grooved and micro wavy surfaces [All droplet figures are not presented at same scale here].

However, from the variation of normalized energies for different volumes of droplet as displayed in Figure 3.6, it has been found that when two curves overlap, they deviate in such a way that for further growth in droplet volume, the configuration with larger pillar numbers will be preferred for droplet stability, as seen by significantly minimized normalized energy values for that arrangement, since the droplet configuration with smallest normalized energy is favored for constant volume of the droplet.

It is known from the earlier discussion (Section 1.4.1) that by increasing the volume of the droplet gradually, a liquid metastable droplet will be formed by advancing front. But as we constrained liquid droplet to stay within the given number of pillars, it will be pinned at the outer edges of the pillar of one rough surface configuration, while acquiring more volume under no gravitational effect. So, regardless of the droplet's size, it will remain in that configuration. For the droplet's contact line to advance, the liquid must be forced to come into touch with the new arrangement. When the liquid comes into touch with new pillars, the droplet's energy is reduced, and the droplet changes shape. As a result, for two consecutive configurations, higher number of pillared surface configuration gives lesser normalized energy values after the overlapping of the curves, as illustrated in Figure 3.6. Thus, for larger droplet volume, transitioning from one anisotropic configuration to the next anisotropic configuration is favored while the spreading is restricted to be unidirectional because the energy required for unidirectional spreading of the droplet is higher in comparison to the energy necessary for transition to the next anisotropic configuration.

81

3.3 Analysis of Contact Angle

The apparent contact angle gives the idea of the wettability of the surfaces upon which the liquid droplet is placed. Surface isotropy/anisotropy can be identified from the contact angles of various shape of the droplets. This study focuses on the examination of contact angle of stationary droplets on rough substrates because of the gentle droplet deposition on the surface. Wetting phenomena on micro V-grooved surfaces are explored first, followed by substrates patterned with micro wavy grooves. After that, wettability comparison between these two micro-structured surfaces will be discussed thoroughly. For the samples stated in Table 2.1, the effect of surface roughness on contact angle and the droplet volume dependency of contact angle are explored.

3.3.1 Effect of Droplet Volume on the Contact Angle for Micro V-Grooved and Micro Wavy Surfaces

Although numerical studies on the wettability of parallel rectangular micro-grooved surfaces have been extensively explored in addition to experimental investigations, there is a considerable lack of such studies on micro V-grooved and wavy surfaces. Geometric parameters similar to those of the experimental study of Li *et al.* which have been specified in the previous chapter (Section 2.4), are used for our simulation work of micro V-grooved surfaces, [104]. After that, to compare the findings for micro V-grooved surfaces with micro wavy surface, same surface roughness parameters have been maintained.

In micro wavy and V-grooved surfaces, the Wenzel wetting state has been detected in all droplet sizes observed in our numerical study within 5 µL for sample surface "$D_g{}^{80}W_g{}^{98}W_p{}^4$" or $H_w{}^{80}\lambda_w{}^{98}$. For this micro V-grooved surface structure, Wenzel wetting state is also matched with the analytic model provided earlier in this chapter in equation 2.16. Because critical

roughness factor (r_{cr}) value for our surface model is 2.72, whereas the roughness factor of our micro V-grooved surface (r) is 1.89, which is substantially lower than r_{cr}. And in the case of micro wavy surface configuration, the critical amplitude height (h_{cr}) has been played the significant role for the observed wetting state. Due to the 80 μm groove height of the surface, amplitude height is 40 μm which is half of the groove height (H_w) of the wavy surface. This is also smaller than the required amplitude height of 40.9 μm, obtained from equation 2.20. That is why, in micro wavy surface arrangement, Wenzel wetting state has also been observed for droplets.In all our simulations, the orthogonal contact angle is greater than the parallel contact angle. This trend has been identified as a common phenomenon in case of anisotropic wetting situations for all droplets lying on rough surfaces, as reported in a number of previous studies[71, 92-107]. The fundamental explanation for this conclusion is the pinning effect of the three-phase contact line, which causes the free energy barrier (FEB) along the perpendicular direction of the grooves to be bigger than along the parallel direction.

The results shown in Figure 3.8 demonstrate that in case of micro V-grooved surfaces, for higher volume of droplets, parallel contact angles are rapidly decreasing, but very slight increment has been attained in orthogonal contact angles for those droplets. Orthogonal contact angles increase from 149.3° to 153.4° (increment of4.1°) for six pillar configurations and from 144.2° to 147.3° (increment of3.1°) for eight pillar setups over the range of 0.5 μL to 4.5 μL droplets beneath micro V-grooved surfaces, while parallel contact angles decrease from 108.5° to 98.2° (decrement of 10.3°) for six pillar configurations. Figure 3.11 depicts the lowest and highest droplet sizes in front and side views to effectively highlight these variations.Water droplets move down the pillars, filling and spreading along the grooves, according to the mechanics of Wenzel wetting. Since the wetting state of our droplets here in Wenzel regardless of the droplet size, when droplet size increases, the droplets stretch further along the grooves, resulting in nearly constant droplet height for this wetting condition with the change in droplet size. However, as the size of the droplet becomes larger, the parallel contact angle decreases due to the lack of pinning by the groove edges along the grooves. As a result, droplets only need to overcome surface tension, which explains why the three-phase contact line progresses down the groove as the droplet volume increases. The almost consistent height of the Wenzel droplets across this 4 μL range of droplet volumes in Figure 3.10 further supports these observations.

83
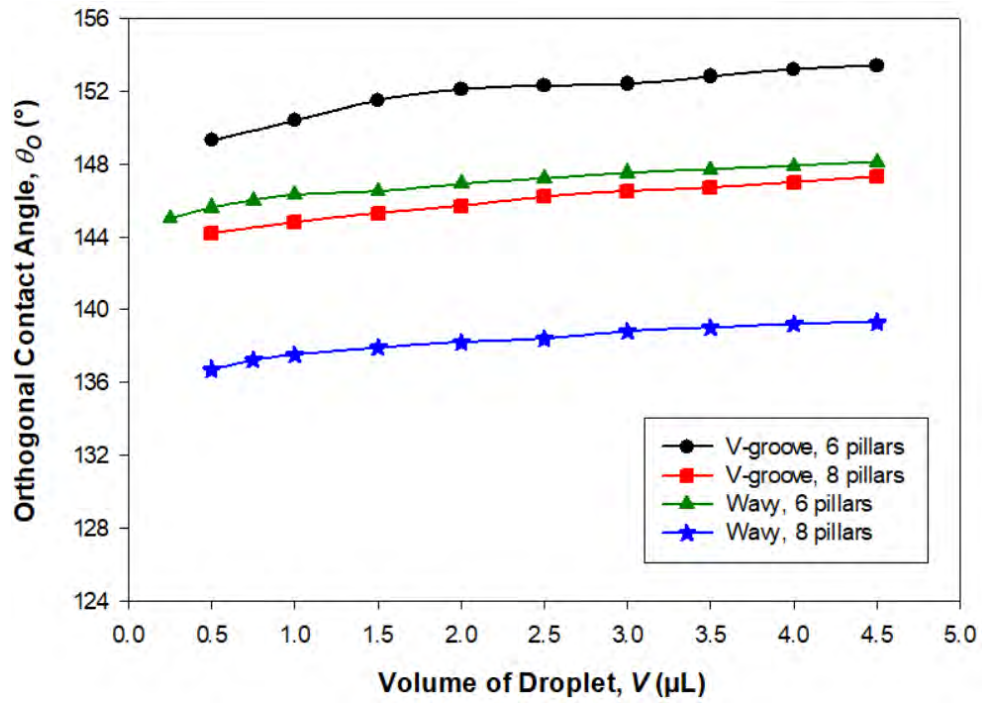
(a)
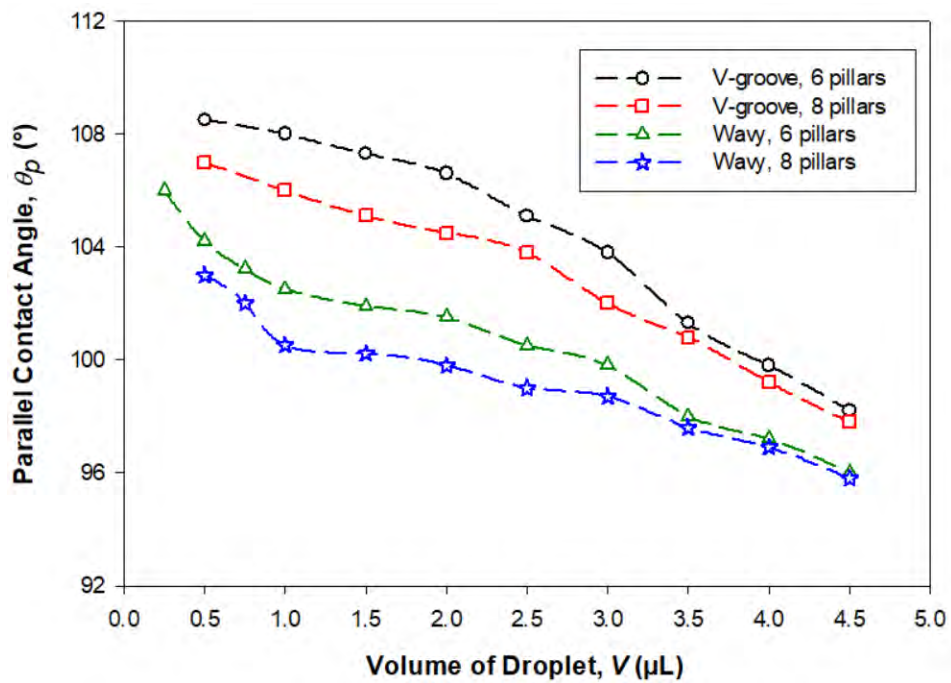
(b)

Figure 3.8: Variation of apparent (a) orthogonal and (b) parallel contact angles of droplets of

Droplets on the wavy surface, on the other hand, show more advancement along the grooves for larger droplet volume and less increment in orthogonal contact angle. Because of no sharp-edged corner at the peak of the wavy surfaces, pinning effect is reasonably less effective than micro V-grooved surfaces. As a result, orthogonal contact angles are found to be smaller for the micro wavy surface configurations than the same for the micro V-grooved ones. Therefore, increasing the volume of the droplet distributes the water farther along the grooves, resulting in a decrease in parallel contact angles. Other trends and demonstrations for droplets on micro wavy surfaces illustrated in Figures 3.8 to 3.11, arefound for the same reasons that have beenexplained for the micro V-grooved surface configurations throughout this section.

Moreover, it is clear from the values of orthogonal and parallel contact angles (Figure 3.8) found for droplets on both micro V-grooved and wavy surfaces that"degree of anisotropy" ($\Delta\theta = \theta_o - \theta_p$for a given volume of droplet) is getting higher for thelarger droplet size on these surfaces (Figure 3.9). Spreading of the droplet along the grooves is mainly responsible for this higher anisotropy for larger droplets, as orthogonal contact angles do not considerably increase in contrast to the reduction rate of the parallel CA for adding more liquid.

In Figure 3.10, variation of the droplet heights (taken from pillar valley or bottom of the surface) has been displayed with the change of droplet size for three samples of micro V-grooved surfaces (six and eight pillared $D_g{}^{80}W_g{}^{98}W_p{}^4$, and eight pillared $D_g{}^{150}W_g{}^{98}W_p{}^4$) and three samples of micro wavy surfaces (six and eight pillared $H_w{}^{80}\lambda_w{}^{98}$, and eight pillared $H_w{}^{150}\lambda_w{}^{98}$). It has already been found that both six and eight pillared $D_g{}^{80}W_g{}^{98}W_p{}^4$ and $H_w{}^{80}\lambda_w{}^{98}$ sample surface configurations demonstrate Wenzel wetting states for all sizes of droplets. Usually, these Wenzel droplets does not vary with the increment of droplet volume. Average heights of these Wenzel droplets are around 1.3 mm and 1.085 mm on micro V-grooved surfaces ($D_g{}^{80}W_g{}^{98}W_p{}^4$) with six and eight pillar configurations respectively and 1.097 mm and 0.96 mm on micro wavy surfaces ($H_w{}^{80}\lambda_w{}^{98}$) with six and eight pillar configurations, respectively. Adding more liquid to the Wenzel droplet resulted in the droplet elongating along

the grooves rather than rising in height, which resulting of almost constant droplet height for different droplet volumes. However, this is not the case with Cassie droplets, height of which are almost 1.6-1.8 times than that of Wenzel droplets. Furthermore, when the volume of the droplet increases, the heights of the Cassie droplets are also growing. Because for Cassie wetting states, further addition of volume to the droplets does not significantly prolong the droplet along the groove direction, but it does increase the orthogonal contact angles at much higher rate. As a consequence, height of the droplet in Cassie state is found to increase with droplet size, which have been observed for $D_g{}^{150}W_g{}^{98}W_p{}^4$ sample of micro V-grooved surface (1.708 mm to 2.1 mm) and $H_w{}^{150}\lambda_w{}^{98}$ sample of micro wavy surfaces (1.51 mm to 1.756 mm). These findings corroborate the experimental results of Rahman *et al.* [99].
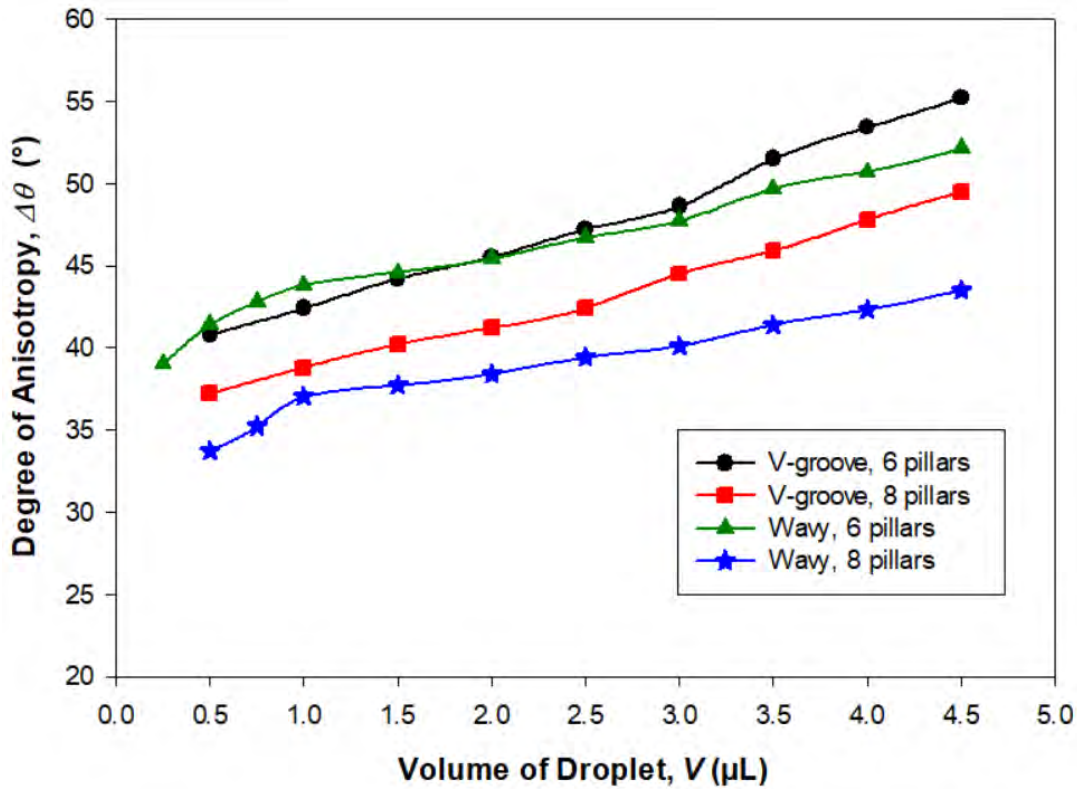
Figure 3.9: Effect of Wenzel droplet volumes on degree of anisotropy for both micro V-grooved and micro wavy surfaces.

Moreover, the orthogonal contact angle is larger for the sample surface when the droplet dwells on a fewer number of pillars for a fixed volume of droplet, as shown in Figure 3.8 (a). For a

particular droplet size, the orthogonal contact angle decreases as the number of pillars on which the droplet is put increases. This is due to the fact that the droplet has to overcome a lower energy barrier at the outer pillar edges for a greater number of pillars. Thus, it has a lesser pinning impact than a droplet on a smaller number of pillars. From droplet energetics we have also observed that, increasing the droplet volume under zero-gravity circumstances will merely increase the contact angle if the droplet is restricted or pinned to the side of the micro pillars because of the higher energy barrier to move to the pillars of the next configuration. And for a given volume of droplet, normalized energy is lower with higher number of pillars configuration than the configuration with smaller number of pillars, which results in a higher orthogonal contact angle for lower number of pillars configurations, which is similar to Anjan *et al.*'s findings for CB state droplets [79, 80]. That is why, for instance, orthogonal contact angles are 151.5° and 145.3° for six and eight pillars of micro V-grooved surfaces respectively and 146.5° and 137.9° for six and eight pillars of micro wavy surfaces respectively, for 1.5 µL droplet.This type of dependency of contact angle on the number of grooves has also been described in computational work of Dokowicz and Nowicki through morphological transitions of droplets [121].
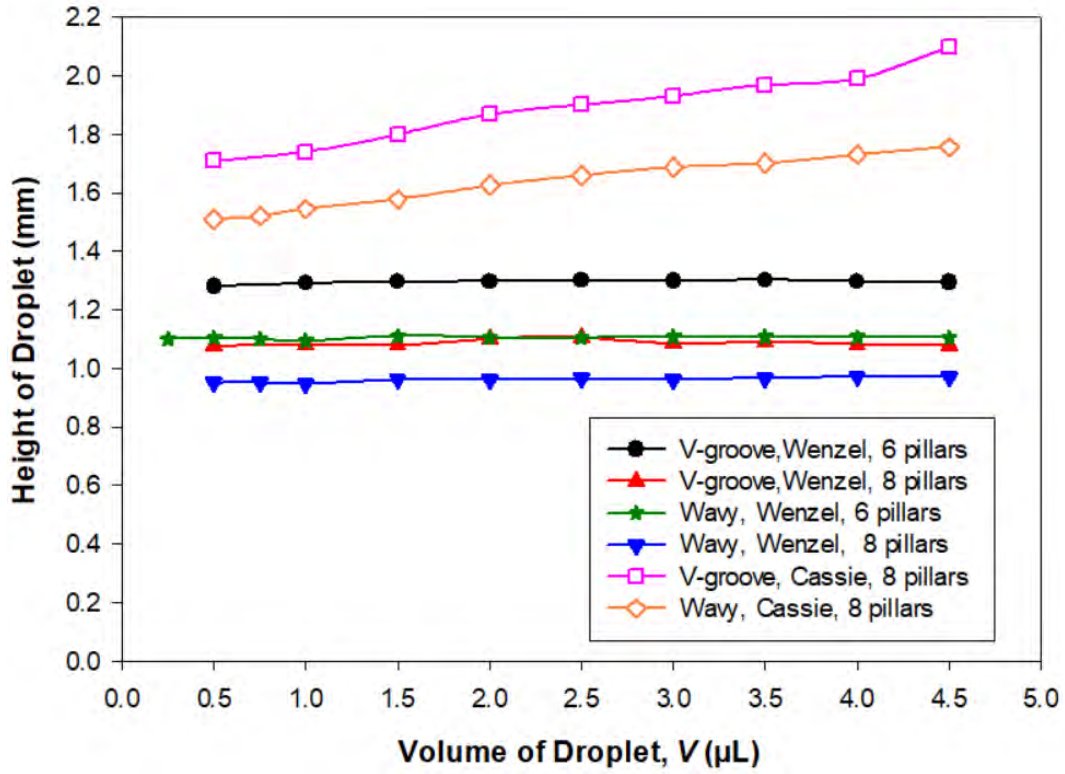
Figure 3.10: Variation and comparison of height of the droplets of different volumes on micro V-grooved and micro wavy surfaces. Non-filled data points refer to Cassie wetting.

Front or Orthogonal View

Side or Parallel View

0.5 µL

$\theta_o = 149.3°$

0.5 µL

$\theta_p = 108.5°$
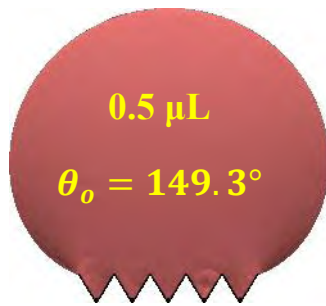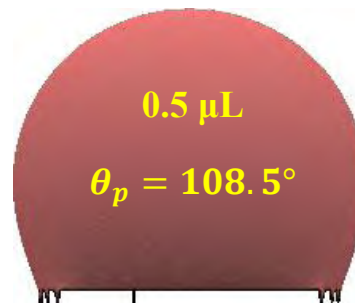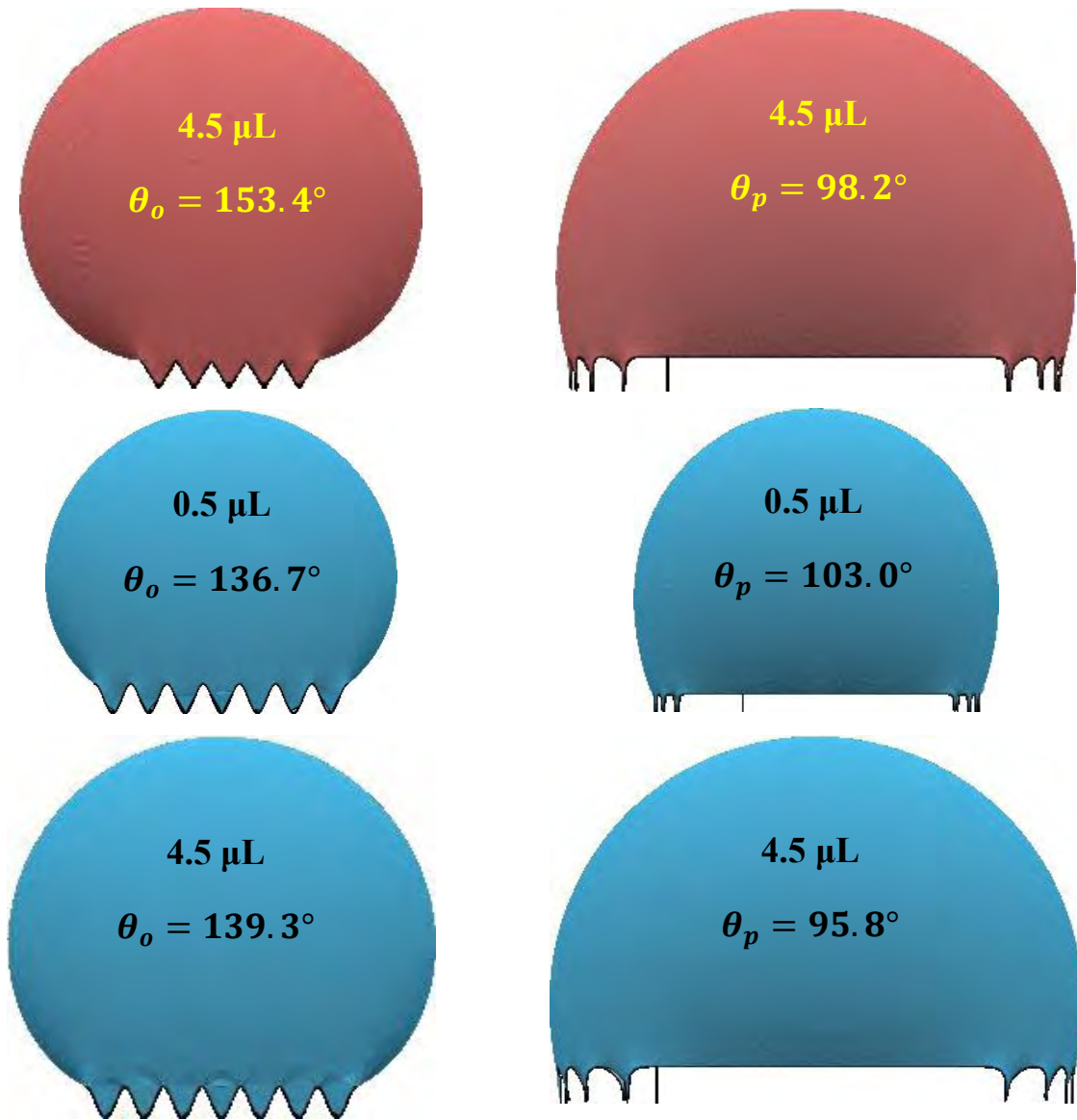
Figure 3.11: Front and side views of smallest (0.5 µL) and largest (4.5 µL) droplets on both micro V-grooved (brick red) and micro wavy (light blue) surfaces along with their apparent orthogonal (θ_o) and parallel (θ_p) contact angles.

The noticeable variation in the shape and spreading of the droplets along the grooves as well as in apparent contact angle for both micro V-grooved and micro wavy surfaces have been quantified by determining the length and width at the droplet base over the specified range of droplet volumes. The length (B) and width (A) of the droplet can be measured from the parallel direction of the grooves or along the grooves (side view of droplet) and orthogonal direction of the grooves or across the grooves (front view of droplet), respectively (Figure 3.12). The ratio

of the length of the droplet to the width of the droplet is termed as "droplet expansion ratio" $(R = {}^B/_A)$.

(a)   (b)
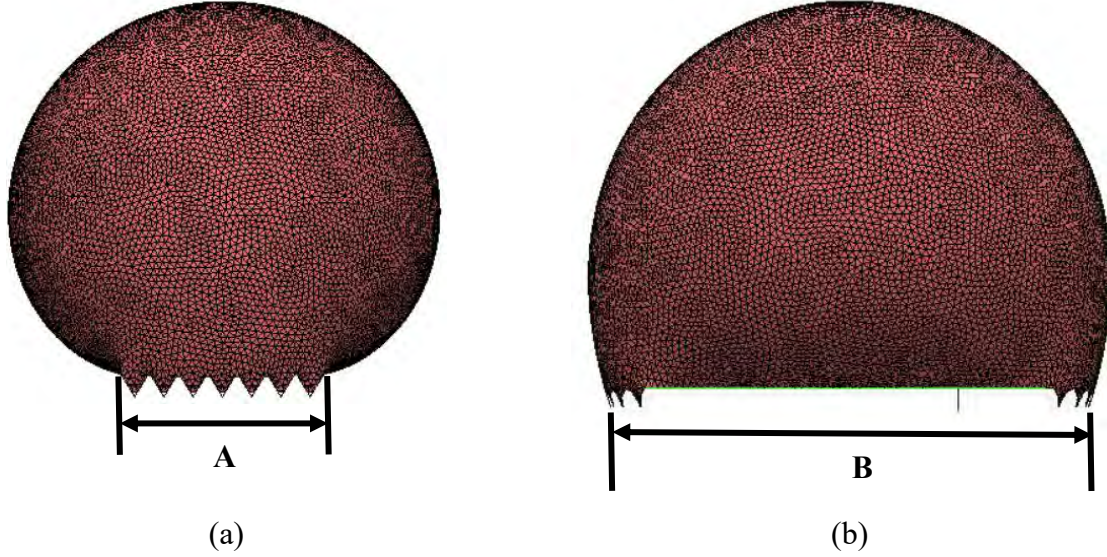
Figure 3.12: (a) Front view (across the grooves direction), and (b) side view (along the groove direction) of the droplet. Here, A and B denotes the width and length of the droplet at the base measured in front and side views respectively.

Figure 3.13 illustrates the relationship between the droplet expansion ratio (R) and droplet size for two microV-grooved surface samples ($D_g{}^{80}W_g{}^{98}W_p{}^4$ and $D_g{}^{150}W_g{}^{98}W_p{}^4$) and two micro wavy surface samples ($H_w{}^{80}\lambda_w{}^{98}$ and $H_w{}^{150}\lambda_w{}^{98}$) with eight pillar configurations. In this case, two samples ($D_g{}^{80}W_g{}^{98}W_p{}^4$ and $H_w{}^{80}\lambda_w{}^{98}$) showed Wenzel wetting (denoted by filled data points) and another two ($D_g{}^{150}W_g{}^{98}W_p{}^4$ and $H_w{}^{150}\lambda_w{}^{98}$) exhibit the Cassie state (represented by non-filled data points). This ratio of expansion (R) for Cassie droplets has been almost constant, whereas for Wenzel droplets, the values of this ratio has been significantly risen with droplet size. For $D_g{}^{80}W_g{}^{98}W_p{}^4$ and $H_w{}^{80}\lambda_w{}^{98}$ samples, this expansion ratio has increased from 2.4 to 3.43 and from 2.0 to 2.55, respectively, because of the Wenzel droplets. However, for Cassie droplets found in $D_g{}^{150}W_g{}^{98}W_p{}^4$ and $H_w{}^{150}\lambda_w{}^{98}$ samples, the value of R is almost constant on around 1.47 and 1.42, respectively. This happens due to the spreading of droplets along the grooves. From the simulation methodology in Chapter 2, it has been already known that the two outermost edges (left and right edges) of the droplets on the surface samples have

been constrained and can only move along those edges without switching across those boundary lines. So, whatever droplet size will be, the width of the droplet (A) will not be increasing in our study. As a result, R is solely dependent on the value of the length of the droplet (B) which is viewed from the parallel direction to the grooves (side view). For Wenzel droplets, the spreading of the droplet grows significantly with the increasing droplet size. Almost constant Wenzel droplet height from Figure 3.10 ensures the fact that droplets will only elongate along the grooves with the increment of the droplet volume, rather than significantly increasing the orthogonal contact angles. However, in case of Cassie droplets, orthogonal contact angles have increased with the increment of droplet size, but parallel contact angles have not changed accordingly. As a result, droplet widths (B) are almost fixed over the whole range (0.5 µL to 4.5 µL) of droplet volumes, resulting in almost constant values of droplet expansion ratio for Cassie droplets. Moreover, droplet expansion ratio values are lower in Cassie droplets than the droplets in Wenzel states. For a fixed 1.5 µL droplets, parallel contact values on samples $D_g{}^{80}W_g{}^{98}W_p{}^4$ and $H_w{}^{80}\lambda_w{}^{98}$ are 105.1° and 100.2° respectively, whereas, they are 130.2° and 123.6° forsamples$D_g{}^{150}W_g{}^{98}W_p{}^4$ and $H_w{}^{150}\lambda_w{}^{98}$, respectively. The latter samples (Cassie droplets) showed much higher contact angle along the groove directions than the former ones (Wenzel droplets), which is the main reason behind this discrepancy of the value of R. Droplet shapes are transforming towards circular or spherical shapes with increasing droplet sizes for Cassie state because of their higher parallel contact angle values. But low parallel contact angles show the elongated droplet shape along the grooves, which substantially increase the droplet width. For parallel micro-grooved surfaces, Rahman and Jacobi discovered similar findings for Wenzel and Cassie droplets [99].
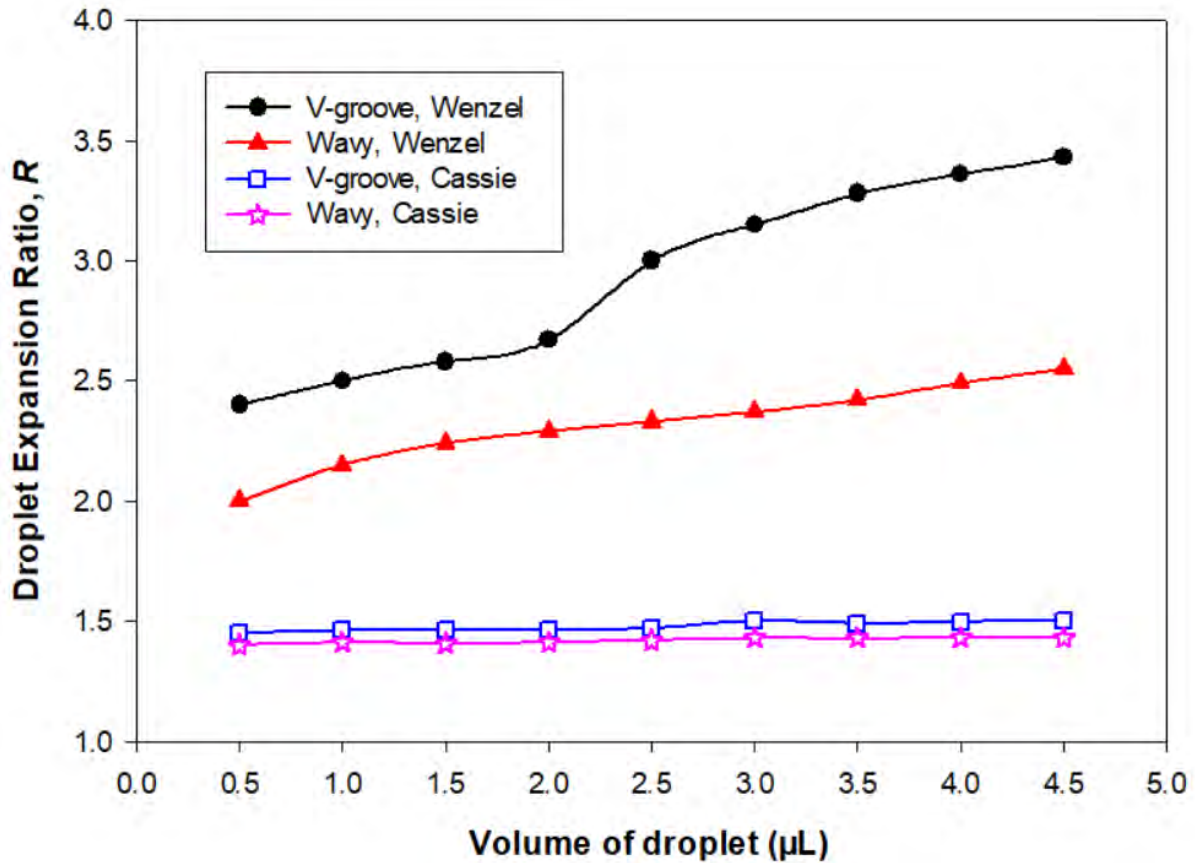
Figure 3.13: Variation and comparison of droplet elongation as a function of droplet volumes on micro V-grooved and micro wavy surfaces. Cassie droplets are represented by non-filled data points.

3.3.2 Effect of Groove Height on the Contact Angle for Micro V-Grooved and Micro Wavy Surfaces

To demonstrate the influence of groove height for droplets deposited on both micro V-grooved and micro wavy surfaces, six sample configurations for each of the surfaces have been identified in Table 2.1 with samples within Series-01 for our simulation. In this particular simulation with 1.5 μL of droplet, eight pillared surface variants have been employed.

92
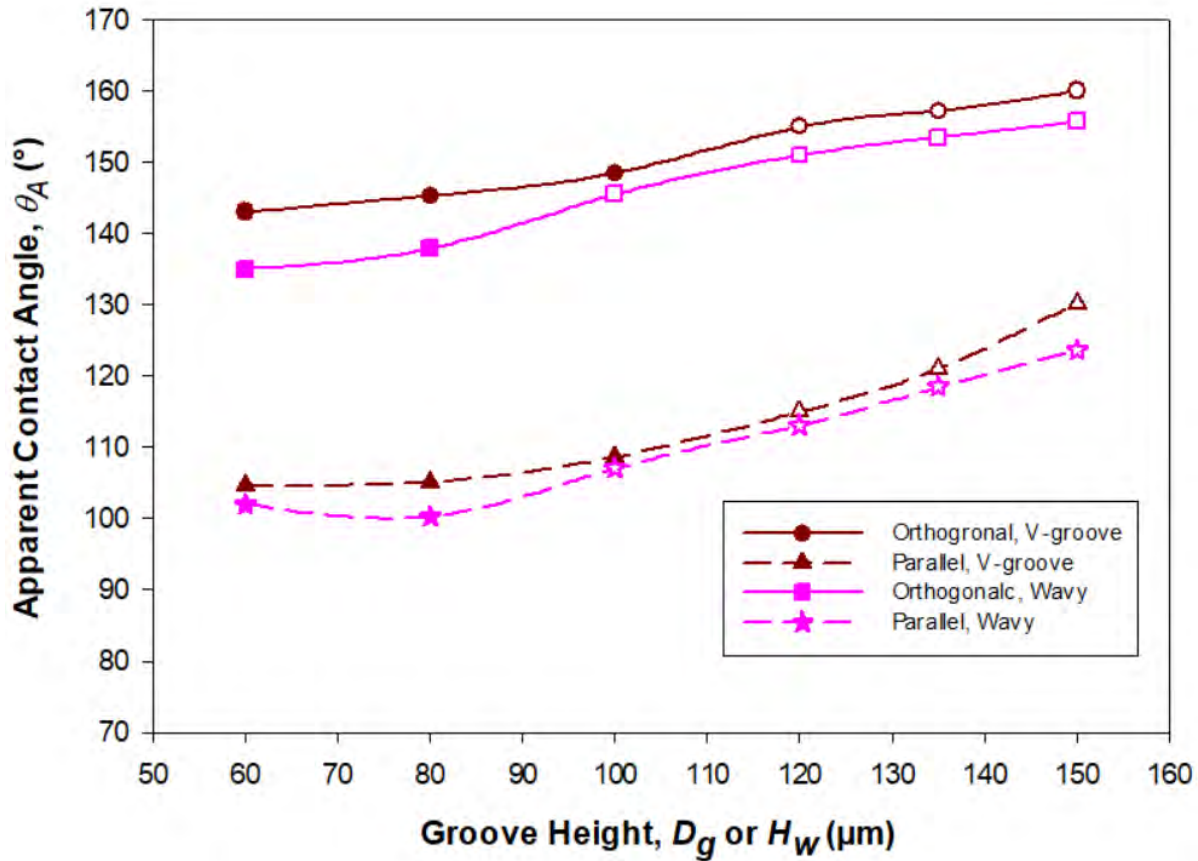
Figure 3.14: Variation of apparent contact angles of 1.5 μLdroplets deposited on eight pillars as a function of groove heighton micro V-grooved and wavy surfaces.

Figure 3.14 illustrates the effect of depth of the grooves of the micro V-grooved and micro wavy surfaces on apparent contact angles in both orthogonal and parallel directions of the grooves, with filled and non-filled data points representing Wenzel and Cassie conditions of wetting, respectively. Because taller pillars are capable of avoiding droplet collapse inside the asperities, the orthogonal contact angle increases as the groove height (or amplitude of the wavy surface) increases in both surface scenarios. This is due to the fact that the energy barrier became greater with the increment of the groove height. Without surpassing that barrier, droplets cannot enter the cavities of rough surfaces. Furthermore, low aspect ratio (D_g/W_g) reduces the capacity of the surface pillars to retain the droplet since they are not tall enough to do so. The Wenzel wetting condition occurs as a consequence, and the orthogonal contact angle decreases. As a result, all of the sample micro V-grooved surfaces with aspect ratios smaller

than 1.15 showed the Wenzel wetting states (1st three sample surfaces of Series-01). Similar variations have been discovered for droplets on parallel micro-grooved surfaces, with aspect ratio playing the dominant role in the wetting transitions [99]. These results are also consistent with investigations of water droplets evaporation process from micro-structured surfaces, which found that droplet curvature increased as the droplet volume reduced for smaller posts, causing the droplet collapsing into the grooves and transitioning to a Wenzel wetting state [122, 123]. However, Cassie wetting condition of droplet has been identified in our instance of micro V-grooved surfaces with greater aspect ratio ($D_g/W_g > 1.2$) and these surfaces have shown comparable high orthogonal contact angle values ($\geq 155°$). These findings of our simulation have also been proved to be in good agreement with the analytically found equation (equation 2.16 in Section 2.7) of the wetting transition requirement for inherently hydrophobic surfaces [117].

However, in the case of wavy surfaces, Cassie wetting condition started to be established considerably before the V-grooved surface for the same conditions. Only the first two samples (within Series-01) of our simulation of micro wavy surface ($H_w^{60}\lambda_w^{98}$ and $H_w^{80}\lambda_w^{98}$) exhibit the Wenzel wetting state, whereas droplets in Cassie mode of wetting are seen on the remaining sample surfaces ($H_w^{100}\lambda_w^{98}$, $H_w^{120}\lambda_w^{98}$, $H_w^{135}\lambda_w^{98}$, and $H_w^{150}\lambda_w^{98}$) with increasing groove depths. This also meets the derived theoretical sinusoidal surface amplitude height condition with no load to achieve the Cassie wetting state, as shown in equation 2.20 of Section 2.7, by Carbone and Mangialardi [118]. According to that equation, when wavelength of the wavy surface, $\lambda_w = 98$ μm and intrinsic contact angle of the material of the substrate = 111°, critical amplitude height of our micro wavy surface is 40.9 μm, above which the wetting condition for our droplets on this specific surface will be in Cassie mode. For the first two samples (within Series-01) of our micro wavy surfaces ($H_w^{60}\lambda_w^{98}$ and $H_w^{80}\lambda_w^{98}$), amplitude heights are 30 μm and 40 μm, respectively, which are less than the critical value. As a result, droplets on micro wavy surfaces are in Wenzel wetting state at these particular sample surfaces. But for the other four sample surfaces ($H_w^{100}\lambda_w^{98}$, $H_w^{120}\lambda_w^{98}$, $H_w^{135}\lambda_w^{98}$, and $H_w^{150}\lambda_w^{98}$), amplitude heights of the surfaces are 50 μm, 60 μm, 67.5 μm, and 75 μm, respectively, which all are significantly larger than the critical amplitude height (40.9 μm) of our micro wavy surface. Also, by dicing and coating a silicon wafer with fluoroalkylsilane, Yoshimitsu*et al.* constructed a succession of

hydrophobic pillar like structures, in which pillar width and spacing were held constant, and the variance in roughness in their samples was caused by a change in pillar height [124]. In their investigation, they discovered that as the pillar height was increased, so did the water contact angle. The prevalent hydrophobicity mode moved from Wenzel to Cassie wetting state when the surface roughness of the pillar structures was increased, which is precisely what happened in our results. Furthermore, our findings are found to be excellent agreement withthe that from the experimental study of Johnson and Dettre [32]. In their study, they discovered that the Wenzel wetting was dominant upto a certain roughness factor for sinusoidal surface. After that limiting point, Wenzel to Cassietransition was observed owing to an increment in the fractional area of air at the cavities because of the higher groove depth [32].

Droplet shapes on both micro V-grooved and micro wavy surfaces consisting of smallest and largest height of grooves are shown in Figure 3.15.

| Front View | Side View | Front View | Side View |

(a)   (b)   (c)   (d)

(e)   (f)   (g)   (h)
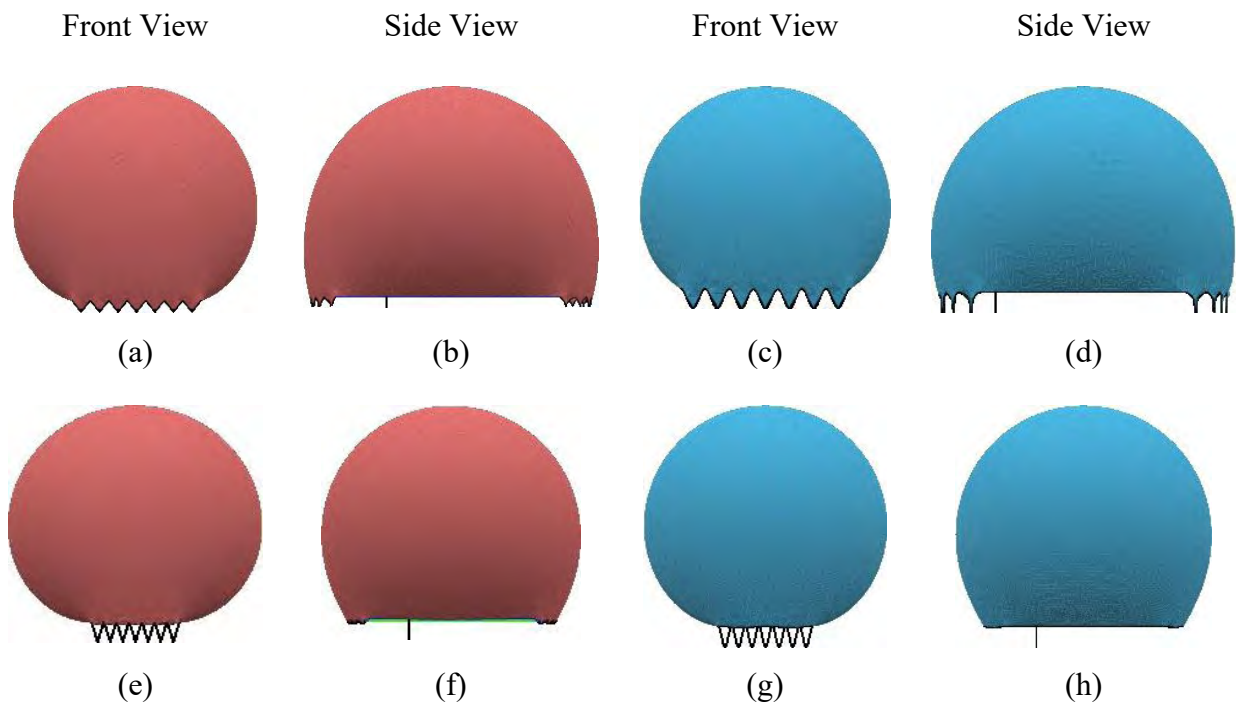
Figure 3.15: Front and side views of 1.5 µL droplets on both micro V-grooved (brick red) and micro wavy (light blue) surfaces with (a-d) smallest (60 µm) and (e-h) largest (150 µm) height of grooves.

For parallel contact angles for both micro V-grooved and micro wavy surfaces, the influence of grove height is practically small and may be considered to be independent of groove height for lower aspect ratio, i.e., for Wenzel droplets, which is quite similar to those reported by these authors on surfaces with parallel rectangular microgrooves [99, 100, 125]. However, for Cassie droplets apparent contact angles are much higher than the Wenzel wetting states. Spreading of the droplet is much less for droplets in Cassie state than Wenzel wetting condition, which is the main reason for this higher parallel contact angle for higher groove heighted Cassie droplets. Greater droplet height and lower droplet expansion ratio for Cassie droplets in Figure 3.10 and 3.13, respectively, also support these higher values of parallel contact angles in case of Cassie droplets observed for the surfaces with deeper grooves.
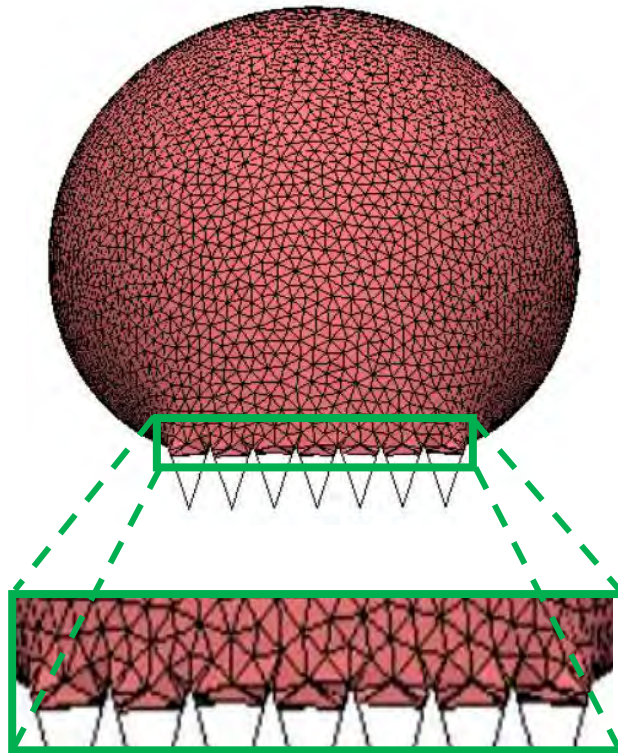
Figure 3.16: The lower meniscus of the droplet is in contact with a very small portion the inclined wall of the deeper grooves of micro V-grooved surface with significant air-gap under the liquid-air interface, resulting in the Composite or Cassie wetting state.

An interesting phenomenon has been observed in the droplets of Cassie wetting condition. Due to the fact that both the micro V-grooved and micro wavy surfaces have inclination of the groove wall, the droplet's bottom meniscus has a tendency to collide with the wall. As we know, when a drop and a surface come into contact, the surface tension force takes over and attempts to fully wet the asperity, resulting in a Wenzel wetting state, which was discovered for all the droplet volumes in our simulation as discussed in the previous subsection. This behavior was addressed by Alen *et al.*, who reported that because of the decreased droplet suspension capacity of V-grooved surfaces, the Wenzel mode of wetting is favored on V-grooved surfaces [101]. However, when the surface roughness factor grows sufficiently and beyond the critical roughness factor, the droplet is unable to completely wet the grooved region due to the increased energy barrier, which prevents the droplet from entering the grooves despite the wall's inclination. However, in Cassie state, due to their lower suspension capability, lower meniscus of droplet still comes into contact with inclined surface of the wall maintaining a significant portion of air-gap under the liquid-air interface in the groove portion of the surfaces. This results in a composite wetting state, which is just another form of Cassie state (Figure 3.16), which has been explained in Section 1.4.1.This is due to the capillary effect, which causes the water molecules to stick to the slanted walls more owing to the adhesion force. And the surface chemistry may modify the capillary effect due to the varied strength of this adhesion force. The adhesion force between water and various surfaces varies, resulting in changes in surface wettability. But surface roughness, rather than surface chemistry, will be the most important element in changing the wetting states on these V-grooved and wavy surfaces.

3.3.3 Effect of Groove Width or Pitch on the Contact Angle for Micro V-Grooved and Micro Wavy Surfaces

In this section, the influence of groove width or pitch on the apparent contact angles of the deposited droplet on micro V-grooved and micro wavy surfaces has been quantitatively explored. To observe the effect of groove width or pitch on the apparent contact angles, five sample surfaces have been examined here by keeping the groove height (= 80 μm) for both surfaces and pillar width (= 4 μm) for micro V-grooved surfaces constant, where only groove

97

widths or pitches for both type sample surfaces have been changed. The specifications of these samples are provided in Table 2.1 within Series-02. Moreover, 1.5 µL volume of droplets are introduced for our simulation study here, with three sorts of configurations such as – six pillared micro V-grooved and micro wavy surfaces as well as eight pillared of micro V-grooved surfaces.

Figure 3.17 depicts the variation of apparent contact angle in both orthogonal and parallel directions of the grooves for varied groove widths or pitches on micro V-grooved and micro wavy surfaces. To begin with on these five sample surfaces of both types with distinct anisotropic topologies, all the droplets are observed in Wenzel wetting states. Analytically derived required conditions for both surfaces (equation 2.16 and 2.20) have likewise been shown to be in excellent agreement with this. With increasing groove widths, perceived contact angles in both directions for Wenzel states decrease for a given droplet size.
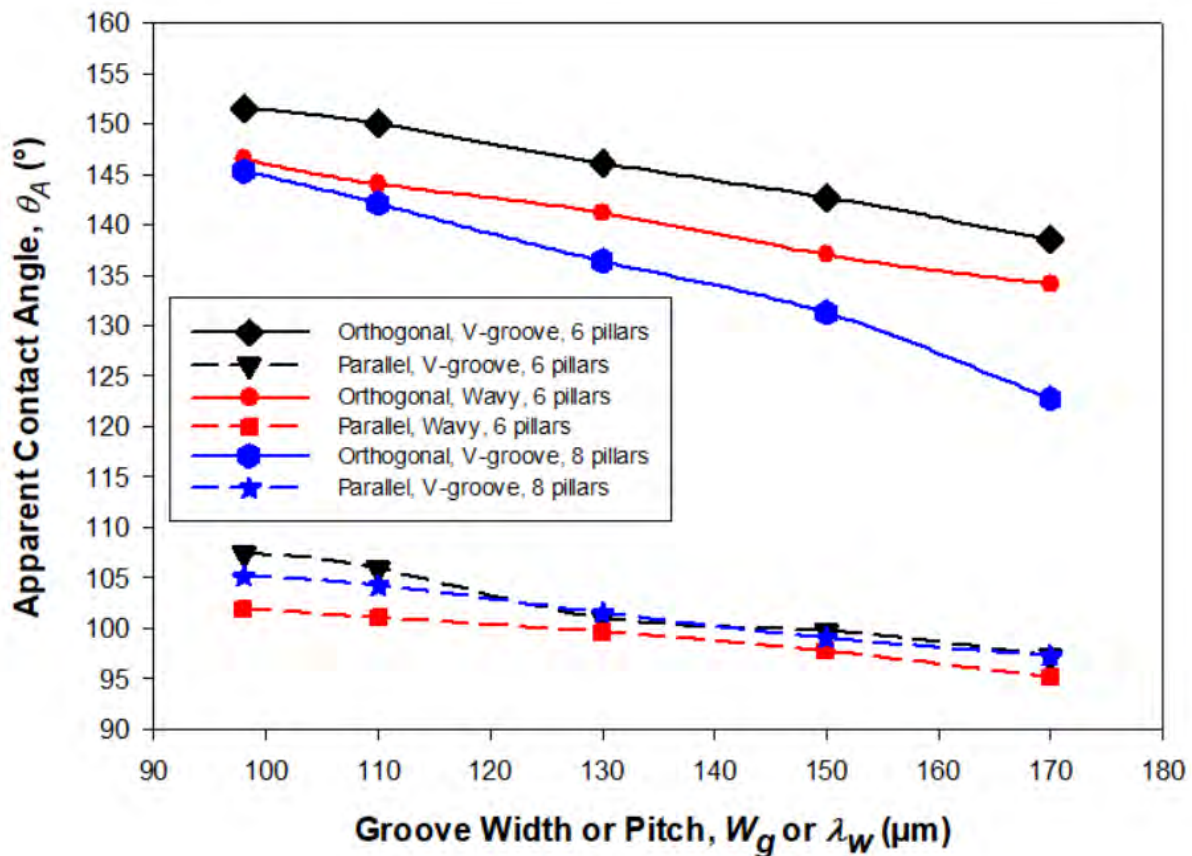
Figure 3.17: Variation of apparent contact angles of 1.5 µLdroplets deposited on various

98

configurations of micro V-grooved and micro wavy surfaces as a function of groove widths or pitches.

For instance, orthogonal contact angles fall from 151.5° to 138.5° (decrement of about 13°) when groove widths are from 98 μm to 170 μm for six pillared micro V-grooved surface configurations. This declining tendency is not only evident for orthogonal contact angle as groove widths increase. Over this growing range of groove widths, parallel contact angles have likewise been lowered by roughly 10°. In this sense, identical groove numbered micro wavy surfaces and higher number of pillar layouts in micro V-grooved surfaces provide similar effects.The intrusion of droplets into the grooves was initially more difficult due to the smaller groove widths. Because the pillar width to groove width ratio decreases as the groove width grows, droplets readily penetrate the asperity of the surfaces. Also, since the aspect ratio (D_g/W_g or H_w/λ_w) is reduced, the arrangement seems to have smaller pillar height, confirming that energy barrier gets reduced, which improves the Wenzel wetting states and reduces the apparent contact angles in both directions. The fluctuation of droplet shape owing to the modification of groove width provide clear representations of this impact in Figure 3.18 and 3.19.

Both of the wetting states of the surfaces - Cassie and Wenzel, further support our findings. In the non-composite or Wenzel wetting state, the impact of groove width on apparent contact angles is diametrically opposed to that in the composite or Cassie wetting condition. In Cassie wetting, apparent contact angles grow, as groove width increases. As a consequence, Wenzel droplets will create lower apparent contact angles with expanding groove widths on the surfaces, as opposed to Cassie wetting state behavior, as shown in our simulation findings. The findings of numerical work of Anjan *et al.* for square and circular shaped pillar like structures [79], experimental findings of Li *et al.* for parallel grooved structure [125], and Park *et al.* for PDMS micro-structured polymer surfaces [126] are all similar with our simulation results. Zhang *et al.* also obtained similar results for hierarchical and non-hierarchical architectures using molecular dynamics simulations, which are consistent with our findings [127]. So, because of their reduced static contact angles, the droplet base length and width rises with the increase in groove widths when seen from both parallel and orthogonal directions, respectively. Furthermore, from Figure 3.17, smaller apparent contact angle for the same number of pillared

surfaces of micro wavy surfaces than micro V-grooved was observed. This occurs due to the lower pinning effect at the peak of the grooves and higher elongation of the droplet along the grooves in wavy surfaces than micro V-grooved surfaces, as was previously discussed.

Front or Orthogonal View   **Side or Parallel View**
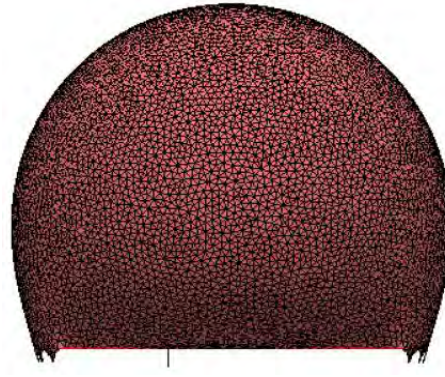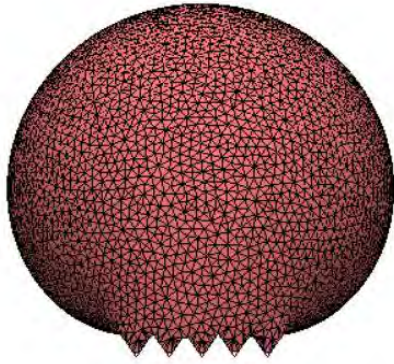
(a) Groove Width = 98 µm
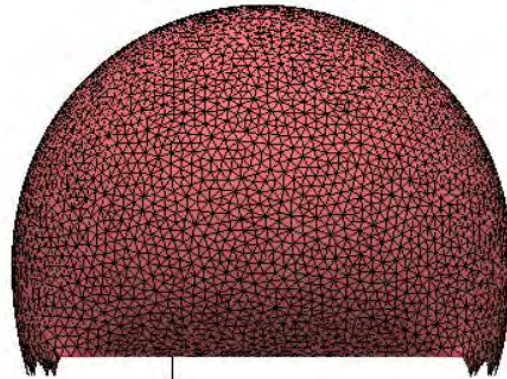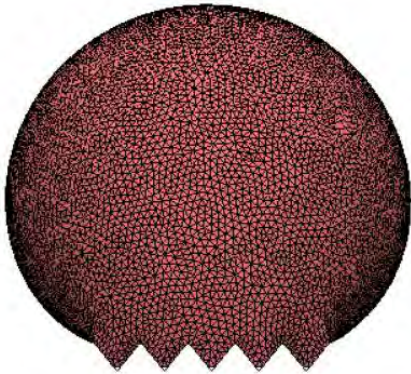
(b) Groove Width = 130 µm
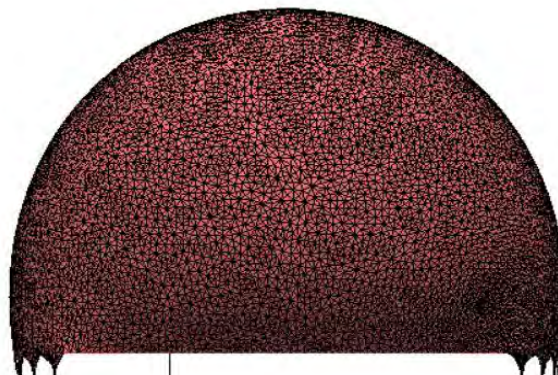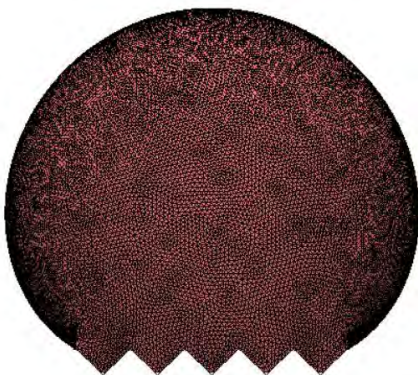
(c) Groove Width = 170 µm

Figure 3.18: Variation of the shape and anisotropy of 1.5 µL droplets on micro V-grooved

surface with 6 pillars for - (a) 98 μm, (b) 130 μm, and (c) 170 μm of groove widths.

Front or Orthogonal View   **Side or Parallel View**
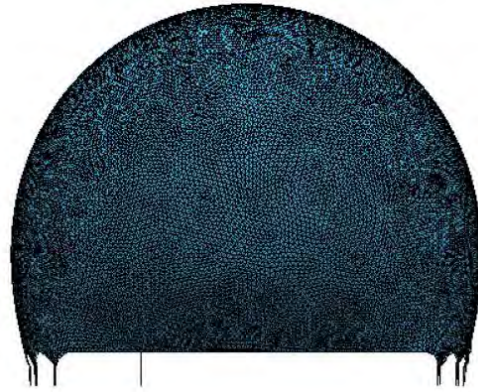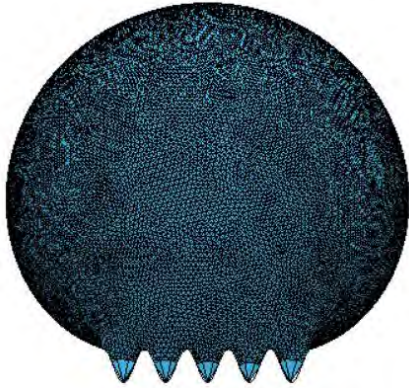
(a) Groove Pitch = 98 μm
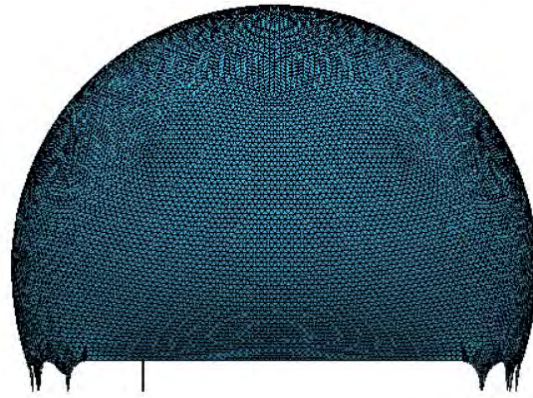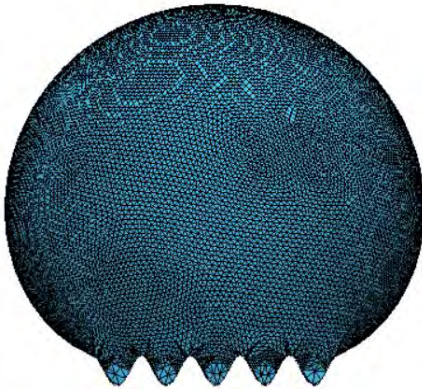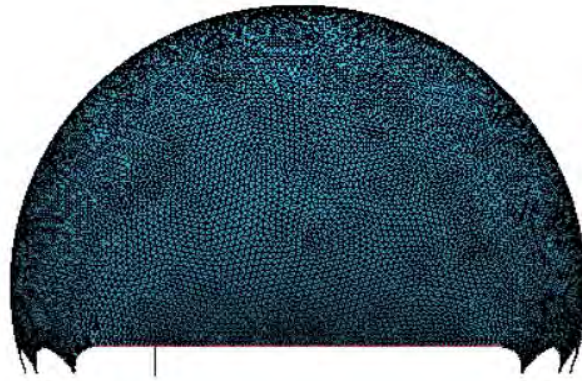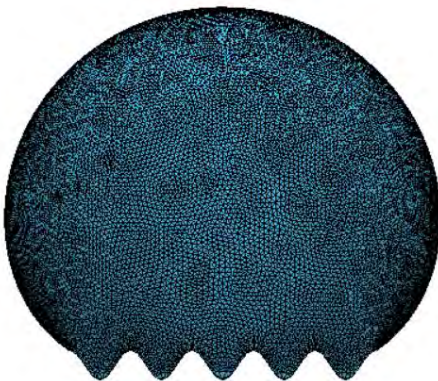
(b) Groove Pitch = 130 μm

Figure 3.19: Variation of the shape and anisotropy of 1.5 μL droplets on micro wavy surface with 6 pillars for - (a) 98 μm, (b) 130 μm, and (c) 170 μm of groove widths or pitches.

3.3.4 Effect of Surface Chemistry on the Contact Angle for Micro V-Grooved and Micro Wavy Surfaces

Chemical modification of the surfaces is another fundamental way for altering the wetting behaviour on a surface. The influence of surface chemistry on apparent contact angles in both directions of the grooves for micro V-grooved and micro wavy surfaces will be numerically investigated in this section.

The term "change of surface chemistry" refers to the changing of the surface material's intrinsic contact angle (θ_{int}) when in contact with the liquids, in this instance water droplets. So far, we have only dealt with a single intrinsic contact angle of surface material (micro-Si), which is 111°, as only droplet volume and surface roughness effects have been established. Now we will look at a wide range of θ_{int} (80° to 140°), to evaluate the nature of anisotropy and apparent contact angles viewed across and along the groove direction. However, $D_g{}^{80}W_g{}^{98}W_p{}^4$and, $H_w{}^{80}\lambda_w{}^{98}$samples, which are common for all series identified in Table 2.1 for micro V-grooved surface and micro wavy surface, respectively, have been used for examining this specific effect on wettability, especially wetting anisotropy.

Orthogonal contact angles, which are 132° and 122° for micro V-grooved and micro wavy surface configurations, respectively, rise to 159.7° and 145.5° for both surfaces when intrinsic contact angle increases from 80° to 140°, as shown in Figure 3.20. In this case, the increment rates of orthogonal contact angles are 27.7° and 23.5° for micro V-grooved and micro wavy surface designs respectively. Not only apparent contact angles viewed from perpendicular direction of the grooves, but also parallel contact angles for these two surface topologies have been discovered in an incremental sequence. This rate of growth in parallel contact angles is 64.7° for micro V-grooved surfaces (63° and 127.7° of parallel contact angles for θ_{int} of 80°

and 140°, respectively) and 51.2° for micro wavy surfaces (70° and 121.2° of parallel contact angles for θ_{int} of 80° and 140°, respectively). So, the apparent contact angles in both directions rise as the intrinsic contact angle increases. However, the rate of rise in parallel contact angles is substantially faster than the rate of increase in orthogonal contact angles. As a result, when the intrinsic contact angle rises, the difference between orthogonal and parallel contact angles diminishes, implying that the degree of anisotropy decreases (Figure 3.21). This indicates that the greater the intrinsic angles, the smaller the amount of energy on the surfaces, making the droplets less reliant on the surfaces' microstructures or grooves. As a consequence, the droplets become more spherical with larger intrinsic contact angles, which will induce isotropic wetting phenomenon. These findings are in good agreement with the numerical work of Song *et al.* for partially grooved surfaces where the grooved area's width is less than the droplet diameter [106].
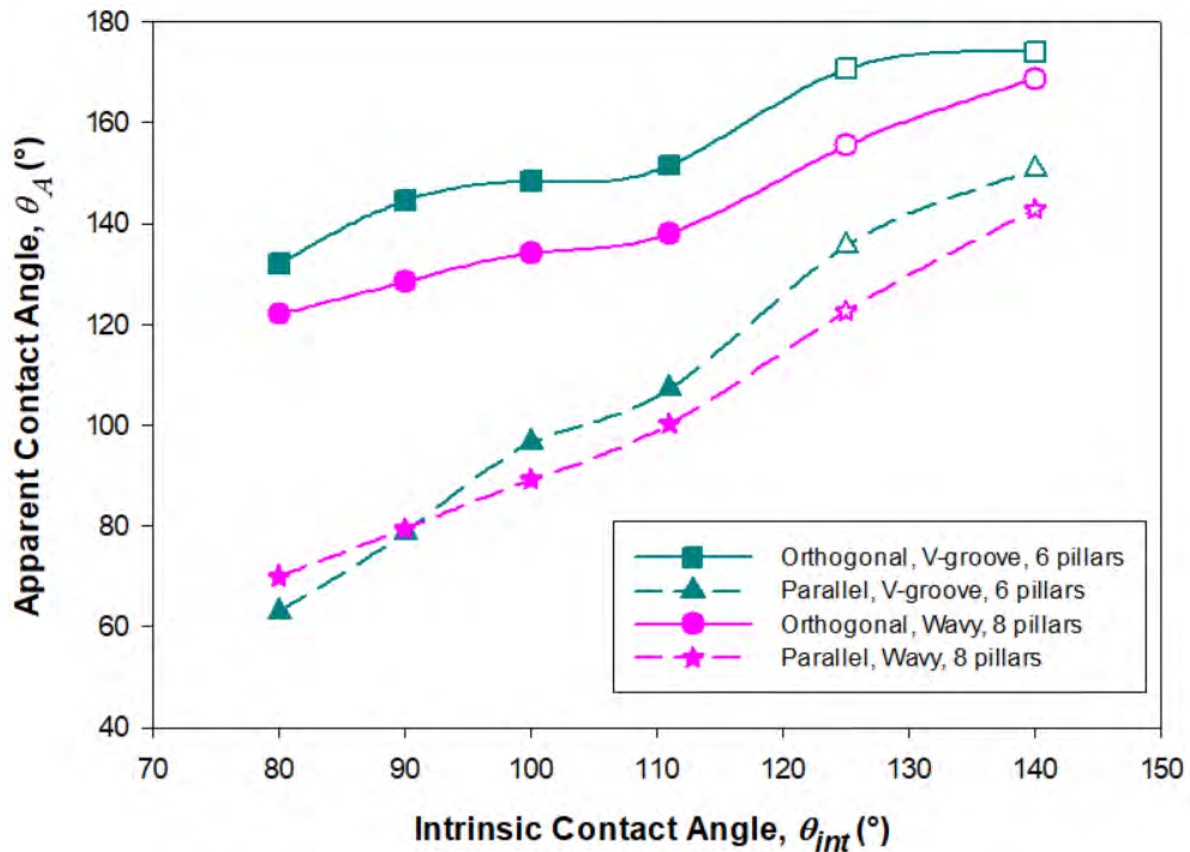
Figure 3.20: Change of apparent contact angles in both orthogonal and parallel directions as a function of intrinsic contact angle for micro V-grooved and wavy surfaces for fixed number of grooves and droplet size. Filled data points indicate Wenzel wetting states.

However, after reaching a specific limit of intrinsic contact angle, the shift of wetting state from Wenzel to Cassie occurs. The wetting state of the droplet has transitioned to Cassie for $\theta_{int} = 125°$ and 140°. This transition is also satisfied by analytically modelled equations (equation 2.16 and 2.20) for micro V-grooved and micro wavy intrinsically hydrophobic surfaces [117, 118]. According to the equation 2.16 and 2.20, the limiting θ_{int} for our micro V-grooved surface and micro wavy surface configurations is about 121.5° and 111°, respectively. As a result, after reaching this key threshold of θ_{int}, the Wenzel to Cassie transition should be detected, which our numerical model has confirmed. For the final two data points for Cassie droplets, droplet morphologies have begun to migrate towards the spherical form from elliptical or elongated ones due to larger contact angles in both directions in Cassie states, which caused lesser anisotropic effect.
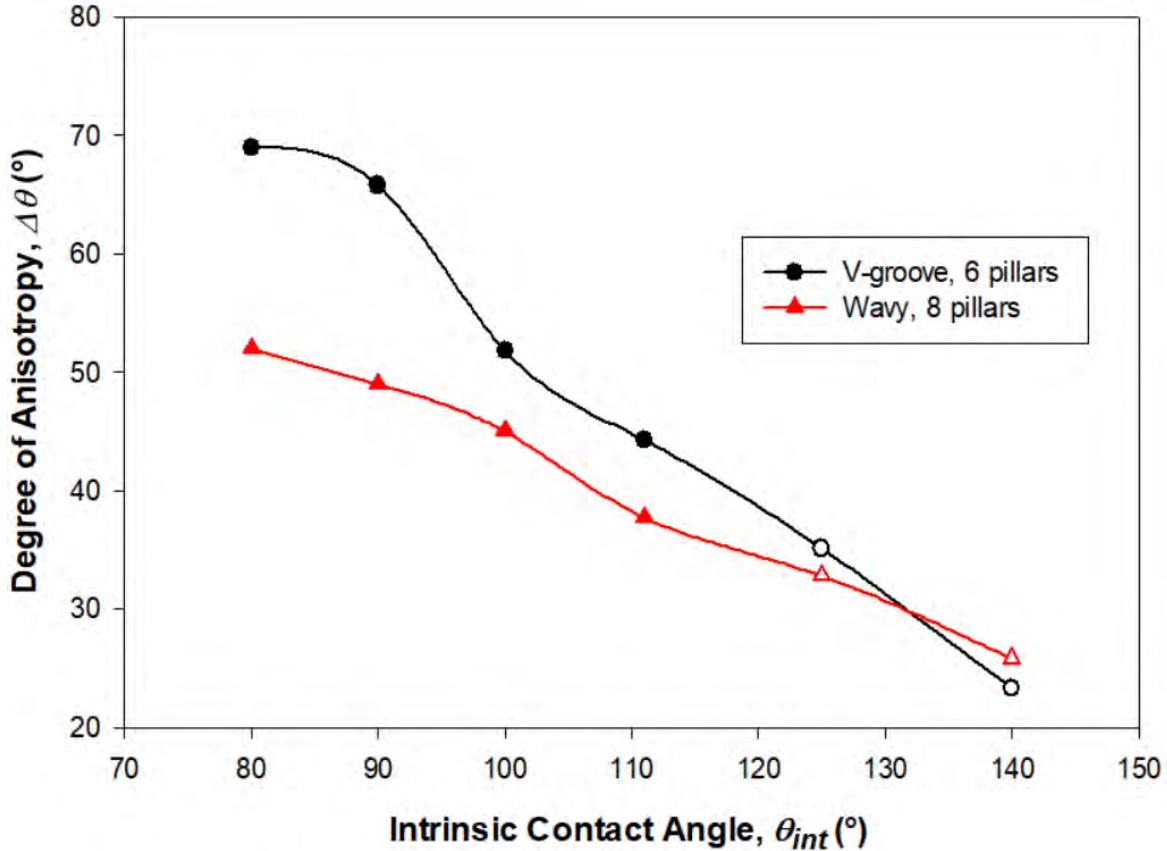
Figure 3.21: Variation in the degree of anisotropy as a function of the intrinsic contact angles. Non-filled data points depict the droplet in Cassie mode.

3.3.5 Effect of Groove Angle on the Contact Angle for Micro V-grooved Surfaces

The variation of apparent contact angle will be investigated with respect to the groove angles (φ) of micro V-grooved surfaces. Groove angle (φ) is the angle created by the two inclined walls of the pillar or groove intersecting at the bottom of the surface or groove (Figure 2.2). Since the surface of the wavy surface follows the sinusoidal curve in our numerical model, it does not have any edge corner, any significant pillar width at the top of the surface as well as precise intersection point at the bottom of the groove, which we have stated earlier. So, indicating the groove angles accurately in case of micro wavy surfaces, is somehow complex. As a result, we have solely looked into themicro V-grooved surfaces to demonstrate the impact of groove angle on the apparent contact angle.

Effects of groove angle (φ) can be observed from two different point of views as follows:

1) Variation of groove height or depth (D_g): When the groove width stays constant, the groove angle decreases with an increase the groove depth.

2) Change of groove width (W_g): Groove angle increases as the groove width increases without corresponding changes in groove height.

In Figure 3.22, these two types of variation have been incorporated together to highlight the effect of groove angle on the apparent contact angle.

In the first case, when φ is getting smaller because of larger groove depths for constant groove widths, both directional apparent contact angles are increased. In the first section (red curve) of Figure 3.22, the smallest ($\varphi = 36.2°$) and larger ($\varphi = 62.98°$) groove angles have been observed for the largest ($D_g = 150$ µm) and lower ($D_g = 80$ µm) groove heights taken in our simulation model, respectively. Lowest groove angle ($\varphi = 36.2°$) have yielded the maximum orthogonal (160°) and parallel contact angle (130.2°), whereas for the larger one ($\varphi = 62.98°$), they have reduced to 145.3° and 105.1°, respectively. So, with the increment of φ (for decreasing groove height), apparent contact angle decreases. This occurs for the same reasons as that of the influence of groove height on the contact angle (discussed in Section 3.3.2). Low groove angles cause the surface configuration to behave like a rough surface with deeper grooves. Deeper grooves may prevent droplets from intruding into the asperities. This is due to the fact that the energy barrier has increased with increased groove depth. Droplets would not be able to enter the voids of rough surfaces until they have passed past that barrier. However, when groove angles start to increase, it indicates that the surface pillars are no longer tall enough to keep the droplet above the pillar, and a low aspect ratio (D_g/W_g) reduces their ability to do so. As a consequence, the orthogonal contact angle decreases. Moreover, Cassie droplets have been generated for lower groove angle configurations in this regard due to the existence of higher aspect ratio ($D_g/W_g > 1.2$). But for higher groove angles, this ratio becomes smaller and after

certain limit ($D_g/W_g < 1.2$), the Wenzel wetting state occurs and orthogonal contact angles are reduced significantly, as shown in Figure 3.22 for surface configurations containing groove angles of $\varphi = 52.2°$ and $\varphi = 62.98°$. Moreover, parallel contact angle shows significant decreasing trend with the increasing values of groove angles, which is corroborated by our prior examination of the groove height effect, where parallel contact angles of Cassie state was detected much larger as groove heights increased.

For the second type of variation, the reliance of groove angle (φ) on groove widths (W_g) has been established for fixed groove depth values (D_g). With the increment of W_g, φ also raises with fixed value of D_g. So, apparent contact angles in both directions decreases with the higher groove angles. So, for the 2nd portion (green curve) of the Figure 3.22, the lowest ($\varphi = 62.98°$) and highest ($\varphi = 93.47°$) groove angles correspond to the smallest ($W_g = 98\mu m$) and largest ($W_g = 170\mu m$) groove width values in our numerical model. In this part, orthogonal contact angle goes down from 145.3° to 122.7° and parallel contact angle reduced from 105.1° to 97.2°, when groove angles have increased from $\varphi = 62.98°$ and $\varphi = 93.47°$. The same reasons as the effects of groove widths on apparent contact angles, as detailed in Section 3.3.3, are responsible for these observations. Droplets readily penetrate the asperity of the surfaces as the groove angle (i.e., which is proportional to the groove width) rises. Lower pillar heights seem to be associated with this kind of topography, indicating a reduced energy barrier, which favors Wenzel wetting state and reduces apparent contact angles in both directions. The obtained results further reveal that the Wenzel droplets exhibit lower apparent contact angles with expanding groove angles on surfaces than Cassie droplets, as also reported by earlier studies [79, 125-127]. Moreover, Cassie to Wenzel wetting state transition have also been observed at lower groove angles, and this occurrence is consistent with the needed conditions for this transition process as specified in the analytical model [117].
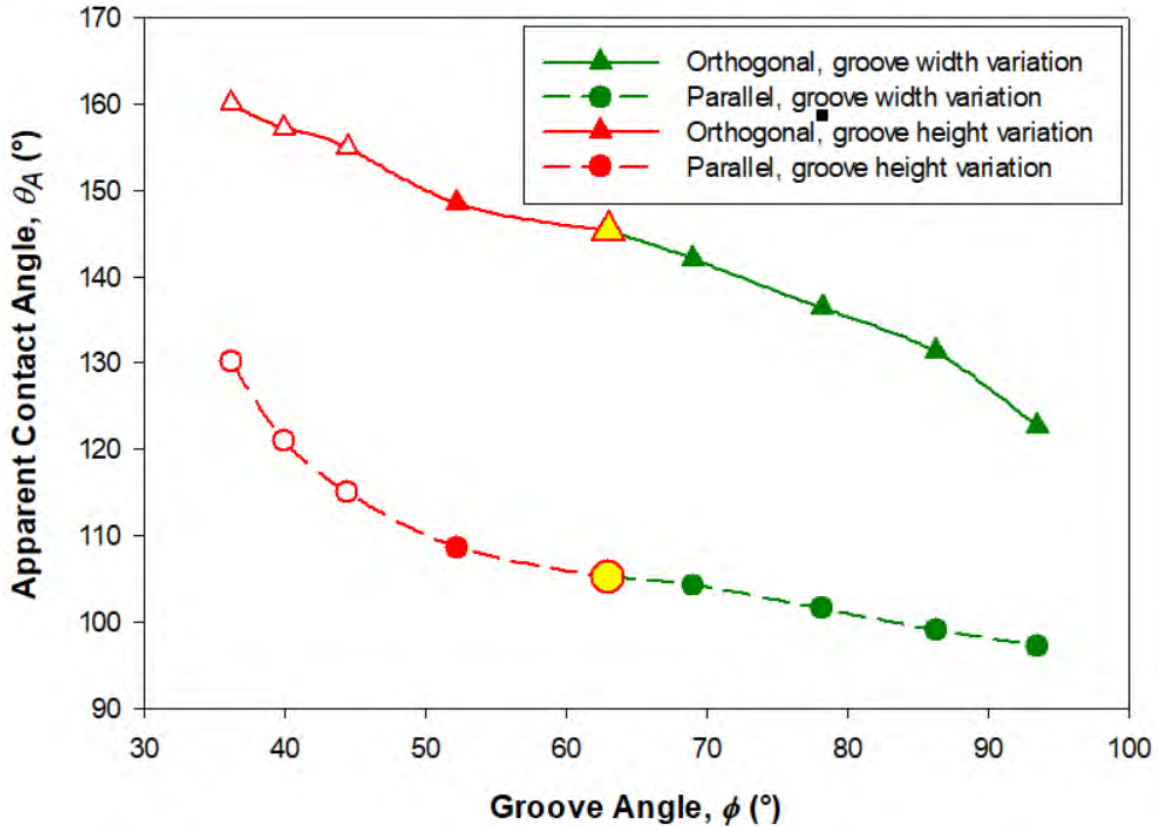
Figure 3.22: Variation of apparent contact angle of droplets as a function of groove angle. Here, for the 'red' portion of the curves, the groove width of the surface is fixed at 98 μm, but groove height varies, whereas for the 'green' portion, the groove height is kept constant at 80 μm while the groove width varies. The yellow data point is the intersection point of these two types of variation (groove height = 80 μm and groove width = 98 μm). The filled data points indicate a Wenzel state of wetting.

3.3.6 Effect of Pillar Width on Contact Angle for Micro V-grooved Surfaces

From the discussion of the preceding chapter, it is clear that there is no distinct and discernible pillar width for the micro wavy surface configurations because of its smooth sinusoidal curvature. As a result, the effect of pillar width on the wettability of micro wavy surfaces is not examined. However, pillar width (W_p) has been discovered to be a significant factor in the wettability of our micro V-grooved surfaces. Thus, we will look at how pillar widths (W_p) of

micro V-grooved surfaces impact the wettability in a form of apparent contact angles in both across and along the groove directions, in this particular section. To begin, groove width (W_g = 98 µm) and groove height (D_g = 80 µm) of the surfaces have been made fixed to all six sample surfaces with varied pillar widths that have been provided in samples of Series-03 in Table 2.1, which include both six and eight pillared configurations.

The variation of apparent contact angles for different values of pillar width is shown in Figure 3.23 for 1.5 µL droplet placed on the above-mentioned surface configurations. For a lower pillar width to groove width ratio (W_p/W_g), Wenzel wetting states have been maintained. That is why, for the first three sample surfaces ($D_g{}^{80}W_g{}^{98}W_p{}^4$, $D_g{}^{80}W_g{}^{98}W_p{}^{15}$, and $D_g{}^{80}W_g{}^{98}W_p{}^{25}$) droplets in the Wenzel state are detected. And no substantial variations have been observed in apparent contact angles for W_p/W_g< 0.26. In this situation, water intrusion into the grooves happened in a similar fashion to that seen for the surface with extremely short pillars, owing to the tiny pillar width and significant groove widths or spacing between the pillar edges. And after raising the pillar widths significantly, Wenzel to Cassie transition of wetting has been observed. So, from W_p = 50 µm to W_p = 100 µm, orthogonal contact angles have been gone down from 144.3° to 124.1° (decrement rate of 20.2°) and parallel contact angle have also reduced from 104.1° to 100° (decrement rate of 4.1°) for six pillared configurations for six pillared configurations. For eight pillared configurations, similar trend has been demonstrated where rate of reduction in contact angles for orthogonal direction to the grooves is 19.5° (134.6° to 115.1°) and for along the groove direction is 5° (104.7° to 99.7°). These findings clearly show that decrement of orthogonal contact angles occurs at a far faster rate, despite the fact that this rate is slower in the case of parallel contact angles. When a droplet is in the composite or Cassie wetting state, solid fraction area at the base of the droplet is the primary cause of three-phase contact line movement and static contact angle fluctuation. Solid fraction area is the region beneath which solid and liquid are in direct contact and it is nothing but the Cassie roughness factor (f), defined in Cassie-Baxter equation (equation 1.12). As a result, droplet on the surface sample ($D_g{}^{80}W_g{}^{98}W_p{}^{50}$) has a lower area of the solid fraction (33.8%) than $D_g{}^{80}W_g{}^{98}W_p{}^{100}$ sample (50.5%). The solid percentage at the drop base and the length of the three-phase contact line have increased for the Cassie state of droplets with an increase in the pillar width. As a

consequence, as the pillar width increases, the apparent contact angle in Cassie wetting is reduced. The Cassie-Baxter hypothesis, which has been around for a long time, predicts the same thing. As a result, our results are logical and consistent with traditional beliefs. Also, due to higher rate of reduction in orthogonal contact angles than parallel ones, anisotropic wetting behavior is reducing with the increment of pillar width and going towards the isotropic condition gradually for Cassie droplets. Figure 3.24 shows an example of variation of the droplet shape with change in the pillar width.

These findings are in good agreement with many experimental and numerical studies reported in the literature. Rahman and Jacobi also experimentally discovered the Wenzel to Cassie transition for larger pillar width to groove width ratio (W_p/W_g) [99]. In another experimental study of droplets on micro-pillar structured hydrophobic surfaces, Yeh and Chen demonstrated similar relationship between solid fraction and apparent contact angles [128]. Similar observations were also found for isotropic Cassie state of wetting on micropillar type surfaces, as reported by Anjan *et al.* [79].
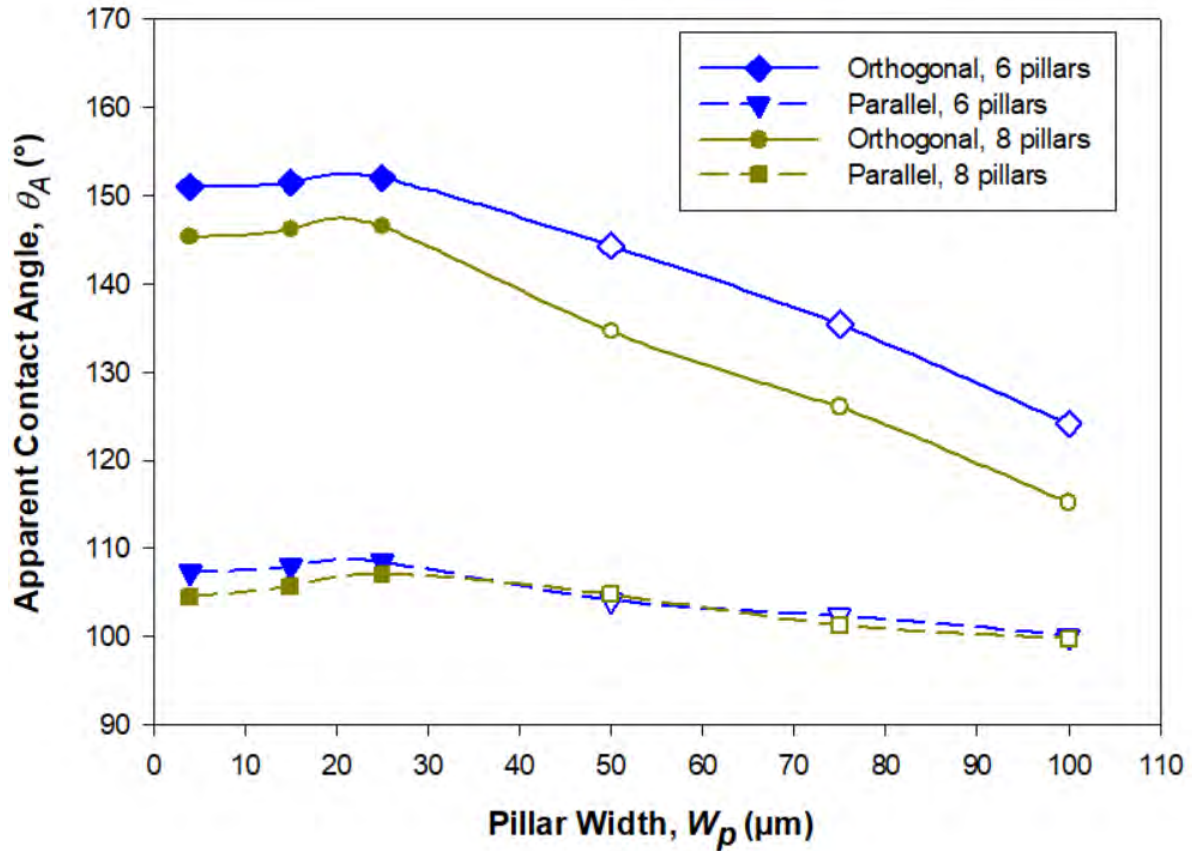
Figure 3.23: Variation of apparent contact angles in both orthogonal and parallel directions as a function of pillar widths for droplet size of 1.5 μL deposited on six and eight pillared micro V-grooved surface configurations. Filled data points indicate Wenzel wetting states.

Front or Orthogonal View   **Side or Parallel View**
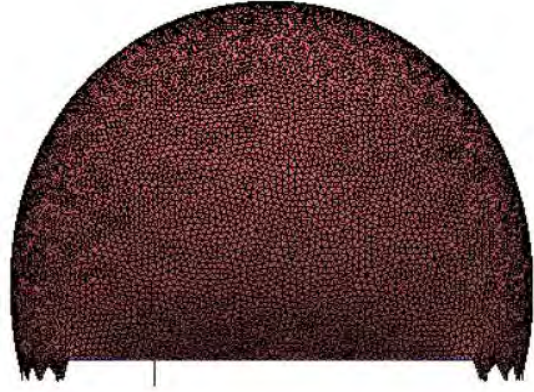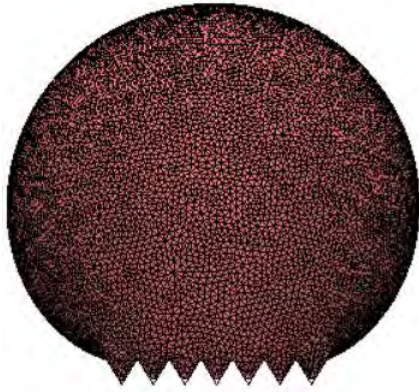
(a) Pillar Width = 4 µm
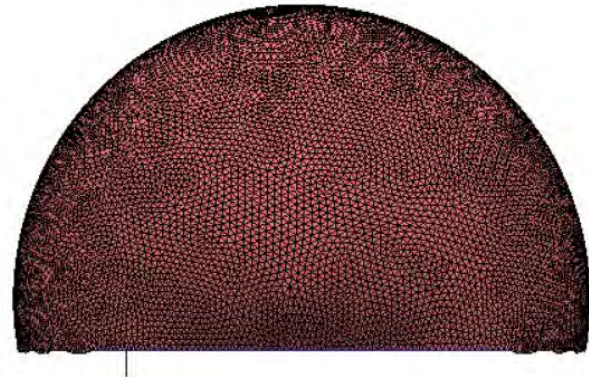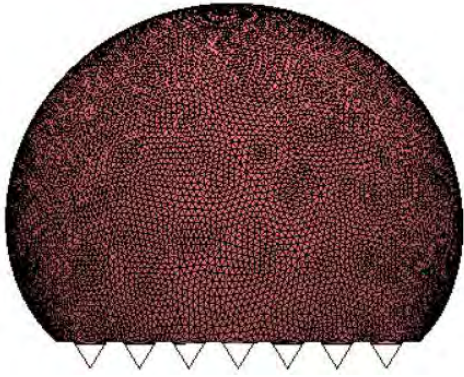
(b) Pillar Width = 50 µm
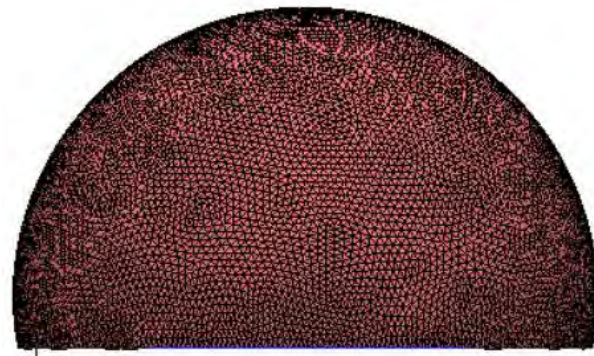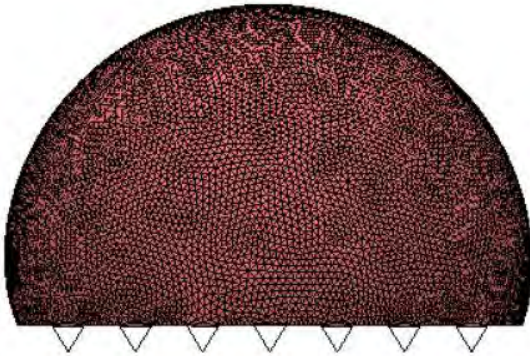
(c) Pillar Width = 100 µm

Figure 3.24: Variation of the shape and anisotropy of 1.5 µL droplet on micro V-grooved surface with 8 pillars for - (a) 4 µm, (b) 50 µm, and (c) 100 µm of pillar widths.

Overall, the results of our research potentially have major implications in a variety of sectors. Specific surface designs may be applied in air conditioning, refrigeration, and microfluidic systems, among other things, based on the volume impact of wettability on micro V-grooved and wavy surfaces, according to the relative stabilities and energetics of the droplets. Furthermore, for specified droplet volumes, the requisite anisotropic effect and wetting states for these rough surfaces can be determined. Surface roughness characteristics can also be induced for improved liquid drainage systems using knowledge of the critical point of wetting transition in these surfaces. The impact of surface roughness characteristics such as groove height, groove width, pillar width, and others has been presented in this research, demonstrating the approach to obtaining desired design structures for a wide variety of applications. The Wenzel state of wetting is better for drainage systems, while the Cassie state is better for rolling droplet-based applications such as self-cleaning, water, or fog collecting. When self-cleaning and water collection are required, superhydrophobic surfaces may also be created by changing the surface chemistry. Aside from these, synthetic surface anisotropy has been shown to be useful in directional water transportation and bio-medical applications.

CHAPTER 04
CONCLUSIONS AND RECOMMENDATIONS

4.1 Conclusions

Micro-scale roughening with grooved structure can result specialized wetting characteristics, some of which may have technological implications in the near future.

The main goal of this research was to study the effect of micro-sized asperities, in the shape of V-grooves and periodic wavy roughness, on the stability and energetics of the liquid droplets and the anisotropic wetting behavior on these surfaces. Surface Evolver was used as the numerical tool to perform a range of simulations and by the process of energy minimization, detailed investigation of the equilibrium droplet shape and associated energies were examined. In the beginning, the numerical simulation is used to investigate wetting on flat smooth surface and it was subsequently extended for surfaces that have been patterned with micro-scale wavy and V-grooves. Validation of the numerical procedure was realized by carrying out comparison of the contact angle analysis with experimental study from the literature, which exhibited excellent agreement having a maximum deviation of less than $\pm 1.5\%$ between the experimental and numerical values. The findings of the present study were also found to be in good agreement with the previously reported analytical and thermodynamical models.The following points, outline the most important findings of this study:

(i)   Because of the pinning effect at the edge and discontinuity of the pillars, the microV-grooved surfaces offered substantially higher apparent orthogonal contact angles than smooth and continuous micro wavy surfaces. As a result, the size of the stable equilibrium droplet for micro wavy surfaces were observed to be smaller than the same on micro V-grooved surfaces.

(ii)   To obtain the most stable equilibrium shape of droplets on both the V-grooved and micro-wavy surfaces, a larger droplet requires a greater number of pillars underneath it. During the variation of droplet size, multiple metastable wetting states for a fixed-sized droplet of liquid were discovered with varying numbers of pillars underneath the droplet.

(iii)   A higher degree of anisotropy was observed for Wenzel state of wettingdue to greater spreading of the liquid droplet along the groove direction. For Cassie droplets, an increase of droplet height was recorded with increase in the droplet volume, while height of the Wenzel dropletswas found to remain relatively constant regardless of droplet size. A larger droplet expansion ratio was observed for the Wenzel state than the Cassie state of wetting.

(iv)   Water droplets,on the surfaces with a smaller groove depth and wider grooves descend down the pillars and spread along the grooves, resulting in lower apparent contact angle, while greater groove height and shorter groove width have the opposite tendency due to the higher aspect ratio and larger energy barrier. Groove angles on the V-grooved surfaces also showed similar wetting characteristics.

(v)   The apparent contact angle in both the parallel and orthogonal directions of the grooves was found to increase for a higher intrinsic contact angle of the surface material, but with faster increment rate of parallel contact angle than orthogonal contact angle, resulting in a lower degree of wetting anisotropy and a shift toward isotropic wetting.

(vi)   Wenzel to Cassie wetting transition occurred after limiting a pillar width, although with lower orthogonal contact angles than the droplets on surfaces with narrower pillar widths than the critical point. This is due to an increase in the solid fraction area underneath the droplet, which aided in the reduction of the anisotropic effects.

On the whole, the simulation findings obtained by using various surface geometries as well as surface energy are in excellent agreement with those obtained via associated experimental and theoretical investigation. As a result of the developed simulation techniques, it is possible to predict the wetting nature with high accuracy, which will greatly assist in the design of micro-structured microwavy and V-grooved rough surfaces with directional wetting characteristics by optimizing geometric parameters such as groove size, shape, and spacing, as well as the nature of the surface coatings required.

4.2 Scopes for Future Work

The following suggestions are proposed for future research works to extend the scope of the present study:

(i)   The present study can be extended to develop numerical models to examine the wetting characteristics on micro-structured surfaces with hierarchical patterns, which has can be highly useful.

(ii)   Similar numerical studies can be carried out for surfaces of woven fabrics as well as chemically striped surfaces both of which has substantial practical applications.

(iii)   The majority of the rough surfaces used in this study are innately hydrophobic. Numerical investigation of the wetting properties of innately hydrophilic surfaces, on the other hand, may be investigated.

(iv)   Dynamic wetting behavior may be studied extensively for both micro V-grooved and wavy surfaces to determine the sliding characteristics of liquid droplets on these surfaces.

REFERENCES

[1]   Lv, C., Hao, P., Yao, Z. and Niu, F., "Departure of Condensation Droplets on Superhydrophobic Surfaces", *Langmuir*, vol.31(8), pp. 2414-2420,2015.

[2]   Liang, Y., Ju, J., Deng, N., Zhou, X., Yan, J., Kang, W. and Cheng, B., "Super-Hydrophobic Self-Cleaning Bead-Like Sio2@ PTFE Nanofiber Membranes for Waterproof-Breathable Applications", *Appl. Surf. Sci.*, vol. 442, pp. 54–64, 2018.

[3]   Choi, C. H., Lee, H. and Weitz, D. A., "Rapid Patterning of PDMS Microfluidic Device Wettability Using Syringe-Vacuum-Induced Segmented Flow in Non-Planar Geometry", *ACS Appl. Mater. Interfaces*, vol. 10(4), pp. 3170–3174, 2018.

[4]   Gibbs, J. W., "A Method of Geometrical Representation of the Thermodynamic Properties of Substances by Means of Surfaces", *Trans. Conn. Acad. Arts Sci.*, pp.382-404, 1873.

[5]   Hautman, J. and Klein, M. L., "Microscopic Wetting Phenomena", *Phy. Rev. Lett.*, vol 67(13), pp. 1763-1766, 1991.

[6]   McHale, G., Shirtcliffe, N. J. and Newton, M. I., "Super-hydrophobic and Super-wettingSurfaces: Analytical Potential?", *Analyst*, vol. 129(4), pp. 284-287, 2004.

[7]   Bhushan, B., "Lessons from nature for green science and technology: an overview and bioinspired superliquiphobic/philic surfaces", *Phil. Trans. R. Soc. A*, vol. 377(2138): 20180274, 2019.

[8]   Wenzel, R. N., "Resistance of Solid Surfaces to Wetting by Water", *Ind. Eng. Chem.*, vol. 28, pp. 988-994, 1936.

[9]   Cassie, A. B. D., Baxter, S., "Wettability of Porous Surfaces", *Trans. Faraday Soc.*, vol. 40, pp. 546-551, 1944.

[10] Barbieri, L., Wagner, E. and Hoffman, P., "Water Wetting Transition Parameters of Perfluorinated Substrates with Periodically Distributed Flat-Top Microscale Obstacles", *Langmuir*, vol. 23(4), pp. 1723-1734, 2007.

[11] Wang, X. and Zhang, Q., "Insight into the Influence of Surface Roughness on the Wettability of Apatite and Dolomite", *Minerals*, vol. 10(2): 114, 2020.

[12] Gao, L. and McCarthy, T. J., "How Wenzel and Cassie Were Wrong", *Langmuir*, vol. 23(7), pp. 3762-3765, 2007.

[13] Nosonovsky, M., "On the Range of Applicability of the Wenzel and Cassie Equations", *Langmuir*, vol. 23(19), pp. 9919-9920, 2007.

[14] Extrand, C. W., "Contact Angles and Hysteresis on Surfaces with Chemically Heterogeneous Islands", Langmuir, vol. 19(9), pp. 3793-3796, 2003.

[15] Shardt, N. and Elliott, J. A. W., "Gibbsian Thermodynamics of Cassie–Baxter Wetting (Were Cassie and Baxter Wrong? Revisited)", *Langmuir*, vol. 34(40), pp. 12191-12198, 2018.

[16] Gao, L. and McCarthy, T. J., "Contact Angle Hysteresis Explained", *Langmuir*, vol. 22, pp. 6234-6237, 2006.

[17] Marmur, A., "Soft Contact: Measurement and Interpretation of Contact Angles", *Soft Matter*, vol. 2, pp. 12-17, 2006.

[18] Kung, C. H., Sow, P. K., Zahiri, B. and Mérida, W**., "**Assessment and Interpretation of Surface Wettability Based on Sessile Droplet Contact Angle Measurement: Challenges and Opportunities",*Adv. Mater. Interfaces*, vol. 6(18), 1900839, 2019.

[19] Barthlott, W. and Neinhuis, C., "Purity of the Sacred Lotus, or Escape from Contamination inBiological Surfaces", *Planta*, vol. 202, pp. 1–8, 1997.

[20] Bhushan, B., and Jung, Y. C., "Micro and Nanoscale Characterization of Hydrophobic and Hydrophilic Leaf Surface", *Nanotechnology*, vol. 17, pp.2758-2772, 2006.

[21] Shirtcliffe, J. N., McHale, G. and Newton, M. I., "Learning from Superhydrophobic

Plants: the Use ofHydrophilic Areas on Superhydrophobic Surfaces for Droplet Control Part of "Langmuir 25[th]Year: Wetting and Superhydrophobicity" Special Issue", *Langmuir*, vol. 25(24), pp. 14121 14128, 2009.

[22] Marmur, A., "The Lotus Effect: Superhydrophobicity and Metastability", *Langmuir*, vol. 20, pp. 3517–3519, 2004.

[23] Neinhuis, C., Koch, K. and Barthlott, W, "Movement and Regeneration of Epicuticular Waxes ThroughPlant Cuticles", *Planta*,vol. 213, pp. 427–434, 2001.

[24] Neinhuis, C., and Barthlott, W, "Characterization and Distribution of Water-Repellant, Self-cleaning Plant Surfaces", vol. 79(6), pp. 667-677, 1997.

[25] Cheng, L., "Marine and Freshwater Skaters: Differences in Surface Fine Structures", *Nature*, vol. 242, pp. 132-133, 1973.

[26] Andersen, N. M., "Fine structure of the body hair layers and morphology of thspirales of semiaquatic bugs (Insects, Hemiptera, Gerromorpha) in relation to life on the water surface", *Vidensk. Meddr. Dansk Naturh. Foren*, vol. 140, pp. 7-37, 1977.

[27] Gao, X. and Jiang, L., "Water Repellant Legs of Water Striders", *Nature*, vol. 432, pp. 36, 2004.

[28] Shi, F., Niu, J., Liu, J., Liu, F., Wang, Z., Feng, X. -Q., and Zhang, X., "Towards Understanding Why a Superhydrophobic Coating is Needed by Water Striders", *J. Adv. Mater.*, vol. 19(17), pp. 2257-2261, 2007.

[29] Wagner, T., Neinhuis, C., and Barthlott, W, "Wettability and Contaminability of Insect Wings as a Function of Their Surface Sculptures", vol. 77(3), pp. 213-225, 1996.

[30] Parker, A. R., and Lawrence, C. R., "Water Capture by a Desert Beetle", *Nature*, vol. 414, pp. 33-34, 2001.

[31] Kim, S. H., Kim, J. -H., Kang, B. -K., and Uhm, H. S., "Superhydrophobic CF*x*Coating via In-Line Atmospheric RF Plasma of He-CF4-H2", *Langmuir*, vol. 21, pp. 12213-12217, 2005.

[32]   Dettre, R. H., and Johnosn, Jr., R. E., "Contact Angle Hysteresis", in *Contact Angle, Wettability, and Adhesion, Advances in Chemistry Ser 43*, chap. 7, pp. 112-135, American Chemical Society, Washington, 1964.

[33]   Onda, T., Shibuichi, S., Satoh, N., and Tsujii, K., "Super Water-Repellant Fractal Surfaces", *Langmuir*, vol. 12, pp. 2125-2127, 1996.

[34]   Shibuichi, S., Onda, T., Satoh, N., and Tsujii, K., "Super Water-Repellant Surfaces Resulting from Fractal Structures", *J. Phys. Chem.*, vol. 100(50), pp. 19512-19517, 1996.

[35]   Khorasani, M. T., Mirzadeh, H., and Kermani, Z., "Wettability of Porous Polydimethylsiloxane Surface: Morphology Study", *Appl. Surf. Sci.*, vol. 242(3), pp. 339-345, 2005.

[36]   Bartell, F. E., and Shepard, J. W., "The Effect of Roughness on Apparent Contact Angles and on Contact Angle Hysteresis. I. The System Paraffin-Water-Air", *J. Phys. Chem.*, vol. 57(2), pp. 211-215, 1953.

[37]   Ebril, H. Y., Demirel, A. L., Avci, Y., and Mert, O., "Transformation of a Simple Plastic into a Superhydrophobic Surface", *Science*, vol. 299, pp. 1377-1380, 2003.

[38]   Bico, J., Marzolin, C., and Quere, D., "Pearl Drops", *EPL*, vol. 47 (2), pp. 220-226, 1999.

[39]   Patankar N.A., "On the Modelling of Hydrophobic Contact Angles on Rough Surfaces", *Langmuir*, 2003, pp. 1249-1253, 2003.

[40]   Li, W., Cui, X. S., and Fang, G. P., "Optimal Geometrical Design for Superhydrophobic Surfaces: Effects of a Trapezoid Microtexture", *Langmuir*, vol. *26*(5), pp. 3194-3202, 2010.

[41]   Su, Y., Ji, B., Zhang, K., Gao, H., and Huang, Y., and Hwang, K., "Nano to Micro Structural Hierarchy is Crucial for Stable Superhydrophobic and Water-Repellent Surfaces", *Langmuir*, vol. *26* (7), pp. 4984-4989, 2010.

[42]   Dong, J., Jin, Y., Dong, H., and Sun, L., "Numerical Calculation Method of Apparent Contact Angles on Heterogeneous Double-Roughness Surfaces", *Langmuir*, vol. *33*(39),

pp. 10411-10418, 2017.

[43] Ding, W., Fernandino, M., and Dorao, C.A., "Conical Micro-structures as a Route for Achieving Super-Repellency in Surfaces with Intrinsic Hydrophobic Properties" *Appl. Phys. Lett.*, vol. 115(5), pp. 053703, 2019.

[44] Teoh, G. H., Jawad, Z. A., Ooi, B. S., Chang, Y. S., and Low, S. C., "Surface-templating of rough interface to efficiently recover aquaculture wastewater using membrane distillation", *Desalination*, vol. 522, pp. 115419, 2022.

[45] Cao, L., Hu, H. H., and Gao, D., "Design and Fabrication of Micro-textures for Inducing a Superhydrophobic Behavior on Hydrophilic Materials", *Langmuir*, vol. 23 (8), pp. 4310–4314, 2007.

[46] Feng, L., Song, Y., Zhai, J., Liu, B., Xu, J., and Zhu, D., "Creation of a Superhydrophobic Surface from an Amphiphilic Polymer", *Angew. Chem. Int. Ed. Engl.*, vol. 42(7), pp. 800-802, 2003.

[47] Kim, J. -H., Liu, G, and Kim, S. H., "Deposition of Stable Hydrophobic Coatings with In-Line CH_4 Atmospheric rf Plasma", *J. Mater. Chem.*, vol. 16 (10), pp. 977-981, 2006.

[48] Patankar, N. A., "Hydrophobicity of Surfaces with Cavities: Making Hydrophobic Substratesfrom Hydrophilic Materials?", *J Adhes. Sci. Technol.,* vol. 23(3),pp. 413-433, 2012.

[49] Abdelsalam, M. E., Bartlett, P. N., Kelf, T., and Baumberg, J., "Wetting of Regularly StructuredGold Surfaces", *Langmuir*, vol. 21, pp. 1753-1757, 2005.

[50] Domingues, E. M., Arunachalam, S., and Mishra, H., "Doubly Reentrant Cavities Prevent Catastrophic Wetting Transitions on Intrinsically Wetting Surfaces", *ACS Appl. Mater. Interfaces*, vol. 9(25), pp. 21532-21538, 2017.

[51] Zhang, W., Wang, D., Sun, Z., Song, J., and Deng, X., "Robust Superhydrophobicity: Mechanisms and Strategies", *Chem. Soc. Rev.*, vol. 50, pp. 4031–4061, 2021.

[52] Rabbani, S., Jafari, R., and Momen, G., "Superhydrophobic micro-nanofibers from

PHBV-SiO$_2$ biopolymer composites produced by electrospinning", *Funct. Compos. Mater.*, vol. 3**,** 2022.

[53] Ntez, R. R., and Andelman, D., "Roughness-Induced Wetting", *Phys. Rev. E*, vol. 55(1), pp. 687-700, 1990.

[54] Tang, J. Z., and Harris, J. G., "Fluid Wetting on Molecularly Rough Surfaces", *J. Chem. Phys.*, vol. 103(18), pp. 8201, 1995.

[55] Alberti, G., and DeSimone, A., "Wetting of rough surfaces: a homogenization approach", *Phil. Trans. R. Soc. A*, vol. 461, pp. 79-97, 2005.

[56] Dorrer, C., and Rühe, J., "Condensation and Wetting Transitions on MicrostructuredUltrahydrophobic Surfaces", *Langmuir*, vol. 23(7), pp. 3820-3824, 2007.

[57] Jung, Y. C., and Bhushan, B., "Wetting Transition of Water Droplets on Superhydrophobic Patterned Surfaces", *Scr. Mater.*, vol. 57, pp. 1057-1060, 2007.

[58] Patankar, N. A., "Transition between Superhydrophobic States on Rough Surfaces", *Langmuir*, vol. 20, pp. 7097-7102, 2004.

[59] Marmur, A., "Wetting on Hydrophobic Rough Surfaces: To Be Heterogeneous or Not to Be?", *Langmuir*, vol. 19(20), pp. 8343-8348, 2003.

[60] Bico, J., Thiele, U., and Quéré, D., "Wetting of Textured Surfaces", *Colloids Surf. A: Physicochem. Eng. Asp.*, vol. 206(1-3), pp. 41-46, 2002.

[61] Milne, A. J. B., and Amirfazli, A., "The Cassie Equation: How It Is Meant to Be Used", *Adv. Colloid Interface Sci.*, vol. 170(1-2), pp. 48-55, 2012.

[62] Yao, C., -W., Alvarado, J. L., Marsh, C. P., Jones, B. G., Collins, M. K., "Wetting Behavior on Hybrid Surfaces with Hydrophobic and Hydrophillic Properties", *Appl. Surf. Sci.*, vol. 290, pp. 59-65, 2014.

[63] Gong, W., Zu, Y., Chen, S., and Yan, Y., "Wetting Transition Energy Curves for a Droplet on a Square-Post Patterned Surface", *Sci. Bull.*, vol. 62(2), pp. 136-142, 2017.

[64] Alen, S. K., Farhat, N., and Rahman, M. A., "Analytical modeling of wetting states and simulation of drop shape on microstructured surfaces", in *2015 11ᵗʰ International Conference on Mechanical Engineering*, vol. 1754(1), Jul. 2016, pp. 050043.

[65] Schiavon, C. S., Moreira, M. L., Cava, S. S., Raubach, C. W., and Jardim, P. L. G., "Wetting-State Transition of Random Surfaces", *Thin Solid Films*, vol. 745, pp. 139102, 2022.

[66] Wilke, K. L., Lu, Z., Song, Y, and Wang, E. N., "Turning Traditionally Non-Wetting Surfaces Wetting Even for Ultra-High Surface Energy", *Proc. Natl. Acad. Sci. U. S. A.*, vol. 119(4), pp. e2109052119, 2022.

[67] Bormashenko, E., Pogreb, R., Whyman, G., Bormashenko, Y., and Erlich, M., "Vibration-Induced Cassie-Wenzel Wetting on Rough Surfaces", *Appl. Phys. Lett.*, vol. 90, pp. 201917, 2007.

[68] Boreyko, J. B., and Chen, C. H., "Self-Propelled Dropwise Condensate on Superhydrophobic Surfaces", *Phys. Rev. Lett.*, vol. 103(18), pp. 184501, 2009.

[69] Liu, G., Fu, L., Rode, A. V., and Craig, V. S. J., "Water Droplet Motion Control on Superhydrophobic Surfaces: Exploiting the Wenzel-to-Cassie Transition", *Langmuir*, vol. 27(6), pp. 2595-2600, 2011.

[70] Long, J., Hyder, M. N., Huang, R. Y. M., and Chen, P., "Thermodynamic Modeling of ContactAngles on Rough, Heterogeneous Surfaces", *Adv. Colloid Interface Sci.*,vol. 118(1-3), pp. 173-190, 2005.

[71] Li, W., and Amirfazli, A., "A Thermodynamic Approach for Determining the Contact AngleHysteresis for Superhydrophobic Surfaces", *J. Colloid Interface Sci.*, vol. 292,pp. 195-201, 2005.

[72] Chen, Y., He, B., Lee, J., and dorrer, N. A., "Anisotropy in the Wetting of Rough Surfaces", *J. Colloid Interface Sci.*, vol. 281, pp. 458–464, 2005.

[73] Chatain, D., Lewis, D., Baland, J. P., and Carter, W. C., "Numerical Analysis of The Shapes and Energies of Droplets on Micropatterned Substrates" *Langmuir*, vol. 22(9), pp.

4237–4243, 2006.

[74] Cui, X., and Li, W., "On the Possibility of Superhydrophobic Behavior for Hydrophilic Materials",*J. Colloid Interface Sci.*, vol. 347(1), pp. 156-62, 2010.

[75] Promraksa, A., and Chen, L. J., "Modelling Contact Angle Hysteresis of a Liquid Droplet Sitting on a Cosine Wave-like Pattern Surface", *J. Colloid Interface Sci.*, vol. 384, pp. 172-181, 2012.

[76] Promraksa, A., Chuang, Y. C., and Chen, L., J., "Study on the Wetting Transition of a Liquid Droplet Sitting on a Square-Array Cosine Wave-like Patterned Surface", *J. Colloid Interface Sci.*, vol. 418, pp. 8–19, 2014

[77] Dubov, A. L., Perez-Toralla, K., Letailleur, A., Barthel, E., and Teisseire, J., "SuperhydrophobicSilica Surfaces: Fabrication and Stability", *J. Micromech. Microeng.*, vol. 23, pp. 125013, 2013.

[78] Guo, H. Y., Li, B., and Feng, X. Q, "Stability of Cassie-Baxter Wetting States on Microstructured Surfaces", *Phys. Rev. E*, vol. 94(4), pp. 042801, 2016.

[79] Goswami, A., and Rahman, M. A., "Numerical study of energetics and wetting stability of liquid droplets on microtextured surfaces", *Colloid Polym. Sci.*, vol. 295(10), pp. 1787–1796, 2017.

[80] Goswami, A., Alen, S. K., Farhat, N., and Rahman, M. A., "Numerical Study of Wetting Stability and Sliding Behavior of Liquid Droplets on Microgrooved Surfaces", *Colloid Polym. Sci.*, vol. 297, pp. 989-1000, 2018.

[81] He, L., Sui, X., Liang, W., Wang, Z., and Akbarzadeh, A., "Numerical Analysis of Anisotropic Wetting of Chemically Striped Surfaces", *RSC Adv*, vol. 8(55), pp. 31735–31744, 2018.

[82] Semprebon, C., and Brinkmann, M., "On the Onset of Motion of Sliding Drops", *Soft Matter*, vol. 10(18), pp. 3325–3334, 2014.

[83] Ding, Y., Jia, L., Yin, L., Dang, C., Liu, X., and Xu, J., "Anisotropic Wetting

Characteristics of Droplet on Micro-grooved Surface", *Colloids Surf. A: Physicochem. Eng. Asp.*, vol. 633-1, pp. 127850, 2022.

[84] Drelich, J., Chibowski, E., Meng, D.D. and Terpilowski, K., "Hydrophilic and Superhydrophilic Surfaces and Materials", *Soft Matter*, vol. 7(21), pp.9804-9828, 2011.

[85] Bikerman, J. J., "The Surface Roughness and Contact Angle", *J. Phys. Chem.*, vol. 54(5), pp. 653-658, 1950.

[86] Good, R. J., Kvikstad, J. A., and Bailey, W. O., "Anisotropic Forces in the Surface of a Stretch-Oriented Polymer", *J. Colloid Interface Sci.*, vol. 35(2), pp. 314-327, 1971.

[87] Hitchcock, S. J., Carroll, N. T., and Nicholas, M. G., "Some Effects of Substrate Roughness on Wettability", *J. Mater. Sci.*, vol. 16, pp. 714-732, 1981.

[88] Nicholas, M. G., Crispin, R. M., and McGurran, B., "Some Effects of Surface Texture on Liquid Behaviour", *Wear*, vol. 109, pp. 305-313, 1986.

[89] Schonhorn, H., "Anisotropic Wetting of Liquids on Finely Grooved Surfaces", *J. Adhes.*, vol. 23(3), pp. 147-161, 1987.

[90] Sung, N. H., Lee, H. Y., Yuan, P., and Sung, C. S. P., "Surface Structure, Topology, and Liquid Wetting Behavior in Oriented Polymers", *Polym. Eng. Sci.*, vol. 29(12), pp. 791-800, 1989.

[91] Feng, L., Li, S., Lim, Y., Li, H., Zhong, L., Zhai, J., Song, Y., Liu, A., Jiang, L., and Zhu, D., "Supe-Hydrophobic Surfaces: From Natural to Artificial", *Adv. Mater.*, vol. 14 (24), pp. 1857-1860, 2002.

[92] Sommers, A. D., and Jacobi, A. M., "Creating Micro-Scale Surface Topology to Achieve Anisotropic Wettability on an Aluminum Surface", *J. Micromech. Microeng.*, vol. 16, pp. 1571-1578, 2006.

[93] Chung, J. Y., Youngblood, J. P., and Stafford, C. M., "Anisotropic Wetting on Tunable Micro-Wrinkled Surfaces", *Soft Matter*, vol. 3, pp. 1163-1169, 2007.

[94] Zhao, Y., Lu, Q., Li, M., and Li, X., "Anisotropic Wetting Characteristics on

Submicrometer-Scale Periodic Grooved Surface", *Langmuir*, vol. 23, pp. 6212- 6217, 2007.

[95]   Zhang, F., and Low, H. Y., "Anisotropic Wettability on Imprinted Hierarchical Structures", *Langmuir*, vol. 23(14), pp. 7793-7798, 2007.

[96]   Xia, D., and Brueck, S. R. J., "Strongly Anisotropic Wetting on One-Dimensional Nanopatterned Surfaces", *Nano Lett.*, vol. 8(9), pp. 2819-2824, 2008.

[97]   Xia, D., He, X., Jiang, Y., -B., Lopez, G. P., and Brueck, S. R. J., "Tailoring Anisotropic Wetting Properties on Submicrometer-Scale Periodic Grooved Surfaces", *Langmuir*, vol. 26(4), pp. 2700-2706, 2010.

[98]   Rahman, M. A., and Jacobi, A. M., "Wetting Behavior and Drainage of Water Droplets on Microgrooved Brass Surfaces", *Langmuir*, vol. 28, pp. 13441-13451, 2012.

[99]   Rahman, M. A., and Jacobi, A. M., "Experimental Investigation of Wetting Anisotropy on Microgrooved Brass Surfaces", in *2013 10th International Conference on Mechanical Enginnering (ICME 2013), Procedia Eng.*, vol. 90, July 2014, pp. 611 – 617.

[100] Rahman, M. A., and Jacobi, A. M., "Drainage of Frost Melt Water from Vertical Brass Surfaceswith Parallel Microgrooves", *Int. J. Heat Mass Transf.*, vol. 55, pp.1596-1605, 2012.

[101] Farhat, N., Alen, S. K., and Rahman, M. A., "Numerical Study of the Wetting and Mobility ofLiquid Droplets on Horizontal and Inclined Flat and Microgrooved Surfaces", in *2014 Proceedings ofthe 6th International Conference on Thermal Engineering (ICTE), Procedia Eng.*, vol. 105, July 2015, pp. 576-585.

[102] Brakke, K. A., "The Surface Evolver", *Exp. Math.*, vol. 1(2), pp. 141–165, 1992.

[103] Asakura, K., and Yan, J., "Ultraprecision micro grooving on brass for surface wettability control", *Adv. Mat. Res.*, vol. 1017, pp. 489-494, 2014.

[104] Li, P., Xie, J., Cheng, J., and Wu, K. K., "Anisotropic Wetting Properties on A Precision-Ground Micro V-Grooved Si Surface Related toTheir Micro-Characterized Variables", *J.*

Micromech. Microeng., vol. 24**,** pp.075004.

[105] Fan, B., Bandaru, P. R., "Anisotropy in the hydrophobic and oleophilic characteristics of patterned surfaces", *Appl. Phys. Lett.*, vol. 111, pp. 261603, 2017.

[106] Song, D., Song, B., Hu, H., Du, X., and Ma, Z., "Contact Angle and Impinging Process of Droplets on Partially Grooved Hydrophobic Surfaces", *Appl. Therm. Eng.*, vol. 85, pp. 356-364, 2015.

[107] Qi, B., Zhou, J., Wei, J., and Li, X., "Study on the wettability and condensation heat transfer of sine-shaped micro-grooved surfaces", *Exp. Therm. Fluid Sci.*, vol. 90, pp. 28-36, 2017.

[108] Shirani, E.,Razmjou, A.,Tavassoli, H.,Landarani-Isfahan, A., Rezaei, S., Kajani, A. A.,Asadnia, M., Hou, J., and Warkiani, M. E., "Strategically Designing a Pumpless Microfluidic Device on an "Inert" Polypropylene Substrate with Potential Application in Biosensing and Diagnostics"*Langmuir*, vol. 33, pp. 5565-5576, 2017.

[109] Li, J., and Guo, Z., "Spontaneous Directional Transportations of Water Droplets on Surfaces Driven by Gradient Structures", *Nanoscale*, vol. 10, pp. 13814-13831, 2018.

[110] Rahman, M. A., and Jacobi, A. M., "Study of the Effects of Microgrooved Geometry on FrostStructure", in *2012 International Refrigeration and Air Conditioning Conference at Purdue*, July 16-19, 2012, pp. 2294 (10 pp).

[111] Brakke, K. A., Surface Evolver Documentation, 2013.

[112] Arfken G (1985), "Mathematical methods for physicists", Third edn. Academic Press, London.

[113] Lamour, G., Hamraoui, A., Buvailo, A., Xing, Y., Keuleyan, S., Prakash, V., Eftekhari-Bafrooei, A., and Borguet, E., "Contact Angle Measurements Using a Simplified Experimental Setup", *J. Chem. Educ.*, vol. 87(12), pp. 1403-1407, 2010.

[114] Ryan, B. J., and Poduska, K. M., "Roughness Effects on Contact Angle Measurements", *Am. J. Phys.*, vol. 76, pp. 1074, 2008.

[115] Tudek, J., Crandall, D., Fuchs, S., Werth, C. J., Valocchi, A. J., Chen, Y., and Goodman, A., "In-situ Contact Angle Measurements of Liquid CO_2, Brine and Mount Simon Sandstone Core Using Micro X-Ray CT Imaging, Sessile Drop, and Lattice Boltzmann Modelling", *J. Pet. Sci. Eng.*, vol. 155, pp. 3-10, 2017.

[116] Gomes, D. J. C., De Souza, N. C., and Silva, J. R., "Using a Monocular Optical Microscope to Assemble a Wetting Contact Angle Analyser", Measurement, vol. 46(9), pp. 3623-3627, 2013.

[117] Alen, S. K., and Farhat, N., *Study of Wetting Behavior and Mobility of Liquid Droplets on Flat and Microgrooved Metal Surfaces*, B.Sc. Engg. Thesis, Department of Mechanical Engineering, Bangladesh University of Engineering and Technology, 2015.

[118] Carbone, G., and Mangialardi, L., "Hydrophobic Properties of a Wavy Rough Substrate", *Eur. Phys. J. E*, vol. 16, pp. 67-76, 2005.

[119] Wan, Y., Lian, Z., Xu, J., Weng, Z., Yin, X., and Yu, H., "Fabrication of the Stainless-Steel Surface with Super Durable One Direction Superhydrophobicity and Two-Direction Anisotropy Wettability", *Micro Nano Lett.*, vol. 9(10), pp. 712-716, 2014.

[120] Li, S. G., Lim, H. S., Lee, D. Y., Kwak, D., and Cho, K., "Tunable Anisotropic Wettability of Rice Leaf-Like Wavy Surfaces", *Adv. Funct. Mater.*, vol. 23(5), 2012.

[121] Dokowicz, M., and Nowicki, W., "Morphological Transitions of Droplets Wetting a Series of Triangular Grooves", *Langmuir*, vol. 32, pp. 7259-7264, 2016.

[122] Kusumaatmaja, K., Blow, M. L., Dupuis, A., and Yeomans, J. M., "The Collapse Transition on Superhydrophobic Surfaces", *EPL*, vol. 81(3), pp. 36003, 2008.

[123] Gross, M., Varnik, F., Raabe, D., and Steinbach, I., "Small Droplet on Superhydrophobic Substrates", *Phys. Rev.* E, vol. 81(5), pp. 051606, 2010.

[124] Yoshimitsu, Z., Nakajima, A., Watanabe, T., and Hashimoto, K., "Effects of Surface Structureon Hydrophobicity and Sliding Behavior of Water Droplets", *Langmuir*, vol. 18(15), pp.5818-5822, 2002.

[125] Li, W., Fang, G., Li, Y., and Qiao, G., "Anisotropic Wetting Behavior Arising from Superhydrophobic Surfaces: Parallel Grooved Structure", *J. Phys. Chem. B*, vol. 112, pp. 7234-7243, 2008.

[126] Park, C. I., Jeong, H. E., Lee, S. H., Cho, H. S., and Suh, K. Y., "Wetting Transition and Optimal Design for Microstructured Surfaces with Hydrophobic and Hydrophilic Materials", *J. Colloid Interface Sci.*, vol. 336, pp. 298-303, 2009.

[127] Zhang, M., Ma, L., Wang, Q., Hao, P., and Zheng, X., "Wettability Behavior of Nanodroplets on Copper Surfaces with Hierarchical Nanostructures", *Colloids Surf. A: Physicochem. Eng. Asp.*, vol. 604, pp. 125291, 2020.

[128] Yeh, K. -Y., and Chen, L. -J., "Contact Angle Hysteresis on Regular Pillar-like Hydrophobic Surfaces", *Langmuir*, vol. 24, pp. 245-251, 2008.

APPENDIX

SURFACE EVOLVER (VERSION 2.70) CODES

Based on a bottom-up method to geometry development, SE geometry is specified using a text file in the necessary format (.fe). To build a body, one first lists the vertices (points in space), edges (directed connection between two vertices), and faces (ordered collection of three or more edges), then combines the faces to generate volume. Codes are also subjected to a number of geometric, energy, and volumetric limitations. Here is a list of the scripts we utilized in our work (comments are preceded by a double forward slash).

A.1 Code for Free Sessile Droplet on Flat Smooth Surface

//this script gives an initial geometry of cubical shape for further computation with SE.

parameter angle = 111 //intrinsic contact angle is 111° for micro-Si surface

parameter vol = 4 //volume of the droplet is specified in microliter

parameter den = 1000*(10^(-9)) //density of water is specified

gravity_constant 0 // start with gravity off

#define T (-cos(angle*pi/180)) // virtual tension of facet on Flat surface

constraint 1 // on the Flat surface

formula: z = 0

energy: // as flat surface is not modeled so edges on the surface will be specified with this energy

      // functions and that results in the same energy we would get if we did include the face.

e1: -T*y

e2: 0

e3: 0

vertices   //points are listed in a space here

1 0 0 0 constraint 1   // 4 vertices Flat surface

2 1 0 0 constraint 1

3 1 1 0 constraint 1

4 0 1 0 constraint 1

5 0 0 1

6 1 0 1

7 1 1 1

8 0 1 1

edges   // given by endpoints and attribute

1 1 2 constraint 1   // 4 edges Flat surface

2 2 3 constraint 1

3 3 4 constraint 1

4 4 1 constraint 1

5 5 6

6 6 7

7 7 8

8 8 5

9 1 5

10 2 6

11 3 7

12 4 8

131

faces   // given by oriented edge loop

1 1 10 -5 -9 frontcolorcyanbackcoloryellow //facet color is given on front and back side

2 2 11 -6 -10 frontcolor cyan backcolor yellow

3 3 12 -7 -11 frontcolor cyan backcolor yellow

4 4 9 -8 -12 frontcolor cyan backcolor yellow

5 5 6 7 8 frontcolor cyan backcolor yellow

bodies   // one body, defined by its oriented faces and volume and density is specified

1 1 2 3 4 5 volume vol density den

read //computation

// 'r' = refinement of the mesh

// 'g' = iteration step

// 'u' = mesh equiangulation

// 'V' = vertex averaging

r

gogo := {{u; V; g50;}20}; //user-defined command the numbers aside corresponds to command repetition

//End of the script

A.2 Code for Micro Wavy Surfaces

// this code is for groove pitch, λ_w = 98 μm, groove height, H_w =80 μm, eight pillar structures

gravity_constant 0 //starts with gravity 0

parameter vol = 1.5

parameter n_p = 8 // pillar numbers

parameter height= 80

parameter pitch= 98

parameter phi= 0

parameter volume_drop = (vol*(10^(9)))

parameter contact_angle = 111 //intrinsic contact angle

parameter GravityAnglePhi = 0 //inclination angle

#define T1 (-cos(angle_1*pi/180))

parameter theta_cos = cos(contact_angle*pi/180)

parameter den = (10^(-15))

constraint 1

formula: z = (sin (2*pi*x/period+pi*phi/180)*height/2)

energy:

e1: -T1*y

e2: 0

e3: 0

constraint 2 nonpositive //left edges

formula: (x-24.5)*(x-24.5004)

constraint 3 nonpositive //right edges

formula: (x-710.4996)*(x-710.5)

vertices

1 24.5 0 40.0 fixed

2 24.5004 0 39.99999999 fixed

3 26.541666666666668 0 39.657794454952416 fixed

4 28.583333333333332 0 38.63703305156273 fixed

5 30.625 0 36.95518130045147 fixed

6 32.666666666666664 0 34.64101615137755 fixed

7 34.708333333333336 0 31.734133611649405 fixed

8 36.75 0 28.284271247461902 fixed

9 38.791666666666664 0 24.350457160348835 fixed

10 40.833333333333336 0 19.999999999999996 fixed

11 42.875 0 15.307337294603595 fixed

12 44.916666666666664 0 10.35276180410084 fixed

13 46.958333333333336 0 5.221047688802063 fixed

14 49.0 0 0 fixed

15 51.041666666666664 0 -5.221047688802053 fixed

16 53.083333333333336 0 -10.352761804100831 fixed

17 55.125 0 -15.307337294603586 fixed

18 57.166666666666664 0 -20.000000000000004 fixed

19 59.208333333333336 0 -24.350457160348824 fixed

20 61.25 0 -28.2842712474619 fixed

21 63.291666666666664 0 -31.734133611649398 fixed

22 65.33333333333333 0 -34.64101615137754 fixed

23 67.375 0 -36.95518130045147 fixed

24 69.41666666666667 0 -38.63703305156273 fixed

25 71.45833333333333 0 -39.657794454952416 fixed

26 73.5 0 -40.0 fixed

27 75.54166666666667 0 -39.65779445495242 fixed

28 77.58333333333333 0 -38.63703305156274 fixed

29 79.625 0 -36.955181300451464 fixed

30 81.66666666666667 0 -34.64101615137754 fixed

31 83.70833333333333 0 -31.734133611649405 fixed

32 85.75 0 -28.28427124746191 fixed

33 87.79166666666667 0 -24.35045716034884 fixed

34 89.83333333333333 0 -20.000000000000018 fixed

35 91.875 0 -15.307337294603583 fixed

36 93.91666666666667 0 -10.352761804100828 fixed

37 95.95833333333333 0 -5.221047688802067 fixed

38 98.0 0 0 fixed

39 100.04166666666667 0 5.221047688802047 fixed

40 102.08333333333333 0 10.35276180410081 fixed

41 104.125 0 15.307337294603599 fixed

42 106.16666666666667 0 20.0 fixed

43 108.20833333333333 0 24.35045716034882 fixed

44 110.25 0 28.284271247461895 fixed

45 112.29166666666667 0 31.734133611649398 fixed

46 114.33333333333333 0 34.641016151377556 fixed

47 116.375 0 36.95518130045147 fixed

48 118.41666666666667 0 38.63703305156273 fixed

49 120.45833333333333 0 39.657794454952416 fixed

50 122.4996 0 39.99999999 fixed

51 122.5 0 40.0 fixed

52 122.5004 0 39.99999999 fixed

53 124.54166666666667 0 39.65779445495242 fixed

54 126.58333333333333 0 38.63703305156274 fixed

55 128.625 0 36.95518130045147 fixed

56 130.66666666666666 0 34.64101615137756 fixed

57 132.70833333333334 0 31.734133611649412 fixed

58 134.75 0 28.284271247461884 fixed

59 136.79166666666666 0 24.35045716034884 fixed

60 138.83333333333334 0 19.999999999999993 fixed

61 140.875 0 15.30733729460362 fixed

62 142.91666666666666 0 10.352761804100831 fixed

63 144.95833333333334 0 5.221047688802037 fixed

64 147.0 0 0 fixed

65 149.04166666666666 0 -5.221047688802079 fixed

66 151.08333333333334 0 -10.352761804100805 fixed

67 153.125 0 -15.307337294603593 fixed

68 155.16666666666666 0 -19.999999999999968 fixed

69 157.20833333333334 0 -24.350457160348817 fixed

70 159.25 0 -28.284271247461916 fixed

71 161.29166666666666 0 -31.734133611649394 fixed

72 163.33333333333334 0 -34.64101615137755 fixed

73 165.375 0 -36.95518130045146 fixed

74 167.41666666666666 0 -38.63703305156273 fixed

75 169.45833333333334 0 -39.65779445495242 fixed

76 171.5 0 -40.0 fixed

77 173.54166666666666 0 -39.657794454952416 fixed

78 175.58333333333334 0 -38.63703305156274 fixed

79 177.625 0 -36.95518130045147 fixed

80 179.66666666666666 0 -34.64101615137756 fixed

81 181.70833333333334 0 -31.734133611649415 fixed

82 183.75 0 -28.284271247461888 fixed

83 185.79166666666666 0 -24.350457160348846 fixed

84 187.83333333333334 0 -19.999999999999996 fixed

85 189.875 0 -15.307337294603624 fixed

86 191.91666666666666 0 -10.352761804100838 fixed

87 193.95833333333334 0 -5.221047688802042 fixed

88 196.0 0 0 fixed

89 198.04166666666666 0 5.221047688802073 fixed

90 200.08333333333334 0 10.352761804100801 fixed

91 202.125 0 15.307337294603588 fixed

92 204.16666666666666 0 19.99999999999996 fixed

93 206.20833333333334 0 24.350457160348814 fixed

94 208.25 0 28.284271247461913 fixed

95 210.29166666666666 0 31.73413361164939 fixed

96 212.33333333333334 0 34.64101615137755 fixed

97 214.375 0 36.95518130045146 fixed

98 216.41666666666666 0 38.637033051562724 fixed

99 218.45833333333334 0 39.65779445495242 fixed

100 220.4996 0 39.99999999 fixed

101 220.5 0 40.0 fixed

102 220.5004 0 39.99999999 fixed

103 222.54166666666666 0 39.657794454952416 fixed

104 224.58333333333334 0 38.63703305156274 fixed

105 226.625 0 36.95518130045147 fixed

106 228.66666666666666 0 34.641016151377535 fixed

107 230.70833333333334 0 31.734133611649415 fixed

108 232.75 0 28.284271247461895 fixed

109 234.79166666666666 0 24.35045716034885 fixed

110 236.83333333333334 0 20.0 fixed

111 238.875 0 15.307337294603629 fixed

112 240.91666666666666 0 10.352761804100844 fixed

113 242.95833333333334 0 5.221047688802046 fixed

114 245.0 0 0 fixed

115 247.04166666666666 0 -5.221047688802068 fixed

116 249.08333333333334 0 -10.352761804100794 fixed

117 251.125 0 -15.307337294603517 fixed

118 253.16666666666666 0 -19.999999999999957 fixed

119 255.20833333333334 0 -24.35045716034881 fixed

120 257.25 0 -28.28427124746191 fixed

121 259.2916666666667 0 -31.73413361164943 fixed

122 261.3333333333333 0 -34.64101615137751 fixed

123 263.375 0 -36.95518130045145 fixed

124 265.4166666666667 0 -38.637033051562724 fixed

125 267.4583333333333 0 -39.65779445495242 fixed

126 269.5 0 -40.0 fixed

127 271.5416666666667 0 -39.65779445495242 fixed

128 273.5833333333333 0 -38.63703305156274 fixed

129 275.625 0 -36.95518130045147 fixed

130 277.6666666666667 0 -34.641016151377535 fixed

131 279.7083333333333 0 -31.734133611649376 fixed

132 281.75 0 -28.284271247461948 fixed

133 283.7916666666667 0 -24.350457160348853 fixed

134 285.8333333333333 0 -20.000000000000004 fixed

137

135 287.875 0 -15.307337294603569 fixed

136 289.9166666666667 0 -10.352761804100778 fixed

137 291.9583333333333 0 -5.2210476888021216 fixed

138 294.0 0 0 fixed

139 296.0416666666667 0 5.221047688802064 fixed

140 298.0833333333333 0 10.352761804100858 fixed

141 300.125 0 15.307337294603514 fixed

142 302.1666666666667 0 19.999999999999954 fixed

143 304.2083333333333 0 24.350457160348803 fixed

144 306.25 0 28.284271247461902 fixed

145 308.2916666666667 0 31.73413361164943 fixed

146 310.3333333333333 0 34.64101615137751 fixed

147 312.375 0 36.95518130045145 fixed

148 314.4166666666667 0 38.637033051562724 fixed

149 316.4583333333333 0 39.65779445495242 fixed

150 318.4996 0 39.99999999 fixed

151 318.5 0 40.0 fixed

152 318.5004 0 39.99999999 fixed

153 320.5416666666667 0 39.65779445495242 fixed

154 322.5833333333333 0 38.63703305156274 fixed

155 324.625 0 36.95518130045147 fixed

156 326.6666666666667 0 34.64101615137754 fixed

157 328.7083333333333 0 31.73413361164938 fixed

158 330.75 0 28.28427124746195 fixed

159 332.7916666666667 0 24.350457160348856 fixed

160 334.8333333333333 0 20.000000000000007 fixed

161 336.875 0 15.307337294603574 fixed

162 338.9166666666667 0 10.352761804100783 fixed

163 340.9583333333333 0 5.221047688802127 fixed

164 343.0 0 0 fixed

165 345.0416666666667 0 -5.2210476888020585 fixed

166 347.08333333333333 0 -10.352761804100854 fixed

167 349.125 0 -15.30733729460364 fixed

168 351.1666666666667 0 -19.99999999999995 fixed

169 353.2083333333333 0 -24.350457160348803 fixed

170 355.25 0 -28.284271247461902 fixed

171 357.2916666666667 0 -31.734133611649426 fixed

172 359.3333333333333 0 -34.64101615137751 fixed

173 361.375 0 -36.95518130045145 fixed

174 363.4166666666667 0 -38.637033051562724 fixed

175 365.4583333333333 0 -39.657794454952416 fixed

176 367.5 0 -40.0 fixed

177 369.5416666666667 0 -39.65779445495243 fixed

178 371.5833333333333 0 -38.637033051562746 fixed

179 373.625 0 -36.95518130045148 fixed

180 375.6666666666667 0 -34.64101615137754 fixed

181 377.7083333333333 0 -31.734133611649384 fixed

182 379.75 0 -28.28427124746195 fixed

183 381.7916666666667 0 -24.35045716034886 fixed

184 383.8333333333333 0 -20.000000000000014 fixed

185 385.875 0 -15.307337294603578 fixed

186 387.9166666666667 0 -10.352761804100787 fixed

187 389.9583333333333 0 -5.221047688802132 fixed

188 392.0 0 0 fixed

189 394.0416666666667 0 5.221047688802054 fixed

190 396.0833333333333 0 10.35276180410085 fixed

191 398.125 0 15.307337294603636 fixed

192 400.1666666666667 0 19.999999999999943 fixed

193 402.2083333333333 0 24.3504571603488 fixed

194 404.25 0 28.2842712474619 fixed

195 406.2916666666667 0 31.73413361164942 fixed

196 408.3333333333333 0 34.6410161513775 fixed

197 410.375 0 36.95518130045145 fixed

198 412.4166666666667 0 38.637033051562724 fixed

199 414.4583333333333 0 39.657794454952416 fixed

200 416.4996 0 39.99999999 fixed

201 416.5 0 40.0 fixed

202 416.5004 0 39.99999999 fixed

203 418.5416666666667 0 39.65779445495243 fixed

204 420.5833333333333 0 38.637033051562746 fixed

205 422.625 0 36.95518130045148 fixed

206 424.6666666666667 0 34.64101615137754 fixed

207 426.7083333333333 0 31.734133611649384 fixed

208 428.75 0 28.284271247461955 fixed

209 430.7916666666667 0 24.350457160348867 fixed

210 432.8333333333333 0 20.000000000000018 fixed

211 434.875 0 15.307337294603583 fixed

212 436.9166666666667 0 10.352761804100792 fixed

213 438.9583333333333 0 5.221047688802136 fixed

214 441.0 0 0 fixed

215 443.0416666666667 0 -5.22104768880205 fixed

216 445.0833333333333 0 -10.352761804100846 fixed

217 447.125 0 -15.30733729460363 fixed

218 449.1666666666667 0 -19.99999999999994 fixed

219 451.2083333333333 0 -24.350457160348796 fixed

220 453.25 0 -28.284271247461895 fixed

221 455.2916666666667 0 -31.73413361164942 fixed

222 457.3333333333333 0 -34.64101615137757 fixed

223 459.375 0 -36.95518130045145 fixed

224 461.4166666666667 0 -38.637033051562724 fixed

225 463.4583333333333 0 -39.657794454952416 fixed

226 465.5 0 -40.0 fixed

227 467.5416666666667 0 -39.65779445495243 fixed

228 469.58333333333 0 -38.637033051562746 fixed

229 471.625 0 -36.955181300451486 fixed

230 473.66666666667 0 -34.64101615137754 fixed

231 475.70833333333 0 -31.73413361164939 fixed

232 477.75 0 -28.28427124746196 fixed

233 479.79166666667 0 -24.350457160348867 fixed

234 481.8333333333 0 -20.00000000000002 fixed

235 483.875 0 -15.307337294603586 fixed

236 485.91666666667 0 -10.352761804100796 fixed

237 487.95833333333 0 -5.221047688802142 fixed

238 490.0 0 0 fixed

239 492.0416666666667 0 5.221047688802044 fixed

240 494.08333333333 0 10.35276180410084 fixed

241 496.125 0 15.307337294603627 fixed

242 498.1666666666667 0 19.999999999999936 fixed

243 500.20833333333 0 24.35045716034879 fixed

244 502.25 0 28.284271247461792 fixed

245 504.2916666666667 0 31.734133611649415 fixed

246 506.3333333333333 0 34.64101615137749 fixed

247 508.375 0 36.9551813004515 fixed

248 510.4166666666667 0 38.63703305156272 fixed

249 512.4583333333334 0 39.657794454952395 fixed

250 514.4996 0 39.99999999 fixed

251 514.5 0 40.0 fixed

252 514.5004 0 39.99999999 fixed

253 516.5416666666666 0 39.65779445495243 fixed

254 518.5833333333334 0 38.63703305156271 fixed

255 520.625 0 36.955181300451486 fixed

256 522.6666666666666 0 34.64101615137762 fixed

257 524.7083333333334 0 31.734133611649394 fixed

258 526.75 0 28.28427124746196 fixed

259 528.7916666666666 0 24.35045716034876 fixed

260 530.8333333333334 0 20.00000000000003 fixed

261 532.875 0 15.307337294603723 fixed

262 534.9166666666666 0 10.352761804100803 fixed

263 536.9583333333334 0 5.221047688802146 fixed

264 539.0 0 0 fixed

265 541.0416666666666 0 -5.22104768880204 fixed

266 543.0833333333334 0 -10.352761804100698 fixed

267 545.125 0 -15.307337294603622 fixed

268 547.1666666666666 0 -19.999999999999932 fixed

269 549.2083333333334 0 -24.350457160348896 fixed

270 551.25 0 -28.284271247461884 fixed

271 553.2916666666666 0 -31.734133611649327 fixed

272 555.3333333333334 0 -34.64101615137756 fixed

273 557.375 0 -36.95518130045144 fixed

274 559.4166666666666 0 -38.63703305156275 fixed

275 561.4583333333334 0 -39.657794454952416 fixed

276 563.5 0 -40.0 fixed

277 565.5416666666666 0 -39.65779445495241 fixed

278 567.5833333333334 0 -38.63703305156275 fixed

279 569.625 0 -36.95518130045143 fixed

280 571.6666666666666 0 -34.641016151377556 fixed

281 573.7083333333334 0 -31.734133611649483 fixed

282 575.75 0 -28.284271247461866 fixed

283 577.7916666666666 0 -24.350457160348874 fixed

284 579.8333333333334 0 -19.999999999999908 fixed

285 581.875 0 -15.307337294603595 fixed

286 583.9166666666666 0 -10.352761804100945 fixed

287 585.9583333333334 0 -5.22104768880201 fixed

288 588.0 0 0 fixed

289 590.0416666666666 0 5.221047688802175 fixed

290 592.0833333333334 0 10.35276180410083 fixed

291 594.125 0 15.307337294603487 fixed

292 596.1666666666666 0 20.00000000000005 fixed

293 598.2083333333334 0 24.350457160348782 fixed

294 600.25 0 28.28427124746178 fixed

295 602.2916666666666 0 31.734133611649412 fixed

296 604.3333333333334 0 34.64101615137749 fixed

297 606.375 0 36.9551813004515 fixed

298 608.4166666666666 0 38.63703305156272 fixed

299 610.4583333333334 0 39.657794454952395 fixed

300 612.4996 0 39.99999999 fixed

301 612.5 0 40.0 fixed

302 612.5004 0 39.99999999 fixed

303 614.5416666666666 0 39.65779445495243 fixed

304 616.5833333333334 0 38.63703305156272 fixed

305 618.625 0 36.955181300451486 fixed

306 620.6666666666666 0 34.64101615137763 fixed

307 622.7083333333334 0 31.734133611649398 fixed

308 624.75 0 28.28427124746197 fixed

309 626.7916666666666 0 24.350457160348768 fixed

310 628.8333333333334 0 20.000000000000036 fixed

311 630.875 0 15.30733729460373 fixed

312 632.9166666666666 0 10.352761804100812 fixed

313 634.9583333333334 0 5.221047688802156 fixed

314 637.0 0 0 fixed

315 639.0416666666666 0 -5.221047688802029 fixed

316 641.0833333333334 0 -10.352761804100687 fixed

317 643.125 0 -15.307337294603613 fixed

318 645.1666666666666 0 -19.999999999999925 fixed

319 647.2083333333334 0 -24.350457160348892 fixed

320 649.25 0 -28.28427124746188 fixed

321 651.2916666666 0 -31.734133611649323 fixed

322 653.3333333333334 0 -34.64101615137756 fixed

323 655.375 0 -36.955181300451436 fixed

324 657.4166666666666 0 -38.63703305156275 fixed

325 659.4583333333334 0 -39.657794454952416 fixed

326 661.5 0 -40.0 fixed

327 663.5416666666666 0 -39.65779445495241 fixed

328 665.5833333333334 0 -38.63703305156275 fixed

329 667.625 0 -36.955181300451436 fixed

330 669.6666666666666 0 -34.641016151377556 fixed

331 671.7083333333334 0 -31.734133611649487 fixed

332 673.75 0 -28.284271247461874 fixed

333 675.7916666666666 0 -24.350457160348885 fixed

334 677.8333333333334 0 -19.999999999999915 fixed

335 679.875 0 -15.307337294603604 fixed

336 681.9166666666666 0 -10.352761804100954 fixed

337 683.9583333333334 0 -5.221047688802019 fixed

338 686.0 0 0 fixed

339 688.0416666666666 0 5.221047688802166 fixed

340 690.0833333333334 0 10.35276180410082 fixed

341 692.125 0 15.307337294603478 fixed

342 694.1666666666666 0 20.000000000000043 fixed

343 696.2083333333334 0 24.350457160348775 fixed

344 698.25 0 28.28427124746198 fixed

345 700.2916666666666 0 31.7341336116494 fixed

346 702.3333333333334 0 34.641016151377485 fixed

347 704.375 0 36.95518130045149 fixed

348 706.4166666666666 0 38.63703305156272 fixed

349 708.4583333333334 0 39.657794454952395 fixed

350 710.4996 0 39.99999999 fixed

351 710.5 0 40.0 fixed

352 24.5 -0.5 40.0 constraint 1 2

353 710.5 -0.5 40.0 constraint 1 3

354 710.5 685.5 40.0 constraint 1 3

355 24.5 685.5 40.0 constraint 1 2

356 24.5 -0.5 726.0

357 710.5 -0.5 726.0

358 710.5 685.5 726.0

359 24.5 685.5 726.0

edges

1 1 2	30 30 31	59 59 60	88 88 89
2 2 3	31 31 32	60 60 61	89 89 90
3 3 4	32 32 33	61 61 62	90 90 91
4 4 5	33 33 34	62 62 63	91 91 92
5 5 6	34 34 35	63 63 64	92 92 93
6 6 7	35 35 36	64 64 65	93 93 94
7 7 8	36 36 37	65 65 66	94 94 95
8 8 9	37 37 38	66 66 67	95 95 96
9 9 10	38 38 39	67 67 68	96 96 97
10 10 11	39 39 40	68 68 69	97 97 98
11 11 12	40 40 41	69 69 70	98 98 99
12 12 13	41 41 42	70 70 71	99 99 100
13 13 14	42 42 43	71 71 72	100 100 101
14 14 15	43 43 44	72 72 73	101 101 102
15 15 16	44 44 45	73 73 74	102 102 103
16 16 17	45 45 46	74 74 75	103 103 104
17 17 18	46 46 47	75 75 76	104 104 105
18 18 19	47 47 48	76 76 77	105 105 106
19 19 20	48 48 49	77 77 78	106 106 107
20 20 21	49 49 50	78 78 79	107 107 108
21 21 22	50 50 51	79 79 80	108 108 109
22 22 23	51 51 52	80 80 81	109 109 110
23 23 24	52 52 53	81 81 82	110 110 111
24 24 25	53 53 54	82 82 83	111 111 112
25 25 26	54 54 55	83 83 84	112 112 113
26 26 27	55 55 56	84 84 85	113 113 114

117	117	147	147	177 177 178	207 207 208
118		148		178 178 179	208 208 209
118	118	148	148	179 179 180	209 209 210
119		149		180 180 181	210 210 211
119	119	149	149	181 181 182	211 211 212
120		150		182 182 183	212 212 213
120	120	150	150	183 183 184	213 213 214
121		151		184 184 185	214 214 215
121	121	151	151	185 185 186	215 215 216
122		152		186 186 187	216 216 217
122	122	152	152	187 187 188	217 217 218
123		153		188 188 189	218 218 219
123	123	153	153	189 189 190	219 219 220
124		154		190 190 191	220 220 221
124	124	154	154	191 191 192	221 221 222
125		155		192 192 193	222 222 223
125	125	155	155	193 193 194	223 223 224
126		156		194 194 195	224 224 225
126	126	156	156	195 195 196	225 225 226
127		157		196 196 197	226 226 227
127	127	157	157	197 197 198	227 227 228
128		158		198 198 199	228 228 229
128	128	158	158	199 199 200	229 229 230
129		159		200 200 201	230 230 231
129	129	159	159	201 201 202	231 231 232
130		160		202 202 203	232 232 233
130	130	160	160	203 203 204	233 233 234

146

237 237 238	267 267 268	297 297 298	327 327 328
238 238 239	268 268 269	298 298 299	328 328 329
239 239 240	269 269 270	299 299 300	329 329 330
240 240 241	270 270 271	300 300 301	330 330 331
241 241 242	271 271 272	301 301 302	331 331 332
242 242 243	272 272 273	302 302 303	332 332 333
243 243 244	273 273 274	303 303 304	333 333 334
244 244 245	274 274 275	304 304 305	334 334 335
245 245 246	275 275 276	305 305 306	335 335 336
246 246 247	276 276 277	306 306 307	336 336 337
247 247 248	277 277 278	307 307 308	337 337 338
248 248 249	278 278 279	308 308 309	338 338 339
249 249 250	279 279 280	309 309 310	339 339 340
250 250 251	280 280 281	310 310 311	340 340 341
251 251 252	281 281 282	311 311 312	341 341 342
252 252 253	282 282 283	312 312 313	342 342 343
253 253 254	283 283 284	313 313 314	343 343 344
254 254 255	284 284 285	314 314 315	344 344 345
255 255 256	285 285 286	315 315 316	345 345 346
256 256 257	286 286 287	316 316 317	346 346 347
257 257 258	287 287 288	317 317 318	347 347 348
258 258 259	288 288 289	318 318 319	348 348 349
259 259 260	289 289 290	319 319 320	349 349 350
260 260 261	290 290 291	320 320 321	350 350 351
261 261 262	291 291 292	321 321 322	
262 262 263	292 292 293	322 322 323	
263 263 264	293 293 294	323 323 324	

351 352 353 constraint 1

352 353 354 constraint 1 3

353 354 355 constraint 1

354 355 352 constraint 1 2

355 356 357

356 357 358

357 358 359

358 359 356

359 352 356

360 353 357

361 354 358

362 355 359

faces

1 351 360 -355 -359 frontcolorlightblue

2 352 361 -356 -360 frontcolorlightblue

3 353 362 -357 -361 frontcolorlightblue

4 354 359 -358 -362 frontcolorlightblue

5 355 356 357 358 frontcolorlightblue

bodies

1 1 2 3 4 5 volume volume_drop density den

A.3 Code for Micro V-grooved Surfaces

// this code is for groove width, W_g = 98 μm, groove height, D_g =80 μm, pillar width, W_p = 98 μm, eight pillar structures

```
gravity_constant 0 //starts with gravity 0
parameter vol = 1.5
parameter n_p = 8 //pillar numbers
parameter dg= 80 // groove height
parameter wp= 4 //pillar width
parameter wg= 98 //groove width
parameter volume_drop = (vol*(10^(9)))
parameter contact_angle = 122 //contact_angle = angle1
parameter n_g = n_p-1.0001
parameter GravityAnglePhi = 0 //inclination angle

parameter angle_1 = contact_angle //contact_angle = angle1
#define T1 (-cos(angle_1*pi/180))
parameter theta_cos = cos(contact_angle*pi/180)

parameter x_2 = 0//var x axis
parameter y_2 = 0 // var y axis
parameter z_2 = 0 // var z axis
```

parameter den = (10^(-15))

parameter aspect_ratio = (dg/wg) //dont change it

parameter ar= (dg/wg)

parameter x_1 = 0 //var x axis

parameter y_1 = -0.5 // var y axis

parameter z_1 = dg // var z axis

parameter g_incline = (180/pi)*(atan(wg/(2*dg)))

parameter incline_cos = (cos(g_incline*pi/180))

parameter incline_sin = (sin(g_incline*pi/180))

parameter incline_tan = (tan(g_incline*pi/180))

parameter wg_1= dg*incline_tan

parameter a_1= n_p*wp+n_g*wg

parameter b_1= a_1

parameter c_1= a_1

parameter g_1 =x_2+0*wp+0*wg_1

parameter g_2 =x_2+1*wp+0*wg_1

parameter g_3 =x_2+1*wp+1*wg_1

parameter g_4 =x_2+1*wp+2*wg_1

parameter g_5 =x_2+2*wp+2*wg_1

parameter g_6 =x_2+2*wp+3*wg_1

parameter g_7 =x_2+2*wp+4*wg_1

parameter g_8 =x_2+3*wp+4*wg_1

parameter g_9 =x_2+3*wp+5*wg_1

parameter g_10 =x_2+3*wp+6*wg_1

parameter g_11 =x_2+4*wp+6*wg_1

parameter g_12 =x_2+4*wp+7*wg_1

parameter g_13 =x_2+4*wp+8*wg_1

parameter g_14 =x_2+5*wp+8*wg_1

parameter g_15 =x_2+5*wp+9*wg_1

parameter g_16 =x_2+5*wp+10*wg_1

parameter g_17 =x_2+6*wp+10*wg_1

parameter g_18 =x_2+6*wp+11*wg_1

parameter g_19 =x_2+6*wp+12*wg_1

parameter g_20 =x_2+7*wp+12*wg_1

parameter g_21 =x_2+7*wp+13*wg_1

parameter g_22 =x_2+7*wp+14*wg_1

parameter g_23 =x_2+8*wp+14*wg_1

constraint 1 //groove perpendicular edges

formula: (x<g_1 ? z=z_2+dg : (x<g_2 ? z=(z_2+dg): (x<g_3 ? z=(z_2+dg-((x-g_2)/incline_tan)) : (x<g_4 ? z=(z_2+dg-((g_4-x)/incline_tan)) : (x<g_5 ? z=(z_2+dg) : (x<g_6 ? z=(z_2+dg-((x-g_5)/incline_tan)) : (x<g_7 ? z=(z_2+dg-((g_7-x)/incline_tan)) : (x<g_8 ? z=(z_2+dg) : (x<g_9 ? z=(z_2+dg-((x-g_8)/incline_tan)) : (x<g_10 ? z=(z_2+dg-((g_10-x)/incline_tan)) : (x<g_11 ? z=(z_2+dg) : (x<g_12 ? z=(z_2+dg-((x-g_11)/incline_tan)) : (x<g_13 ? z=(z_2+dg-((g_13-x)/incline_tan)): (x<g_14 ? z= (z_2+dg) :(x<g_15 ? z=(z_2+dg-((x-g_14)/incline_tan)): (x<g_16 ? z=(z_2+dg-((g_16-x)/incline_tan)):(x<g_17 ? z= (z_2+dg) :(x<g_18 ? z=(z_2+dg-((x-g_17)/incline_tan)): (x<g_19 ? z=(z_2+dg-((g_19-x)/incline_tan)):(x<g_20 ? z= (z_2+dg) :(x<g_21?z=(z_2+dg-((x-g_20)/incline_tan)):(x<g_22?z=(z_2+dg-((g_22-x)/incline_tan)) :(x<g_23 ? z= (z_2+dg) : z_2+dg))))))))))))))))))))))))

energy:

e1: (x<g_1 ? -T1*y : (x<g_2 ? -T1*y: (x<g_3 ? -T1*y : (x<g_4 ? -T1*y : (x<g_5 ? -T1*y : (x<g_6 ? -T1*y : (x<g_7 ? -T1*y : (x<g_8 ? -T1*y : (x<g_9 ? -T1*y : (x<g_10 ? -T1*y : (x<g_11 ? -T1*y : (x<g_12 ? -T1*y : (x<g_13 ? -T1*y : (x<g_14 ? -T1*y : (x<g_15 ? -T1*y : (x<g_16 ? -T1*y : (x<g_17 ? -T1*y :(x<g_18 ? -T1*y : (x<g_19 ? -T1*y : (x<g_20 ? -T1*y :(x<g_21 ? -T1*y : (x<g_22 ? -T1*y : (x<g_23 ? -T1*y: -T1*y)))))))))))))))))))))))

e2: 0

e3: 0

constraint 2 nonpositive //left edges

formula: (x-g_1)*(x-g_2)

constraint 3 nonpositive //right edges

formula: (x-g_22)*(x-g_23)

vertices

1 g_1 y_2 z_2+dg fixed

2 g_2 y_2 z_2+dg fixed

3 g_3 y_2 z_2 fixed

4 g_4 y_2 z_2+dg fixed

5 g_5 y_2 z_2+dg fixed

6 g_6 y_2 z_2 fixed

7 g_7 y_2 z_2+dg fixed

8 g_8 y_2 z_2+dg fixed

9 g_9 y_2 z_2 fixed

10 g_10 y_2 z_2+dg fixed

11 g_11 y_2 z_2+dg fixed

12 g_12 y_2 z_2 fixed

13 g_13 y_2 z_2+dg fixed

14 g_14 y_2 z_2+dg fixed

15 g_15 y_2 z_2 fixed

16 g_16 y_2 z_2+dg fixed

17 g_17 y_2 z_2+dg fixed

18 g_18 y_2 z_2 fixed

19 g_19 y_2 z_2+dg fixed

20 g_20 y_2 z_2+dg fixed

21 g_21 y_2 z_2 fixed

22 g_22 y_2 z_2+dg fixed

23 g_23 y_2 z_2+dg fixed

24 x_1 y_1 z_1 constraint 1 2

25 x_1+a_1 y_1 z_1 constraint 1 3

26 x_1+a_1 y_1+b_1 z_1 constraint 1 3

27 x_1 y_1+b_1 z_1 constraint 1 2

28 x_1 y_1 z_1+c_1

29 x_1+a_1 y_1 z_1+c_1

30 x_1+a_1 y_1+b_1 z_1+c_1

31 x_1 y_1+b_1 z_1+c_1

edges

1 1 2 no_refine fixed

2 2 3 no_refine fixed

3 3 4 no_refine fixed

4 4 5 no_refine fixed

5 5 6 no_refine fixed

6 6 7 no_refine fixed

7 7 8 no_refine fixed

8 8 9 no_refine fixed

9 9 10 no_refine fixed

10 10 11 no_refine fixed

11 11 12 no_refine fixed

12 12 13 no_refine fixed

13 13 14 no_refine fixed

14 14 15 no_refine fixed

15 15 16 no_refine fixed

16 16 17 no_refine fixed

17 17 18 no_refine fixed

18 18 19 no_refine fixed

19 19 20 no_refine fixed

20 20 21 no_refine fixed

21 21 22 no_refine fixed

22 22 23 no_refine fixed

23 24 25 constraint 1

24 25 26 constraint 1 3 color blue//rightedge

25 26 27 constraint 1

26 27 24 constraint 1 2 color green//leftedge

27 28 29

28 29 30

29 30 31

30 31 28

31 24 28

32 25 29

33 26 30

34 27 31

faces

1 25 34 -29 -33 color lightred //front

2 24 33 -28 -32 color lightred //right

3 23 32 -27 -31 color lightred //back

4 26 31 -30 -34 color lightred //left

5 27 28 29 30 color lightred //top

153

bodies

1 1 2 3 4 5 volume volume drop density